Titre: Title:	Valorization of Low-Grade Phosphate Fine Waste by Carbo-Chlorination Route
Auteur: Author:	Ahmed Najjar
Date:	2023
Type:	Mémoire ou thèse / Dissertation or Thesis
Référence: Citation:	Najjar, A. (2023). Valorization of Low-Grade Phosphate Fine Waste by Carbo-Chlorination Route [Mémoire de maîtrise, Polytechnique Montréal]. PolyPublie. https://publications.polymtl.ca/55225/

URL de PolyPublie: PolyPublie URL:	https://publications.polymtl.ca/55225/
Directeurs de recherche: Advisors:	Jamal Chaouki
Programme: Program:	Génie chimique

POLYTECHNIQUE MONTRÉAL

affiliée à l'Université de Montréal

Valorization Of Low-Grade Phosphate Fine Waste By Carbo-Chlorination Route

AHMED NAJJAR

Département de génie chimique

Mémoire présenté en vue de l'obtention du diplôme de *Maîtrise ès sciences appliquées*

Génie chimique

Août 2023

POLYTECHNIQUE MONTRÉAL

affiliée à l'Université de Montréal

Ce mémoire intitulé :

Valorization Of Low-Grade Phosphate Fine Waste By Carbo-Chlorination Route

présenté par **Ahmed NAJJAR**

en vue de l'obtention du diplôme de *Maîtrise ès sciences appliquées*

a été dûment accepté par le jury d'examen constitué de :

Jean-Philippe HARVEY, président
Jamal CHAOUKI, membre et directeur de recherche
Yassine TAHA, membre

ACKNOWLEDGMENTS

First and foremost, I am grateful to God for all His graces and blessings that enabled me to undertake and achieve my research work successively.

I would like to express my sincere gratitude to my advisor Prof. Jamal Chaouki for giving me the opportunity to conduct my master's study under his supervision. I have learned a lot from his guidance, expert advice, and vast engineering knowledge. Additionally, I would like to express my gratitude to the members of my thesis committee, Prof. Jean-Philippe Harvey and Prof. Yassin Taha, for graciously accepting the task of evaluating my thesis project and for their invaluable insights and constructive feedback. My indebtedness extends to my mentor, Dr. Adrián Carrillo García, whose unwavering support, valuable theoretical recommendations, and assistance have been instrumental in the accomplishment of my research project.

I am also thankful to Afshin Fallahi for his unwavering willingness to assist at any given moment. Furthermore, I would like to extend my appreciation to Prof. Mohammad Latifi, Dr. Ahmad-reza, and Dr. Jaber Shabanian for their invaluable advice and support throughout my studies. I am forever grateful to the dedicated technicians and staff of the Department of Chemical Engineering for their exceptional support. Warm gratitude is extended to Polytechnique Montreal and the OCP group for their financial support and provision of essential resources for this project. My heartfelt acknowledgment extends to the entire PEARL group for fostering a friendly and conducive environment.

I express my utmost gratitude to my beloved parents, Amel and Farhat, for their unceasing motivation and unwavering belief in my abilities. Finally, I would like to extend my deepest appreciation to my wonderful wife, whose unwavering support and encouragement have been a constant source of strength throughout my thesis journey. I am especially grateful to my three-year-old son, Ayoub, whose innocent curiosity and boundless energy have brought immense joy and served as an endless source of inspiration. His presence and infectious spirit serve as a constant reminder of life's true priorities. Ayoub, thank you for being my little ray of sunshine, bringing boundless love and laughter into our lives, and undoubtedly contributing to my success.

RÉSUMÉ

Le phosphore, dérivé d'une grande variété de minéraux, joue un rôle essentiel dans la croissance des plantes, des animaux et de la vie humaine. Il revêt une importance capitale en agriculture en tant qu'engrais indispensable. Face aux ressources naturelles limitées et à l'absence de substitut cohérent, il est crucial de relever ces défis. Pour répondre à une demande croissante, une approche en deux volets est nécessaire: explorer les minerais de phosphate à faible teneur et recycler efficacement le phosphore à partir des déchets. Ces mesures garantissent une utilisation durable du phosphore en agriculture et dans d'autres pratiques industrielles.

Cette étude se concentre sur l'extraction du phosphore à partir de matériaux de phosphate, spécifiquement sous forme de composés phosphorés chlorés, en utilisant la carbochloration avec du chlore gazeux et du carbone. Deux échantillons industriels de déchets de phosphate à faible et haute teneur ont été soumis à une réaction de carbochloration en utilisant un mélange gazeux de Cl_2 et de N_2 dans un réacteur en quartz en laboratoire.

Avant de débuter la phase expérimentale, une étude thermodynamique approfondie et une revue exhaustive de la littérature ont été réalisées afin de déterminer la composition optimale des réactifs et les conditions appropriées, notamment la température, le débit de gaz et la pression. L'échantillon de minerai de phosphate à haute teneur a été examiné dans un premier temps à différents intervalles de temps (allant de 30 minutes à 7 heures) et à différentes températures (de 600 °C à 700 °C) afin d'identifier les conditions expérimentales conduisant à la meilleure conversion du phosphore.

Ensuite, le minerai de phosphate à faible teneur a été testé dans les conditions optimales présélectionnées pour valider la faisabilité du processus de carbochloration avec les déchets industriels de phosphate à faible teneur. En combinant les prédictions thermodynamiques avec l'analyse élémentaire ICP, la microanalyse SEM-EDS et l'examen XRD des produits solides de réaction, des interprétations éclairantes des phénomènes et des mécanismes de réaction lors de la carbochloration des déchets de phosphate à faible teneur ont été obtenues.

Les résultats obtenus ont révélé que le rendement maximal de récupération du phosphore pour les phosphates à haute et faible teneur était respectivement de 70 % et 76 %, atteint à une température de 700 °C pendant une durée de 7 heures. Cette réaction relativement lente a été attribuée à l'interaction solide-solide entre le carbone et le minerai, principalement régie par la diffusion du carbone à travers le minerai. De plus, la formation progressive de $CaCl_2$ a recouvert les particules

solides, réduisant ainsi la surface de contact entre le gaz de chlore et le minerai, entravant ainsi sa diffusion et ralentissant la progression de la réaction. L'analyse thermodynamique et l'analyse XRD-LECO ont fourni des informations précieuses sur la décomposition du carbonate-fluorapatite ($Ca_{9.55}(PO_4)_{4.96}F_{1.96}(CO_3)_{1.28}$), qui subit une décarbonatation et conduit principalement à la formation de fluorapatite ($Ca_5(PO_4)_3F$) et à la libération de CO et de CO_2. Ensuite, à des températures et des durées de réaction plus élevées, la fluorapatite se décompose en $CaCl_2$, $POCl_3$, CO et CO_2. D'autre part, la calcite ($CaCO_3$), la dolomite ($CaMg(CO_3)_2$) et le silicate (SiO_2) forment principalement les produits suivants : CO, CO_2, $CaCl_2$, $MgCl_2$, $SiCl_4$.

Enfin, pour mieux comprendre la carbochloration appliquée à la valorisation des phosphates à faible teneur, une étude a été réalisée, incluant un schéma de procédé, sa simulation et une étude techno-économique. L'évaluation a été menée dans le contexte du traitement d'un million de tonnes métriques de minerai de phosphate à faible teneur par an, conduisant à la production de 50 tonnes par heure de $POCl_3$ avec une pureté impressionnante de 99,99 %. Sur la base de cette capacité de production, les dépenses d'investissement projetées (CAPEX) pour le processus s'élevaient à 165 millions de dollars américains, accompagnées de frais d'exploitation annuels (OPEX) de 233 millions de dollars américains. En fin de compte, le coût de production estimé pour le $POCl_3$ s'est établi à 640 dollars américains par tonne métrique.

ABSTRACT

Phosphorus, derived from a wide variety of minerals, is essential for the growth of plants, animals, and human life. It serves a vital role in agriculture as an indispensable fertilizer. With finite natural resources and no consistent substitute, addressing these challenges is crucial. To cope with rising demands, a two-fold approach is needed: exploring low-grade phosphate ore and efficiently recycling phosphorus from waste. These measures ensure sustainable phosphorus use in agriculture or other industrial practices.

This study focuses on the extraction of phosphorus from phosphate materials, specifically in the form of phosphorus-chlorinated compounds, utilizing carbochlorination with gaseous chlorine and carbon. Two industrial samples of low and high-grade phosphate wastes were tested by carbochlorination reaction with Cl_2 and N_2 gaseous mixture using a lab-scale quartz reactor.

Before commencing the experimental phase, an in-depth thermodynamic study and comprehensive literature review were conducted to determine the optimal composition of reagents and the appropriate conditions, including temperature, gas flow rate, and pressure. The high-grade phosphate ore sample was initially examined at various time intervals (ranging from 30 minutes to 7 hours) and temperatures (600 °C to 700 °C) to identify the experimental conditions that yielded the highest phosphorus conversion.

Subsequently, the low-grade phosphate ore was tested under the preselected optimal conditions to validate the feasibility of the carbochlorination process with industrial low-grade phosphate waste. By combining thermodynamic predictions with ICP elemental analysis, SEM-EDS, and XRD examination of the solid reaction products, insightful interpretations of the occurring phenomena and reaction mechanisms during the carbochlorination of low-grade phosphate waste were obtained.

The obtained results revealed that the maximum phosphorus recovery for high and low-grade phosphates was 70% and 76%, respectively, achieved at a temperature of 700 °C over a 7-hour duration. This relatively slow reaction rate was ascribed to the solid-solid interaction between carbon and ore, predominantly governed by carbon diffusion through the ore. Furthermore, the gradual formation of $CaCl_2$ covered the solid particles, resulting in reduced contact surface area between chlorine gas and the ore, thereby impeding its diffusion and hindering the progress of the reaction. Thermodynamic analysis and XRD-LECO analysis provided valuable insights into the

decomposition of carbonate-fluorapatite ($Ca_{9.55}(PO_4)_{4.96}F_{1.96}(CO_3)_{1.28}$), undergoes decarbonization and yields primarily to the formation of fluorapatite ($Ca_5(PO_4)_3F$) and liberation of CO and CO_2. Then, for higher temperatures and reaction times, the fluorapatite decomposes into $CaCl_2$, $POCl_3$, CO and CO_2. In the other hand, calcite ($CaCO_3$), dolomite ($CaMg(CO_3)_2$) and silicate (SiO_2) forms mainly CO, CO_2, $CaCl_2$, $MgCl_2$, $SiCl_4$, products.

Lastly, in order to gain a comprehensive understanding of carbochlorination as applied to the valorization of low-grade phosphate, an investigation was conducted including a process flowsheet, its simulation, and a techno-economic study. The assessment was carried out in the context of processing 1 million metric tons per year of low-grade phosphate ore, leading to the production of 50 tons per hour of $POCl_3$ with an impressive purity of 99.99%. Based on this production capacity, the projected capital expenditure (CAPEX) for the process amounted to 165 million US dollars, accompanied by annual operating expenses (OPEX) of 233 million US dollars. Ultimately, the estimated production cost for $POCl_3$ was determined to be 640 US dollars per metric ton.

TABLE OF CONTENTS

LIST OF TABLES

LIST OF FIGURES

LISTE OF SYMBOLS AND ABBREVIATIONS

a	Cost constant
ACC	Annual Capital Charge
b	Cost constant
BPL	Bone Phosphate of Lime
CRF	Capital Recovery Factor
FCI	Fixed Capital Investment
FCOP	Fixed Cost of Production
TCOP	Total Cost of Production
$Ca_{10}(PO_4)_6(Cl)_2$	Chlorapatite
$Ca_{10}(PO_4)_6(OH)_2$	Hydroxyapatite
$Ca_{10}(PO_4)_6F_2$	Fluorapatite
Ca_2SiO_4	Dicalcium silicates
$Ca_3(PO_4)_2$	Tricalcium phosphate
$Ca_{9.55}(PO_4)_{4.96}F_{1.96}(CO_3)_{1.283}$	Carbonate-fluorapatite
$CaCO_3$	Calcite
$CaMg(CO_3)_2$	Dolomite
$CaMgSi_2O_6$	Diopside
CaO	Calcium oxide
$CaSiO_3$	Monocalcium silicates
C_{IE}	Installed equipment cost
CO	Carbon monoxide
CO_2	Carbon dioxide
C_{PE}	Equipment cost
f_i	Installation factor
f_n	Material cost factor
i	Discount rate
j	Year
n	Equipment lifetime
S	Size parameter

CHAPTER 1 INTRODUCTION

Phosphorus is vital for the life of plants, humans, and animals, as it plays a crucial role in soil fertility and global food security. However, the primary source of phosphorus currently utilized, phosphate rock, is a finite resource that cannot be renewed.[1]

Recent statistics indicate a more than threefold increase in global phosphate rock production (with 26-34% P_2O_5) over the past five decades because of its extensive range of applications [2, 3]. Approximately 95% of the global production of phosphate rock is utilized by the fertilizer industry. The remaining portion is processed to produce elemental phosphorus, which serves as the primary raw material for manufacturing different phosphate compounds.[4] Indeed, phosphorus is regarded as the highest capacity anode material for sodium-ion batteries and is also among the most attractive anode materials for lithium-ion batteries due to their wide range of applications, including portable electronic devices, transportation such as electric vehicles, and renewable energy storage systems contributing to achieving a secure, cost-effective, environmentally friendly, and sustainable energy future.[5] Given this growth and the finite nature of phosphate resources, the depletion of economically viable phosphorus reserves is imminent in the near future. To overcome the increasing phosphor demand as well as the environmental issues that present stockpiling of minerals wastes, the exploitation of low-grade phosphate ores and the recycling of phosphorus from waste materials are crucial. [2, 6]

Phosphoric acid is manufactured through a sequence of unit operations, mainly by reacting phosphate with sulfuric acid. Depending on the process's operational conditions, different qualities and purities of phosphoric acid are obtained.[7] In turn, fertilizers are produced by attacking apatite, the most common form of phosphate, with phosphoric acid through several reaction mechanisms. Naturel phosphate used for both phosphoric acid and fertilizer production undergoes several pre-treatment operations, which can involve physical and/or chemical processes.[7] These processes are currently confronted with numerous environmental challenges stemming from the substantial quantities of waste generated. In the phosphate industry, these wastes include waste rocks, concentrator tailings, and phosphate sludge.[8] Typically, these materials are accumulated on the surface in large waste rock piles, covering extensive areas within the mine site [9, 10]. The accumulation of these wastes poses a potential source of pollution due to their chemical characteristics and grain size, some of them being very fine powders. During the extraction of

sedimentary phosphate ores, large volumes of rocks are excavated without undergoing sorting and are stored as stockpiles. Additionally, the beneficiation process involves techniques such as crushing, screening, washing, and flotation for the concentration of the carbon-fluorapatite from associated gangue minerals. As a result, the enrichment plants generate significant quantities of sludge and flotation tailings, which are deposited together as phosphate sludge in basins covering several hectares. The abundance of these by-products during the mining operations of sedimentary phosphate ore presents a major challenge in terms of storage capacity and dust control. These waste materials diminish arable lands, modify topography, and mar the natural landscapes.[10, 11]

As mentioned before, the phosphate industry produces a continuous stream of diverse waste materials, such as carbonated and/or siliceous waste rocks, clayey sludge, and phosphogypsum. These waste products accumulate in significant quantities, ranging from 5 to 10 tons of waste per ton of concentrated phosphate apatite.[6] The proper management of these wastes has become a prominent concern, considering their impact on the public, the environment, and financial aspects. To align with the goals of sustainable mining and a circular economy, researchers are actively investigating eco-friendly and green approaches for recycling and managing phosphate mine waste rocks and tailings. Over the past two decades, researchers have focused their efforts on developing several chlorination techniques to valorize various raw materials and solid industrial waste. Among these techniques, carbochlorination has been mainly used to produce metallic chlorides in the presence of a reducing agent and chlorine. This process presents an economical and efficient path to extract the metals as it reduces the melting and boiling points of the resultant chlorides compared to the metal or the oxide forms. [12-14]

The current research study, in partnership with OCP Group, proposes the carbochlorination of low-grade phosphate ore as a promising method for extracting phosphorus in the form of phosphorus chlorinated compounds. This process involves reducing the phosphate ore in the presence of chlorination agents and reductive reagents, which can result in the formation of phosphoryl chloride. This product can then be used as an essential reagent in the synthesis of valuable chemical products, e.g., phosphate esters and phosphine oxides, or to synthesize phosphoric acid, as part of the value chain of OCP Group. While thermodynamics are initially used to understand the reactions taking place and the process operating conditions, the project focuses on proof of concept and feasibility, technical and economic, of the carbochlorination of the phosphate ore.

CHAPTER 2 LITERATURE REVIEW

Phosphorus “P” is a critical nutrient required for all forms of life, much like nitrogen. The most prevalent form of phosphorus used by living organisms is phosphate “PO_4^{3-}”. This is a naturally occurring non-metal mineral resource that is classified as non-renewable. This mineral is essential for plant growth and development as it is involved in many metabolic processes including photosynthesis, protein synthesis, and respiration. Furthermore, phosphorus acts as a primary constituent in the molecule ATP (adenosine triphosphate) and serves as a central building block of nucleic acids, including DNA and RNA. Besides, this vital element is necessary to produce proteins and other essential compounds.[15-17] Figure 2.1 provides a representation of phosphorus’ role of in plant growth.[18] As phosphate plays a critical role in plant growth, it is a key factor in ensuring food supply and supporting life on our planet. [19]

An average soil typically contains about 0.05% (w/w) of phosphorus content. However, due to its poor solubility and fixation in the soil, only 0.1% of the total phosphorus is available for the plant. Consequently, this limited availability significantly affects plant size and productivity. Therefore, it is essential to supplement the soil with phosphorus through fertilizers. [20, 21]

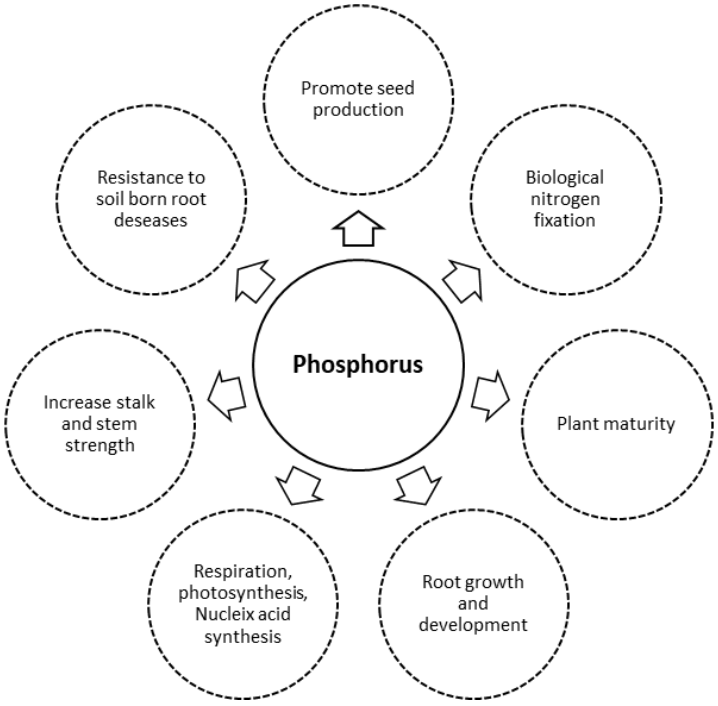

Figure 2.1 Role of Phosphorus on plant growth [18]

Considering fertilizers provide a portion of a plant's phosphorus requirements, the remaining content of phosphorus must come from the native soil. This highlights the indispensability of phosphorus for plant growth and the importance of maintaining adequate levels in the soil through fertilization and other management practices. Additionally, the sustainable management and efficient use of phosphate resources are crucial for meeting the increasing demand for food and maintaining the health of ecosystems.[22-24]

2.1 Phosphate's overview

Since its discovery in 1669, phosphorus has been extensively used in industries such as chemical, food, aviation, agriculture, and aerospace, with the phosphoric acid and fertilizers industries being the predominant consumers. [25] Given the significant economic and vital values associated with phosphorus, it is not surprising that the demand for phosphate has been steadily increasing over the years. In 2019, the global consumption of P_2O_5 was estimated at 47 million tons, it is predicted to reach 50 million tons by 2023.[26]

Currently, most of the phosphate rock, approximately 66%, is allocated to produce fertilizers, including solid diammonium phosphate (DAP), mono ammonium phosphate (MAP), and triple superphosphate (TSP). The types of fertilizers and their respective production routes can be found in Figure 2.2.

Apart from the fertilizer industry, the animal feed and food sectors represent 6% and 9% of worldwide phosphorus consumption respectively, while the remaining 19% is utilized in various industrial products such as detergents and metal phosphate coatings.[25, 27] For instance, in 2017 in China, considered a compelling case study to understand this resource's allocation, the phosphate rock was primarily allocated to produce fertilizers (75.6%), yellow phosphorus (11.1%), and animal feed (12.2%). The remaining amount is being used for other purposes (0.5%) or exported (0.6%). [25]

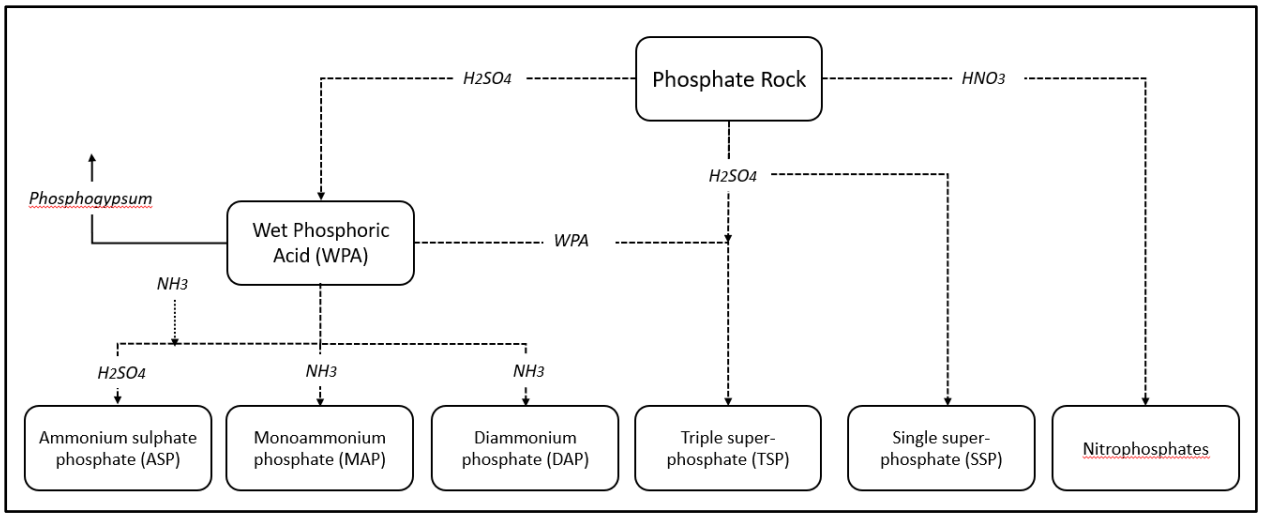

Figure 2.2 The manufacturing process of the different types of phosphate-based fertilizers [28]

2.1.1 Global distribution of phosphate resources

According to the US Geological Survey, the estimated reserves of the world's phosphate rock in 2016 were around 17 billion tons, with additional basic reserves estimated at nearly 50 billion tons. Although phosphate resources are abundant worldwide as they can be found in over 60 countries, their distribution is far from uniform. In fact, in 2021, over 80% of phosphate reserves are found in Morocco, the United States, South Africa, Jordan, and China; Morocco being the country with the biggest reserves (Table 2.1). [29, 30] Figure 2.3 illustrates the phosphate rock reserves in Morocco and other major countries.[31]

Table 2.1 Global phosphate production in 2021 (Leading phosphate producers in 2021) [30]

Country	Deposit type	Phosphate mineral	Gangue mineral	2021 production (Mt)	Reserves (Mt)
China	*Ig, *Sd, *Mt, *Gu	Fluoapatite, Collophane, francolite, monazite	Dolomite, clay,, aluminium silicate, quartz, zircon, goethite, chlorite	85	3200
Morocco	Sd	Apatite	Dolomite, calcite, aluminium silicate, quartz	38	50000
United States	Ig, Sd, Mt, Gu	Monazite francolite, wavellite, crandallite	Dolomite, calcite, aluminium silicate, quartz, goethite	22	1000
Russia	Ig, Sd	Monazite, francolite, fluorapatite, hydroxyapatite	Ilmenite, pyrite, mica, magnetite, calcite etc.	14	600
Jordan	Sd	N.A	N.A	9.2	1000

*Ig: Igneous rocks**,** *Sd: Sedimentary rocks**,** *Mt: Metamorphic rocks, *Gu: Guano

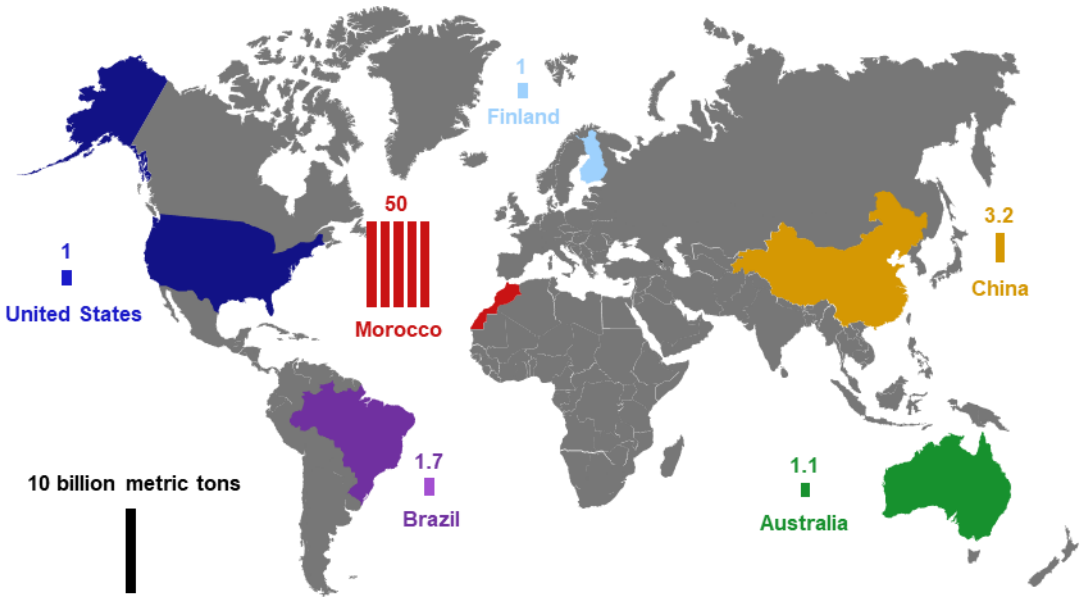

Figure 2.3 The phosphate rock reserves of Morocco and some other main countries [31]

2.1.2 Phosphate deposits

Generally, phosphate deposits are classified into three categories (Figure 2.4): [32-35]

b) Igneous: derived from magma crystallization. This type of rock is formed at very high temperatures and is characterized by its high degree of purity, with a P_2O_5 content typically between 4-15% and can be enriched up to 35-40%.

c) Sedimentary: formed by diagenesis through the cementation of particles. Igneous rock is altered into particles of different sizes and through erosion by water, ice, and wind, sediment is formed. This type of rock is characterized by its high degree of impurity throughout its formation process. 80% of the world's phosphate reserves are of sedimentary origin, with a P_2O_5 content for sedimentary deposits between 10% to 30% and can be enriched up to 30-35%.

d) Metamorphic: sedimentary rocks that have taken on another form under very high temperature and pressure conditions. 15 to 20% of the world's phosphate reserves are of igneous and metamorphic origin.

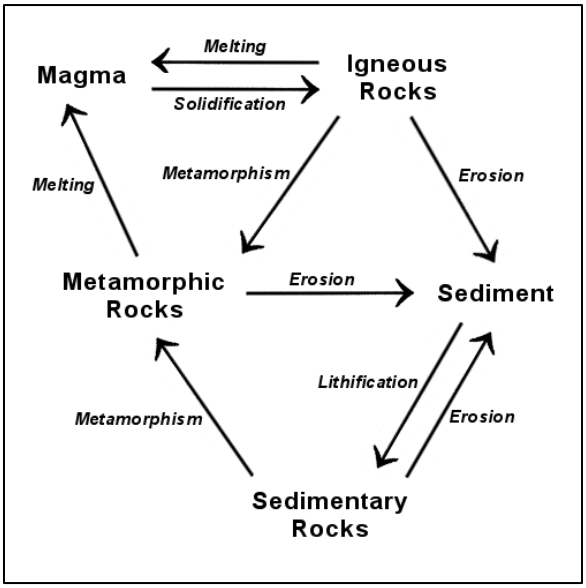

Figure 2.4 Diagram of the rock cycle [35]

2.1.3 Phosphate minerals and impurities

There are over 200 known phosphate minerals, from which the apatite group is the most abundant, accounting for roughly 95% of the phosphorus present in the Earth's crust. A summary of some types of phosphatic minerals is shown in Table 2.2. [36]

Table 2.2 The most abundant phosphate minerals [36]

Phosphate mineral	Type	Occurrence	Formula
Apatite	Fluorapatite	Ig*, Sd*, Mt*	$Ca_5(PO_4)_3F$
	Chlorapatite	Ig, Mt	$Ca_5(PO_4)_3Cl$
	Hydroxyapatite	Ig, Sd, Mt	$Ca_5(PO_4)_3OH$
	Carbonate-Fluorapatite	Sd, Mt	$Ca_5(PO_4, CO_3)_3(F, O)$
	Carbonate-Hydroxyapatite	Sd, Mt	$Ca_5(PO_4, CO_3)_3(OH, O)$
Monazite	Monazite-(Ce)	Ig, Sd, Mt (REE)	$CePO_4$
Xenotime	Xenotime-(Y)	Ig, Mt (REE)	YPO_4
Monetite	-	Ig, Sd	$CaHPO_4$
Other phosphate minerals: Vivianite, Xenotime, Variscite, Wavellite, Whitlockite, Brushite, Struvite *Ig: Igneous rocks**,** *Sd: Sedimentary rocks**,** *Mt: Metamorphic rocks			

The composition and type of impurities present in phosphate depend on their origin and formation conditions. Table 2.3 shows the main impurities of phosphate rock with their advantages and disadvantages, as well as the acceptable limit of these impurities in the rock.

Table 2.3 The properties of the main impurities present in phosphate rock.

Component	Source	Acceptable limit	Advantage	Disadvantage	Ref
MgO	Dolomite, phoscorite, ankerite	Content < 1%	Nutrient	Higher content increases the phosphoric acid viscosity and decrease its filterability (P2O5 losses)	[37, 38]
CaO	Calcite, dolomite, fluorite, gypsum, apatite, ankerite	Ratio CaO to P_2O_5 < 1.6%	Enhance the reactivity of phosphate	Raise the consumption of sulfuric acid and foam formation during the wet Process	[37, 38]
SiO_2	Quartz, sand mining	Content < 2%	Lead to SiF4 formation, which is less toxic and corrosive than H2SiF6	Cause the erosion of equipment and affect the filtration of phosphogypsum	[39]
F_2	Fluorapatite, fluorite, francolite	Content < 4%	May be collected as a co-product	Affect the filtration of phosphogypsum and lead to corrosion and mud formation	[37, 38]
Cl_2	Chlorapatite	Content < 0.03%	-	Cause the erosion of equipment	[39]

Hence, igneous phosphate minerals may contain a variety of phosphate minerals that are rarely found in sedimentary minerals and vice versa.

2.2 Phosphate ore treatment

In this section, a comprehensive examination of the methodologies, including physical beneficiation, wet processes, and dry processes, employed to manufacture premium-quality phosphate products suitable for applications in phosphoric acid, fertilizers, and various other phosphate compounds, is provided. The emphasis will be placed on the production of phosphoric acid, serving as an illustrative example of the wet and thermal processes. In fact, the two primary industrial methods exist for the production of phosphoric acid are: the wet process and the dry process, also known as the electrical furnace method. While the dry process yields a purer, technical-grade acid, it's also considerably more expensive to execute compared to the wet process method for producing phosphoric acid (Figure 2.5).[10]

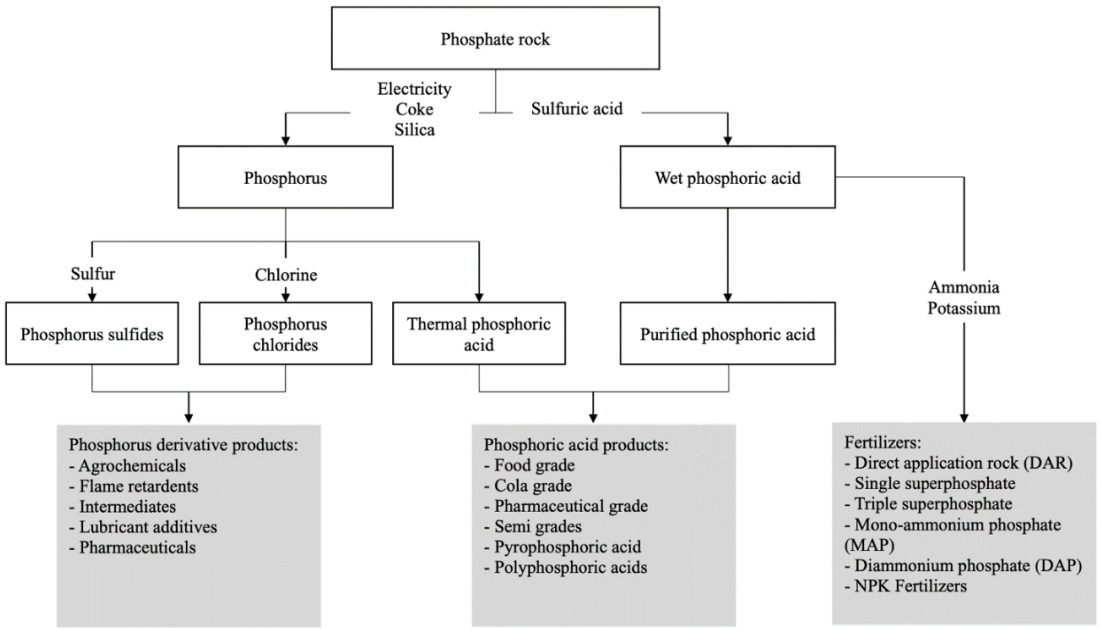

Figure 2.5 An overview of phosphate rock enhancement and processing methods [2]

2.2.1 Physical beneficiation

Physical beneficiation is the process of separating valuable minerals, especially phosphate-bearing minerals, from unwanted gangue minerals based on their distinct physical properties, including magnetic, gravity, electrostatic, and flotation characteristics. This process involves various treatments such as crushing, grinding, screening, washing, and flotation, depending on factors like the size of the ore and the presence of gangue minerals. etc.[40, 41] The main goals of physical beneficiation are to improve the grade of the extracted mining product by eliminating unnecessary minerals and to remove toxic metals commonly associated with phosphate rock, such as arsenic, chromium, lead, mercury, nickel, vanadium, and cadmium. [42]

The comminution process involves reducing the size of particles to facilitate the release of carbonates from the pockets of apatite. This size reduction through crushing and grinding is particularly beneficial for subsequent treatments, such as leaching reactions.[43] Mukhopadhyay introduced an innovative beneficiation process for phosphate rock, focusing on segregating phosphorus-containing heavy metal-free minerals based on their crystal nature, distinct from non-phosphorus-containing minerals.[44] The process involves grinding the crystals to a sand-like size (0.5-1.0 mm), followed by screening or sieving to collect the appropriate substrate. Subsequently, specific gravity separation is carried out to isolate heavy materials (specific gravity > 2.82), which

are then dried to extract phosphate-containing minerals with specific crystallinity.[44] Despite claiming cost-effectiveness, the invention was never evaluated on a larger scale. Decreasing particle size can enhance process efficiency; however, fine grinding can also raise capital costs due to the higher energy required for comminution, thus limiting further particle separation and extraction. Consequently, certain physical beneficiation steps, such as crushing and grinding, cannot selectively extract heavy metals during the decontamination process.[45] Fine grinding is an essential step in achieving particle liberation, but our primary focus lies in exploring treatments like flotation to extract heavy metals effectively. Flotation is a dynamic and selective process extensively employed in mineral processing to separate valuable elements finely ground from gangue minerals in a mixture. By using froth flotation, we can suspend impurities and conveniently recover them from the medium.[46] When it comes to heavy metals, they can be extracted either when associated with gangue material or individually, depending on the design parameters that allow for selectivity. This property is well-recognized and utilized in wastewater treatment, where heavy metals bond to a specific agent through adsorption and are then separated by filtration.[47] Peng et al. explored various technologies for remediating heavy metals in contaminated sediments, taking into account sediment characteristics like metal load, particle size distribution, and metal species distribution. They proposed the use of flotation for particles smaller than 63 μm, achieving an impressive 80% removal of heavy metals from anaerobic sediments.[48] The study also identified the presence of metal ions, including heavy metals, in the sediment in sulfide form. However, the authors highlighted the significance of assessing the sulfides' oxidation degree, as both low and high oxidation intensities can significantly influence the removal efficiency.[48, 49]

The effective physical beneficiation treatment, or a combination of treatments, primarily depends on the liberation size of phosphate from its gangue minerals.[40] Additionally, the process may be influenced by the geological factors and mineral composition of the ore, particularly the nature of the gangue material and the presence of heavy metals. In cases where sedimentary calcareous phosphate rocks with significant carbonate content are involved, the physical beneficiation process can become more intricate or even challenging. This difficulty arises because carbonate minerals closely resemble the desired minerals, making their efficient removal through flotation or other physical separation methods problematic due to their similar physical and surface properties.[40, 41] Furthermore, the design of the beneficiation processes must be carefully executed to enable

effective and selective removal of heavy metals, as inadequate design may result in soluble phosphorus loss.[44] Consequently, it is essential to explore novel removal techniques that can address the issues related to heavy metal removal during the physical beneficiation stage.

2.2.2 Wet process

Phosphoric acid can be derived from phosphate rock through digestion with mineral acids such as nitric, hydrochloric, phosphoric, or sulfuric. The conventional method, often referred to as the "wet process", typically uses sulfuric acid. A by-product of this process is calcium sulfate.[50] The particular form of calcium sulfate that precipitates: dihydrate, hemihydrate, or anhydrite, depends on factors like temperature and the concentrations of P_2O_5 and SO_4 in the solution, as illustrated in Figure 2.6.[51]

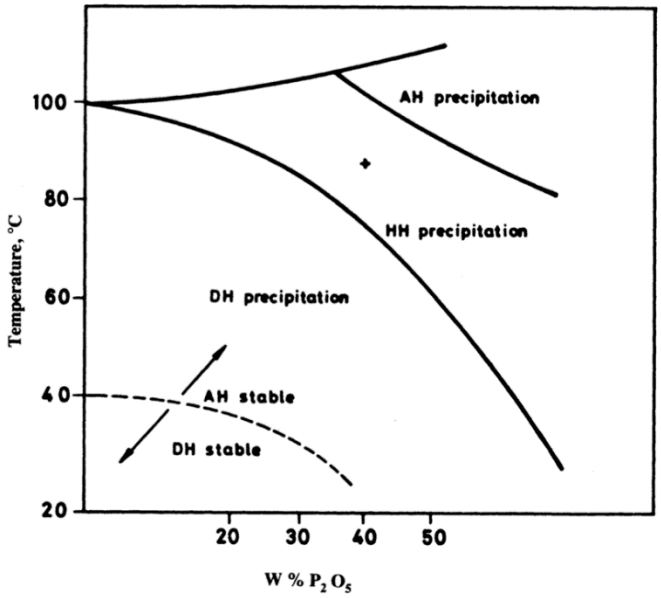

Figure 2.6 Areas represent dihydrate (DH), hemihydrate (HH), and anhydrate (AH) forms of gypsum. determined by the temperature and the P_2O_5 concentration present in the phosphoric acid solution [52]

The tricalcium phosphate found in phosphate rock interacts with concentrated H_2SO_4, resulting in the production of phosphoric acid and an insoluble form of calcium sulfate salt. This reaction allows for the direct separation of phosphoric acid via filtration due to the insolubility of the calcium sulfate salt. The equation below showcases the overarching reaction involved in the production of phosphoric acid using H_2SO_4 as a reactant.[2]

$$CaF_2.3Ca_3(PO_4)_2 + 10\ H_2SO_4 + 20\ H_2O \rightarrow 10\ (CaSO_4.2H_2O) + 2\ HF + 6\ H_3PO_4$$

the dihydrate method can be applied to a broad spectrum of phosphate rocks, yielding a weak acid with a P_2O_5 concentration of 26–30%. This weak acid is then concentrated to 50–54% through evaporation in order to fulfill the requirements for fertilizer production.[53]

The di-hemihydrate process with two-stage filtration, also known as the Central Prayon process, is employed to produce approximately 50% of phosphoric acid, achieving a P_2O_5 efficiency of 98%. The reaction between tricalcium phosphate and H_2SO_4 is restricted by an insoluble layer of $CaSO_4$.[2] However, this can be mitigated through the recirculation of phosphoric acid, which enables the solubilization of the substance as monocalcium phosphate. This then turns into calcium sulfate after undergoing precipitation with sulfuric acid.[54]

2.2.3 Dry process

Phosphoric acid production through the thermal route is carried out in two stages. Initially, elemental phosphorus is extracted from phosphate rock. Subsequently, this elemental phosphorus is oxidized with air to produce P_2O_5, which is then hydrated to form phosphoric acid. The procedure involves combining ground phosphate rock with a slurry composed of water, clay, and various waste streams rich in phosphorus.[55, 56] This mixture is then heated to a temperature between 1450 °C and 1500 °C in an electric resistance furnace, this mixture is combined with cokes and gravel, resulting in the production of phosphorus. As depicted in the following reaction, this method yields gaseous phosphorus, carbon monoxide, and a liquid form of slag.

$$2\ Ca_3(PO_4)_2 + 6\ SiO_2 + 10\ C \rightarrow P_4 + 10\ CO + 6\ CaSiO_3$$

The second step in phosphoric acid production involves the oxidation of elemental phosphorus with air to produce P_2O_5. Subsequently, the generated P_2O_5 reacts with diluted phosphoric acid and the water present in the acid to produce phosphoric acid, as per the following reactions.

$$P_4 + 5\ O_2 \rightarrow 2\ P_2O_5$$

$$P_2O_5 + 3\ H_2O \rightarrow 2\ H_3PO_4$$

It's important to note that these reactions are exothermic, with the heat released being utilized for high-temperature steam generation.[2]

While thermal phosphoric acid is highly pure, its production is costly due to the considerable amount of energy required [57, 58]. Consequently, it is primarily produced for specific applications that necessitate exceptionally pure acid quality, such as metal surface treatment in the microelectronics industry and acidification of beverages.[57]

The OCP Group specializes in the extraction, processing, and commercialization of phosphate and its derived products.[59] Every year, over 23 million tonnes of minerals are extracted from the Moroccan underground, which holds three-quarters of the world's reserves.[60] Primarily used in fertilizer production, the phosphates come from deposits in Khouribga, Ben Guérir, Youssoufia, and Boukraa. Depending on the case, the ore undergoes one or several processing operations such as washing/flotation, drying, calcination, flotation, dry enrichment, and more.[61, 62]

Once processed, it is either exported or delivered to the chemical industries of the group in Jorf Lasfar or Safi to be transformed into marketable derived products: basic phosphoric acid, purified phosphoric acid, and solid fertilizers.[63]

2.3 Chlorination and carbochlorination processes

2.3.1 Applications of chlorination and carbochlorination

Chlorine is a highly reactive element that has been widely utilized by metallurgists for the extraction of valuable elements from their bearing materials. With the depletion of high-grade ores and primary sources, the treatment of leaner and more complex ores, as well as the recycling of secondary materials, has become necessary. Over the past two decades, researchers have focused their efforts on developing several chlorination techniques for the treatment of various raw materials and solid industrial wastes. Carbochlorination produces mainly metallic chlorides under dry conditions in the presence of a reducing agent. The carbochlorination reaction offers a notable advantage in terms of the low melting and boiling points of the resultant chlorides and the variation in their vapor pressures at different chlorination temperatures, which makes it an economical and efficient way compared to traditional extraction processes. [12, 13, 64]

For instance, Cl_2 was applied for non-ferrous metals extraction such as PbS, ZnS, FeS_2, and $CuFeS_2$ and the results showed interaction of these metals with Cl_2 even at ambient temperature. At around 300 °C, the Fe and sulfur chlorides produced were converted into vapor and separated, leaving behind concentrated valuable metal chlorides, e.g., $CuCl_2$, $PbCl_2$, and $ZnCl_2$, in the chlorination

residues. In addition, more than 95% of Cu in the ore was extracted at 300 ˚C as water-soluble $CuCl_2$.[65-67] Moreover, the next case study discussed enhancing lean chromite ores and/or concentrate. physically improving this material is physically challenging. To overcome this, chromite chlorination was conducted in the presence of a reducing agent, such as CO. The results show carbochlorination, i.e., Cl_2+CO, of mentioned materials results in iron extraction at temperatures around 550 ˚C.[68, 69] It was reported that performing the reaction under higher temperatures results in the complete extraction of chromite elements in the form of chlorides, i.e., $FeCl_3$, $CrCl_3$, $MgCl_2$ and $AlCl_3$. In addition, pure $MgCl_2$ can be collected by selective condensation of the gas phase. The third illustration demonstrates the selectivity of the chlorination process when oxygen is present. This approach was employed to selectively chlorinate specific elements within chromite in addition to magnesium oxide purification by selectively chlorinating and eliminating iron oxides.[69-71]

Many studies have been conducted on the chlorination and carbochlorination of ores and metal oxides using various gaseous chlorinating agents on a laboratory scale. Recent investigations have been devoted to the chlorination technique for the separation and extraction of valuable metals from raw and residual materials, including the recovery of tantalum (Ta), cobalt (Co), nickel (Ni), molybdenum (Mo), and vanadium (V) from their bearing materials. Other studies have explored the reactivity and kinetics of the interaction of chlorine with several rare earth element oxides. Moreover, a low-temperature treatment of copper concentrate has been identified as an effective method, and decontamination of various non-ferrous residues is possible through chlorination.

These findings highlight the significant potential of chlorination processes in various applications. [12, 72-77] Figure 2.7 provides a visual representation of the experimental setup employed for the carbochlorination experiment to convert cerium and neodymium oxides into their chlorides. [78]

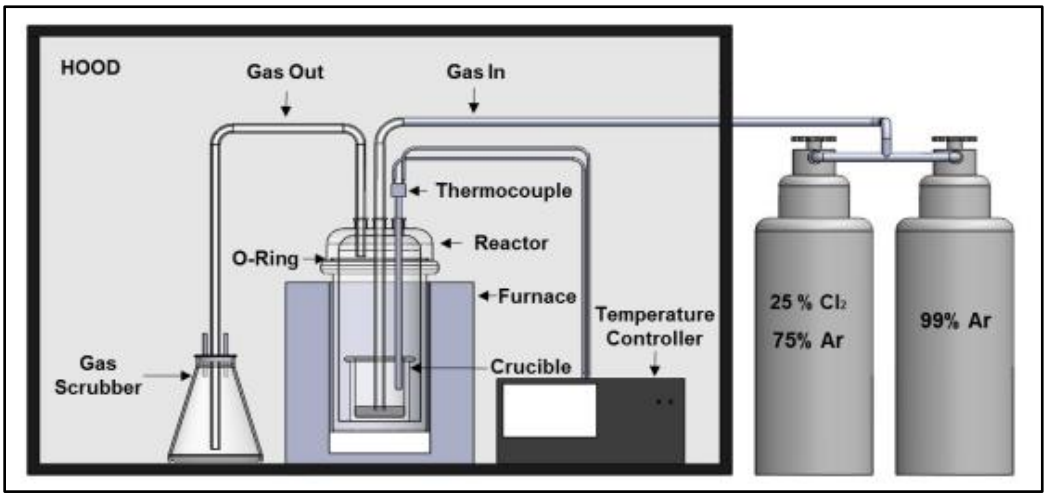

Figure 2.7 Schematic diagram of the experimental setup for the carbochlorination experiment [78]

2.3.2 Chlorination and carbochlorination kinetics

For the kinetic study of carbochlorination, TGA analysis was applied. Therefore, the extracted results were studied by employing a proper mathematical approach for the estimation of activation energy and reaction mechanism.

The particle shape effect was considered in mathematical models as presented in the following equations (2.1 to 2.7). These mathematical equations are valid when the overall reaction rate if affected by the rate-controlling step, i.e., the slowest step.[79]

$$1-(1-X)^{\frac{1}{F_p}}=kt \tag{2.1}$$

$$X=kt\ for\ F_p=1 \tag{2.2}$$

$$1-(1-X)^{\frac{1}{2}}=kt\ for\ F_p=2 \tag{2.3}$$

$$1-(1-X)^{\frac{1}{3}}=kt\ for\ F_p=3 \tag{2.4}$$

$$X^2=kt\ for\ F_p=1 \tag{2.5}$$

$$X+(1-X)Ln(1-X)=kt\ for\ F_p=2 \tag{2.6}$$

$$1 - 3(1 - X)^{\frac{1}{3}} + 2(1 - X) = kt \; for \; F_p = 3 \quad (2.7)$$

where k is reaction constant, t is reaction time, X is the extent of reaction, i.e., the ratio of the weight of the reacted fraction to initial weight, F_p is particle shape factor, i.e.,1, 2, and 3 for infinite slabs, long cylinders, and for spheres.

For the calculation of gas-solid reaction activation energy, by employing TGA with a linear temperature program the following Equation (2.8) can be applied.

$$\frac{dX}{dt} = kf_1(p_A)f_2(X)f_3(d) \quad (2.8)$$

In this context, X represents the extent of the reaction, p_A stands for the partial pressure of the reactive gas(es), and d indicates the average particle size. The impact of the partial pressure of the reactive gases, reaction extent, and particle size on the reaction rate is represented by functions $f_1(pA)$, $f_2(X)$, and $f_3(d)$ respectively. Additionally, the temperature's influence on the reaction rate is governed by the Arrhenius law, given by Equation (2.9), where in the rate constant k is utilized.

$$k = k_0 exp(-E_a/RT) \quad (2.9)$$

2.3.3 Chlorination and carbochlorination thermodynamics

The phase stability diagrams display regions of stability for condensed phases within a ternary system while maintaining isothermal conditions and considering the other constraints along the remaining axis. These diagrams serve as a rapid means to estimate the predominant phases. It is assumed that all phases are composed of pure substances, and the diagrams do not consider mixed phases in their basic form. Furthermore, phase diagrams are valuable tools for comprehending intricate solid-state phase transformations in systems with multiple components, such as determining optimal conditions for chlorination reactions.[80-82]

The phase stability diagrams are constructed based on a set of reactions involving the condensed phases and their likelihood to take place, considering their ΔG (Gibbs free energy change) at 400 °C, while also considering different partial pressures of chlorine and oxygen. [81, 83] This specific temperature was selected due to various studies indicating that several chlorination reactions involving rare earth elements (LREE), transition metals like zirconium and iron oxides, and other

uncommon metal oxides can occur at this temperature. Figure 2.8 illustrates one example of phase stability diagram for ternary Ln−O−Cl system.

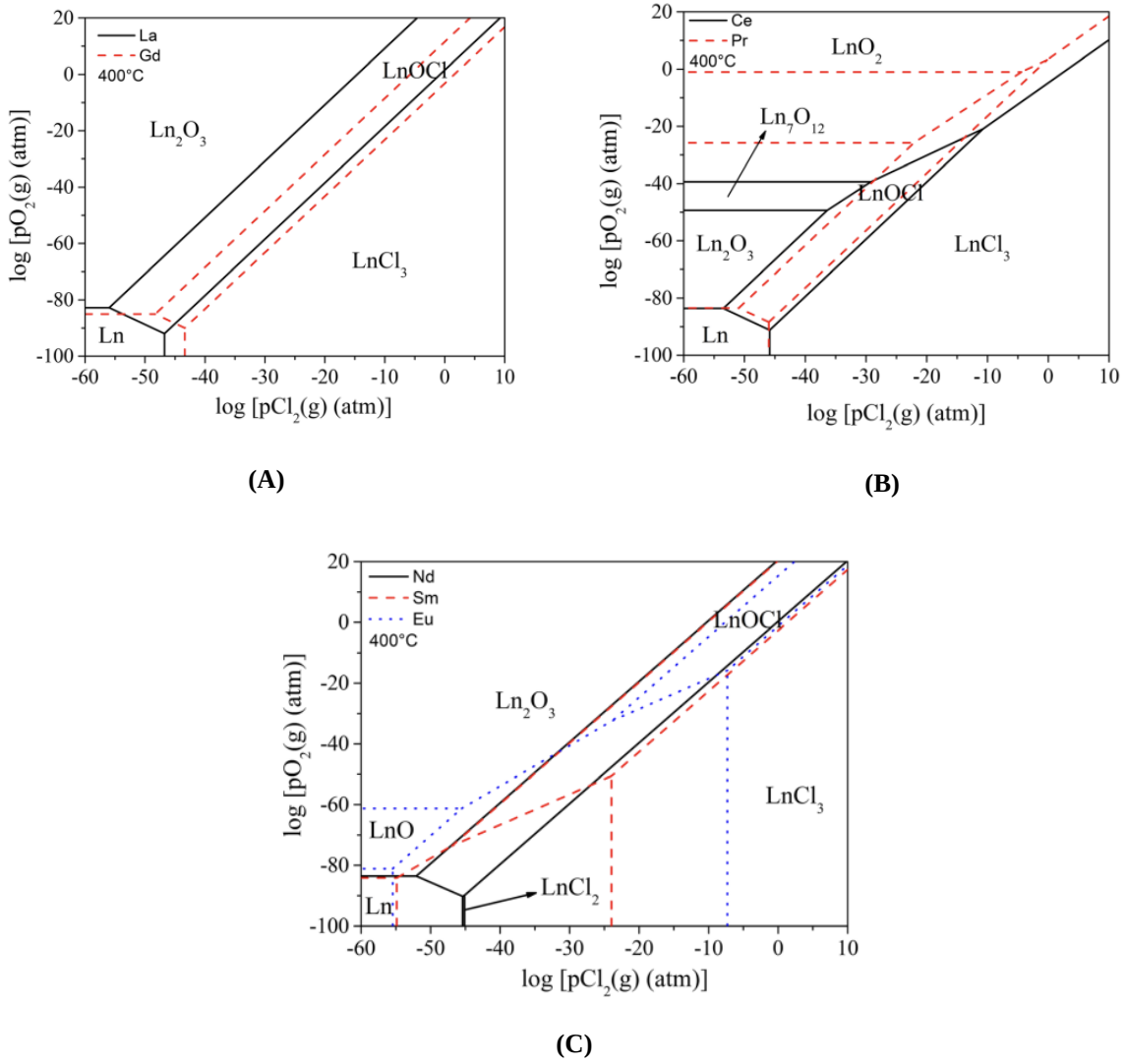

Figure 2.8 Phase stability diagram for ternary Ln−O−Cl systems (A) Ln: La, Gd at 400 °C, (B) Ln: Ce, Pr at 400 °C, and (C) Ln: Nd, Sm, Eu at 400 °C [82]

CHAPTER 3 OBJECTIVES

The main scope of this project is to valorize the low-grade phosphate fine wastes by extracting phosphorus in the form of chlorinated compounds by the carbochlorination route. More precisely, as the application of this process on the phosphate ore is new, this project focuses to prove the technical and economic viability of the carbochlorination process.

This study focused on examining the feasibility of carbochlorination, with particular attention given to the following three sub-objectives:

1) Conduct in-depth thermodynamic analysis of the carbochlorination reactions using FactSage software. (CHAPTER 5)
2) Evaluate, experimentally the process feasibility (proof of concept) and establish the reaction mechanism (CHAPTER6)
3) Perform an Aspen simulation, followed by a techno-economic evaluation. (CHAPTER7)

CHAPTER 4 MATERIAL AND METHODOLOGY

In this chapter, an overview is presented of the materials utilized in the study, including details about the sampling procedure. Additionally, an exploration is conducted into the various analytical characterizations carried out on the materials, the description of the experimental setup, and the utilization of FactSage software, along with the protocols applied for simulation.

4.1 Materials

4.1.1 Phosphate ore

In the present study, two types of ore were used as a feed, a low and a high-grade phosphate ore given by the Office Chérifien des Phosphates (OCP) in Morocco. Based on the mineralogical analysis utilizing QEMSCAN, the low-grade phosphate ore, which is basically a fine phosphate tailing, consists of four primary mineral groups: carbonates, silicates, oxides, and phosphates. The apatite-based minerals, predominantly carbonate-fluorapatite, constitute approximately 65% of the ore composition, while the remaining 35% comprises gangue minerals, mainly carbonates like calcite and dolomite, as well as quartz, feldspar, and other silicates. The size of this fine waste ore is generally below 45 µm. The mineralogy obtained by QEMSCAN is given in Figure 4.1.

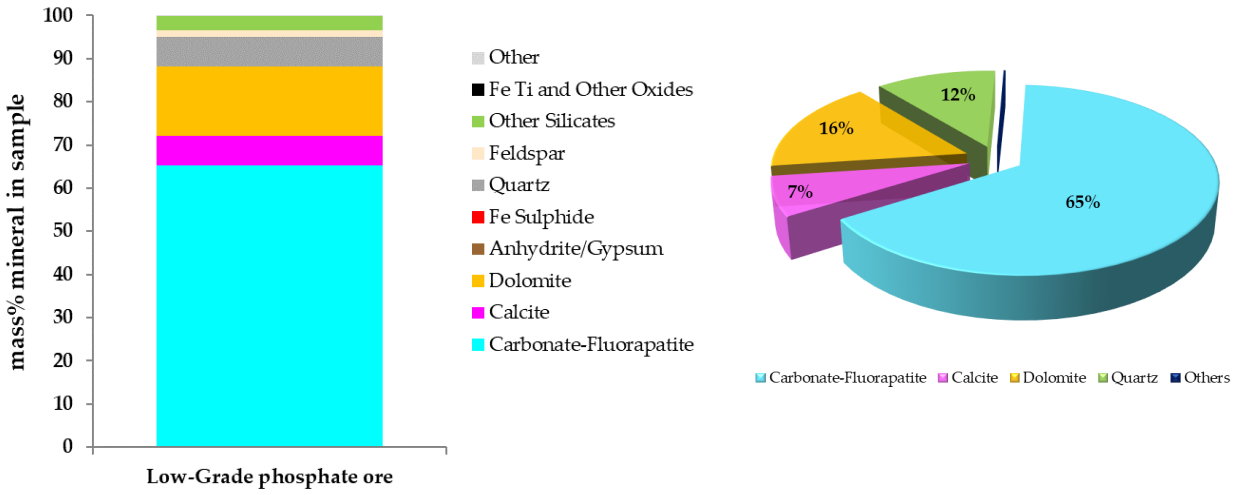

Figure 4.1 Low-grade phosphate ore mineralogy analyzed by QEMSCAN

On the other hand, the high-grade phosphate exhibits a broader particle size distribution, extending beyond 500 µm. The mineralogical analysis, presented in Figure 4.2, demonstrates that the

predominant mineral phase is carbonate-fluorapatite (> 95% for particles larger than 45 µm), while minor constituents primarily comprise calcite, dolomite, and silicates.

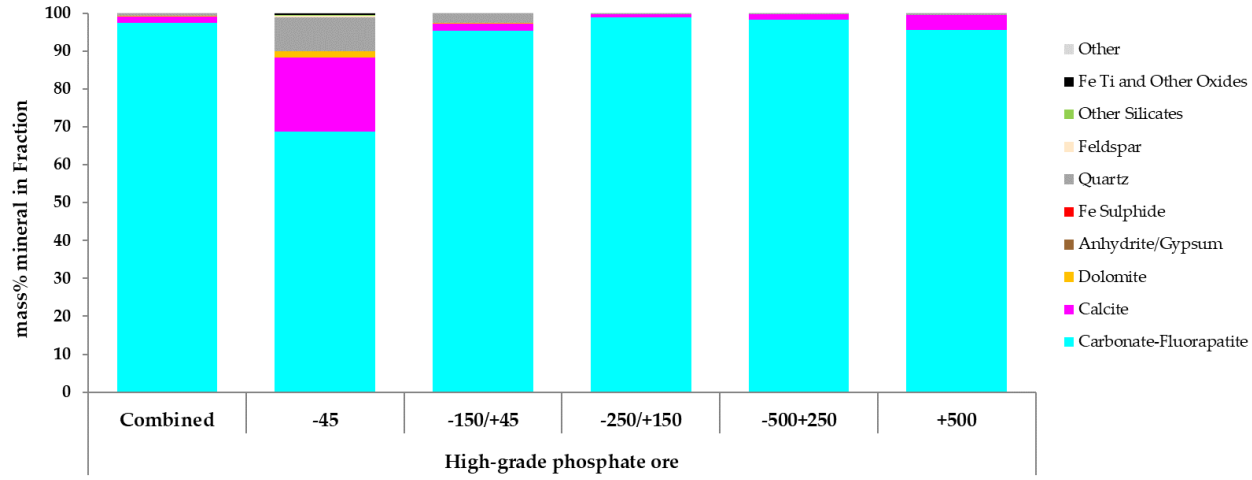

Figure 4.2 High-grade phosphate ore mineralogy analyzed by QEMSCAN

The ore samples provided for experimentation are received in the form of substantial 20 kg batches. In order to ensure uniformity in characteristics, it is essential to reduce these large samples to an appropriate representative size prior to conducting any experiments or testing. To achieve this, the following preparatory steps were carried out in accordance with the guidelines outlined in ASTM C702. Initially, a 5 kg portion of the ore was meticulously mixed to homogenize the sample and facilitate subsequent separation techniques. Subsequently, the coning and quartering method was employed to progressively reduce the sample quantity to approximately 1 kg. Further refinement was accomplished using the riffle splitter method, which reduced the mass to 50 grams, meeting the required size for experimentation. To ensure an adequately dried sample, any residual moisture was eliminated by subjecting the ore sample to a drying cycle in a furnace set at a temperature of 90-100 ℃ for approximately 24 hours. This crucial step guarantees the complete removal of free water, thus enabling a reliable and consistent analysis. For a particular particle size range, a sieve shaker was used to achieve it.

4.1.2 Chemicals

Activated charcoal has been deliberately selected as the carbon-bearing substance for carbochlorination in the phosphate ore study. High purity activated charcoal, acquired from Sigma Aldrich, serves as the ideal reducing agent for this experimental investigation.

To generate the required chlorine gas on a laboratory scale, Trichloroisocyanuric acid (TCCA) and hydrochloric acid (HCl 37%), both procured from Sigma Aldrich, are employed as essential reactants. In the process, it is imperative to ensure the dryness of the input chlorine gas. This is achieved through the utilization of sulfuric acid (H_2SO_4 98%) sourced from Thermo fisher scientific, which efficiently acts as a drying agent. Additionally, sodium hydroxide pellets were procured from Sigma Aldrich to prepare a basic solution to neutralize the exhaust chlorine gas.

4.2 Thermodynamic study of the phosphate ore's carbochlorination

FactSage, a thermodynamic software developed at Polytechnique Montreal, was used to perform a preliminary thermodynamic study to verify the feasibility of the carbochlorination process of the phosphate ore. In this regard, several solid and gas chlorination agents, i.e., chlorine gas (Cl_2), magnesium chloride ($MgCl_2$), calcium chloride ($CaCl_2$), zinc chloride ($ZnCl_2$), ammonium chloride (NH_4Cl), sodium chloride (NaCl) and carbon tetrachloride (CCl_4), were simulated. This study was performed using the FactPS (pure substances) and FToxid (stoichiometric metal oxides) databases. Initially, the "Reaction module" within the FactSage software was utilized to compute variations in extensive thermodynamic properties (H, G, V, S, Cp, A) for the carbochlorination reactions involving fluorapatite ($Ca_5(PO_4)_3F$) and the specified reagents. Specifically, the calculation of the standard free energy ($\Delta G°$) was performed to ascertain the spontaneity of the reaction, where a negative $\Delta G°$ indicates a spontaneous process. This approach enabled a thorough investigation into the spontaneity of the carbochlorination reaction of fluorapatite when subjected to various chlorination agents outlined in the study.

After selecting the most appropriate reagents (spontaneous reaction) and in order to define the range of temperature and reactant concentrations to maximize phosphorus trichloride ($POCl_3$) production, the phase diagram with each reactant was plotted by using the "Phase Diagram" module in FactSage. This thermodynamic module calculates, plots, and edits systems, i.e., unary, binary or tertiary, for several combinations of T, P, V, composition, activity, chemical potential,

etc. Herein we were interested in the effect of temperature and reactants concentration on the products and phases that are produced to allow a better understanding of the system's reactions.

Finally, and based on the results from the phase diagram module, the "Equilib" module was used to determine the optimum reactions parameters, i.e., phosphate ore, chlorination agent, and reducing age ratios, to maximize apatite's conversion and phosphorus oxychloride's production.

Although the first study focused on fluorapatite as the mineral of interest, the phosphate ore also contains gangue minerals, mainly dolomite ($CaMg(CO_3)_2$), calcite ($CaCO_3$), and silicate (SiO_2), see Figure 4.1. Thus, following the same procedure, thermodynamics of the carbochlorination reaction of these minerals were also studied under the same conditions to predict the main products and phases resulting from the reaction.

4.3 Experimental setup

4.3.1 Setup implementation and description

A fundamental step to obtain the desired purposes is assembling the experimental setup and making it operational. Since the use of chlorine gas cylinders is restricted at the Polytechnique laboratory, a lab-scale chlorine gas generator was prepared. Figure 4.3 shows a schematic representation of the chlorine gas generator.

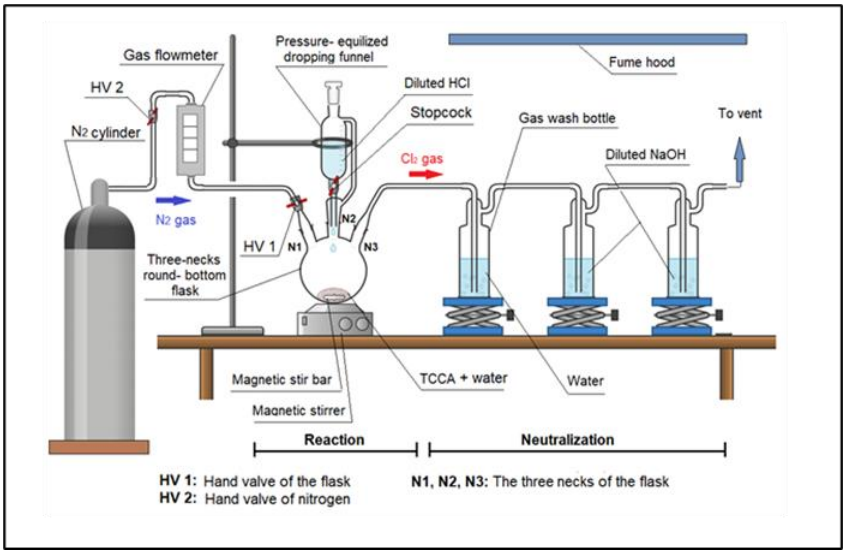

Figure 4.3 Schematic of the chlorine gas generator setup

The chlorine gas (Cl_2) was generated by reacting the trichloroisocyanuric acid $C_3N_3O_3Cl_3$ (TCCA) with concentrated hydrochloric acid (HCl), this reaction allows for a controlled and safe flow of chlorine gas. The reaction is driven essentially by entropy, and it simply proceeds at room temperature without heat. Besides the ease of operation, this reaction is quantitative, so the addition of a calculated amount of chlorine is easy to implement.

The carbochlorination experiments were carried out inside fume-hood to ensure the safe handling of any harmful off-gases. A schematic and a real picture of the experimental setup are illustrated in Figure 4.4 and Figure 4.5.

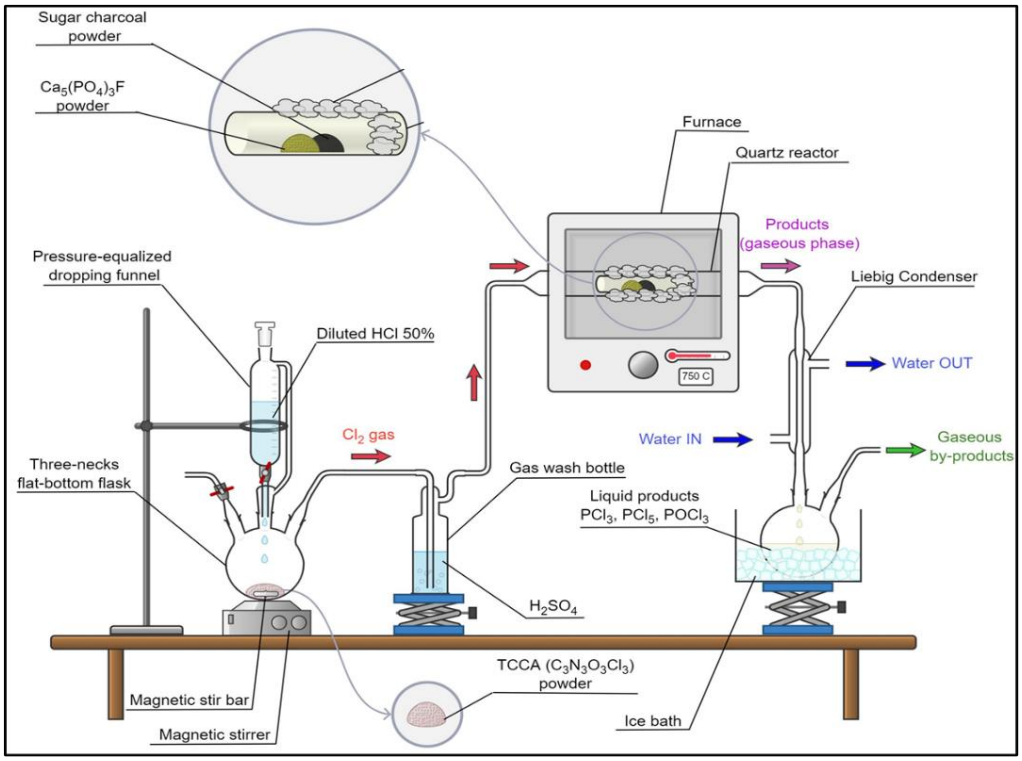

Figure 4.4 Schematic of the carbochlorination experimental setup

The outlet of the quartz reactor was connected to a two-necks receiver flask (collector) immersed in an ice-water bath so that phosphorus chlorinated product condensate downward. The non-condensable gases, including mainly CO_2, CO, and unreacted Cl_2, left the receiver flask through the second neck. These gaseous were routed and bubbled through two consecutive washing bottles containing a caustic soda scrubbing solution to neutralize any excess chlorine gas and any other by-product gases. The remaining non-condensable gases were sent to the fume hood vent.

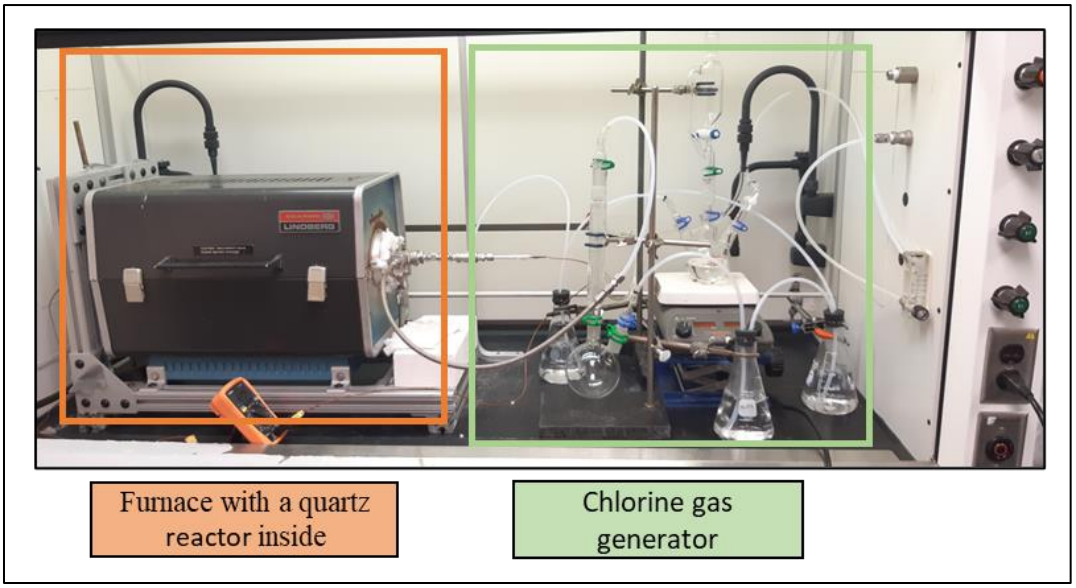

Figure 4.5 Lab-scale carbochlorination experimental setup

4.3.2 Experimental procedure

In this project, the same sample preparation was used for each carbochlorination experiment while varying process parameters. Prior to each test, the phosphate ore and carbon were weighed, mixed, and placed at the bottom of the quartz tube reactor. Then, the reactor was tightly sealed to the stainless-steel body and purged with a continuous nitrogen flow introduced at a constant rate of 2 ml/min for 10 to 20 minutes. This purge was to ensure an oxygen-free environment.

Once the furnace reached the desired temperature, the quartz reactor was inserted inside the furnace while keeping the nitrogen flow. Then, the reactor was heated until attaining the targeted temperature. Once the temperature was attained, the flow of nitrogen was adjusted, and the chlorine gas was introduced at a flow rate adjusted for each test. The chlorine gas generator was monitored throughout the test by adjusting the hydrochloric acid rate regularly through the stopcock of the pressure-equalized dropping funnel.

When the test was complete, after the total consumption of TCCA, the reactor was cooled down and purged with nitrogen. The quartz reactor was then removed from the furnace and the sample was retrieved, weighed, and stored for ICP and XRF analysis.

4.4 Characterization techniques

4.4.1 ICP-OES

Inductively Coupled Plasma Optical Emission Spectrometry (ICP-OES) is a potential analytical method employed to determine the elemental composition of samples. It achieves this using an inductively coupled plasma to atomize and excite the elements, subsequently measuring the emitted light for accurate quantification. An Agilent 5100 SVDV ICP-OES model was used to determine the elemental concentration of our sample before and after treatment.

This method requires liquid samples for accurate elemental analysis. For the preparation step before analysis, the solid sample was prepared by acid digestion. This digestion consists of digesting 1 g of sample with concentrated nitic acid (HNO_3) and hydrogen peroxide (H_2O_2) under a high temperature of 100 ºC for 2 hours. Then, the digested sample is filtered and diluted before sending to the ICP for analysis.

4.4.2 LECO

The LECO is an analytical method applied to determine the elemental concentration of carbon. This technique operates by combusting a sample at 1000 ºC, creating an oxidizing atmosphere that converts carbon and sulfur into carbon dioxide and sulfur dioxide, respectively. The resulting gases are then analyzed using an infrared detector, which generates a signal proportional to their concentration. This study employed LECO to determine the carbon concentration present in the samples before and after carbochlorination treatment. Prior to chemical analysis with the LECO, the phosphate ore underwent furnace drying at 150 ºC for 24 hours to eliminate any moisture content. By validating the collected carbon content data, it was possible to accurately determine the mass balance of our system and understand carbon's contribution to the carbochlorination reaction.

4.4.3 QEMSCAN

QEMSCAN, or Quantitative Evaluation of Materials by Scanning Electron Microscopy, is an advanced analytical technique that utilizes Scanning Electron Microscopy-Energy Dispersive X-ray Spectroscopy (SEM-EDS) and specialized software to characterize the mineral composition of a sample. By capturing high-resolution images and elemental data, QEMSCAN enables detailed analysis of mineral grain size, liberation, and associations within the sample. QEMSCAN was

applied in this study to the phosphate ore samples before treatment to gain insights into the mineral grain and liberation size, as well as to study the mineral associations within individual particles.

4.4.4 SEM-EDS

Scanning Electron Microscopy (SEM) coupled with Energy Dispersive X-ray Spectroscopy (EDS) is a powerful imaging and elemental analysis technique. SEM generates high-resolution images of the sample's surface, while EDS identifies and quantifies the elements present based on the characteristic X-rays emitted when the sample is bombarded with an electron beam. In this study, SEM-EDS was employed to examine the morphology and elemental composition of the samples, both before and after the carbochlorination treatment of the phosphate ore.

4.4.5 XRD

X-ray Diffraction (XRD) is a non-destructive analytical method used to study the crystallographic structure and mineral phases of materials. When X-rays are directed at a sample, they diffract off the atomic lattice, producing distinctive diffraction patterns. These patterns serve as a fingerprint for the crystal structure of the minerals present in the sample. By comparing the observed diffraction peaks with a database of known mineral patterns, XRD can precisely identify the minerals and their relative abundances in the analyzed material. XRD is a widely employed technique in geology, material science, and many other scientific fields for mineral identification and crystallographic studies.

CHAPTER 5 THERMODYNAMIC ANALYSIS

The thermodynamic calculations were performed using the reaction module database on the software to test different combinations of chlorination and carbochlorination reactions of fluorapatite at various conditions. As the carbonate-fluorapatite $Ca_5(PO_4, CO_3)_3F$ was not included in the database of FactSage v. 8.2, the thermodynamic analysis was performed on fluorapatite $Ca_5(PO_4)_3F$. In addition, the possible reactions suggested are under a nitrogen atmosphere (as inert and balance gas) and involve the formation of phosphorus oxychloride $POCl_3$ and phosphorus trichloride PCl_3 as the main desired products.

The most widely used reducing agents in chemical reactions are carbon (C) and carbon monoxide (CO). Carbon serves dual roles in the reaction process. Firstly, from a thermodynamic perspective, carbon creates a low oxygen potential atmosphere, reducing the likelihood of oxide formation and promoting chloride formation [84]. Secondly, from a kinetic standpoint, carbon is believed to facilitate the creation of reaction intermediates, leading to higher levels of reaction advancement at a given time and an overall increase in the reaction rate [84, 85]. The literature suggests that in chlorination reactions, the use of carbon as a reducing agent enhanced the kinetic of the carbochlorination reaction of calcium pyrophosphate better than CO. [86] The observed phenomenon can be attributed to the formation of calcium chloride during the reaction, which, at higher temperatures, undergoes melting, resulting in the development of a compact layer on the solid substrate. This layer, in turn, hinders effective contact between the gaseous carbon monoxide CO and the solid utilized. Moreover, the solid carbon can disperse the formed calcium chloride salt, thereby creating free pathways for chlorine gas diffusion and facilitating access to the reaction zone. [86] Herein, carbon as a reducing agent, and several chlorine salts, i.e., $MgCl_2$, $CaCl_2$, $ZnCl_2$, NaCl, NH_4Cl, and CCl_4, and chlorine, Cl_2, were evaluated in this thermodynamic study.

To execute the plan, we evaluated the free Gibbs energy changes ($\Delta G°$) as a function of the temperature, ranging from 100 to 1200 °C, for the overall chlorination and carbochlorination reactions listed below (R1 to R13). Figures 5.1 and 5.2 present the relationship between the standard Gibbs free energy and temperature for the chlorination and carbochlorination equations.

$2\ Ca_5(PO_4)_3F + 18\ Cl_2 \rightarrow 9\ CaCl_2 + CaF_2 + 6\ POCl_3 + 9\ O_2$ (R1)

$2\ Ca_5(PO_4)_3F + 18\ Cl_2 + 9\ C \rightarrow 9\ CaCl_2 + CaF_2 + 6\ POCl_3 + 9\ CO_2$ (R2)

$2\ Ca_5(PO_4)_3F + 18\ Cl_2 \rightarrow 9\ CaCl_2 + CaF_2 + 6\ PCl_3 + 12\ O_2$ (R3)

$2\ Ca_5(PO_4)_3F + 18\ Cl_2 + 9\ C \rightarrow 9\ CaCl_2 + CaF_2 + 6\ PCl_3 + 12\ CO_2$ (R4)

$2\ Ca_5(PO_4)_3F + 18\ MgCl_2 \rightarrow 9\ CaCl_2 + CaF_2 + 6\ POCl_3 + 9\ O_2 + 18\ Mg$ (R5)

$2\ Ca_5(PO_4)_3F + 18\ MgCl_2 + 9\ C \rightarrow 9\ CaCl_2 + CaF_2 + 6\ POCl_3 + 9\ CO_2 + 18\ Mg$ (R6)

$2\ Ca_5(PO_4)_3F + 18\ CaCl_2 \rightarrow 9\ CaCl_2 + CaF_2 + 6\ POCl_3 + 9\ O_2 + 18\ Ca$ (R7)

$2\ Ca_5(PO_4)_3F + 18\ CaCl_2 + 9\ C \rightarrow 9\ CaCl_2 + CaF_2 + 6\ POCl_3 + 9\ CO_2 + 18\ Ca$ (R8)

$2\ Ca_5(PO_4)_3F + 18\ ZnCl_2 \rightarrow 9\ CaCl_2 + CaF_2 + 6\ POCl_3 + 9\ O_2 + 18\ Zn$ (R9)

$2\ Ca_5(PO_4)_3F + 18\ ZnCl_2 + 9\ C \rightarrow 9\ CaCl_2 + CaF_2 + 6\ POCl_3 + 9\ CO_2 + 18\ Zn$ (R10)

$2\ Ca_5(PO_4)_3F + 36\ NaCl \rightarrow 9\ CaCl_2 + CaF_2 + 6\ POCl_3 + 9\ O_2 + 36\ Na$ (R11)

$2\ Ca_5(PO_4)_3F + 36\ NaCl + 9\ C \rightarrow 9\ CaCl_2 + CaF_2 + 6\ POCl_3 + 9\ CO_2 + 36\ Na$ (R12)

$2\ Ca_5(PO_4)_3F + 9\ CCl_4 \rightarrow 9\ CaCl_2 + CaF_2 + 6\ POCl_3 + 9\ CO_2$ (R13)

In fact, as per a positive $\Delta G°$ (> 100 kJ/ mol Cl_2), the chlorination route of $Ca_5(PO_4)_3F$ (without a reducing agent) is not feasible in the temperature interval of 100 - 1200 °C (Figure 5.1).

In the case of carbochlorination reactions, the reactions involving chlorine salts were also non-spontaneous (positive free Gibbs energy) (Figure 5.2). On the other hand, the carbochlorination reactions with Cl_2 and CCl_4 presented a negative $\Delta G°$ value for the same temperature, resulting in favorable and spontaneous reactions from a thermodynamic point of view. In summary, the thermodynamic data indicated that the fluorapatite could only react with chlorine gas and carbon tetrachloride in the presence of a reducing agent leading to the formation of the phosphorus-chlorinated compounds.

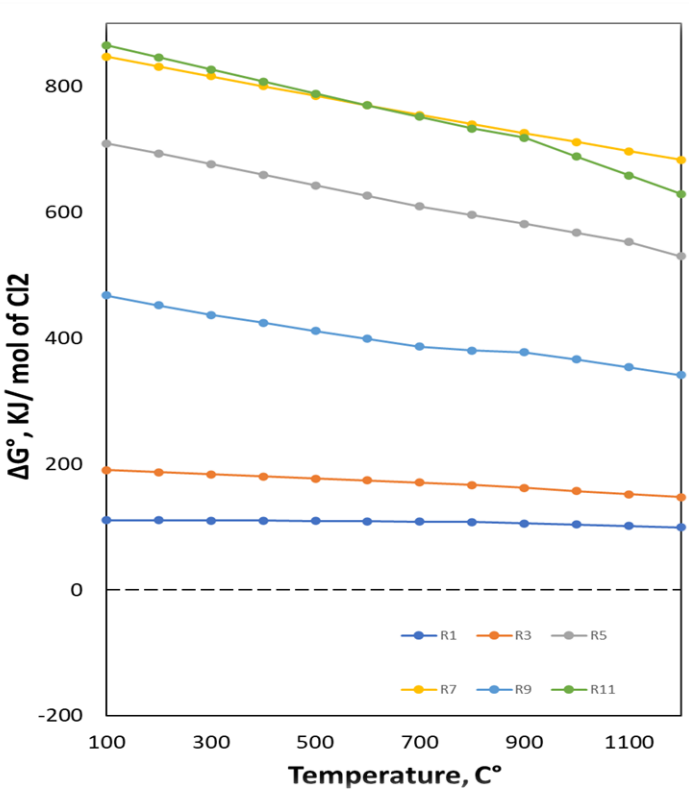

Figure 5.1 Standard free energy change of the chlorination reactions

Between both reactions, carbon tetrachloride (CCl_4) was optimal as it plays the role of chlorination and reducing agent at the same time. However, this chemical is an ozone-depleting substance that is banned from usage under the Montreal Protocol on Substances that Deplete the Ozone Layer. The regulation of CCl_4 in the Montreal Protocol suggests that, presently, emissions should be zero. Therefore, the use of CCl_4 was neglected for the rest of the project and thermodynamic studies and experimental trials proceeded using a combination of Cl_2 and C.

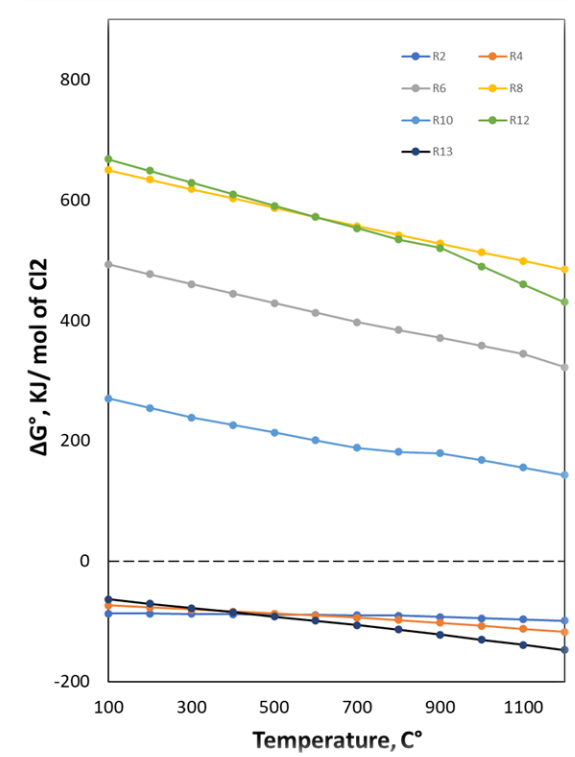

Figure 5.2 Standard free energy change of the carbochlorination reactions

To facilitate predicting the optimal operating conditions and predominant phases, FactSage‘s module “Predom” was employed, plotting the isothermal predominance area diagrams for the system: P-O-Cl at various temperatures. Figure 5.3 illustrates the evolution of the phase stability area of the P-O-Cl system as a function of the partial pressure of oxygen within the temperature range studied.

According to the studied conditions, phosphorus oxychloride ($POCl_3$) was stable for a high partial pressure of chlorine gas and a low oxygen potential. Moreover, it is noticeable that the predominance area of the $POCl_3$ is better extended at a lower temperature, particularly at 700 °C. However, decreasing the temperature below 500C delimits the $POCl_3$ predominance area again.

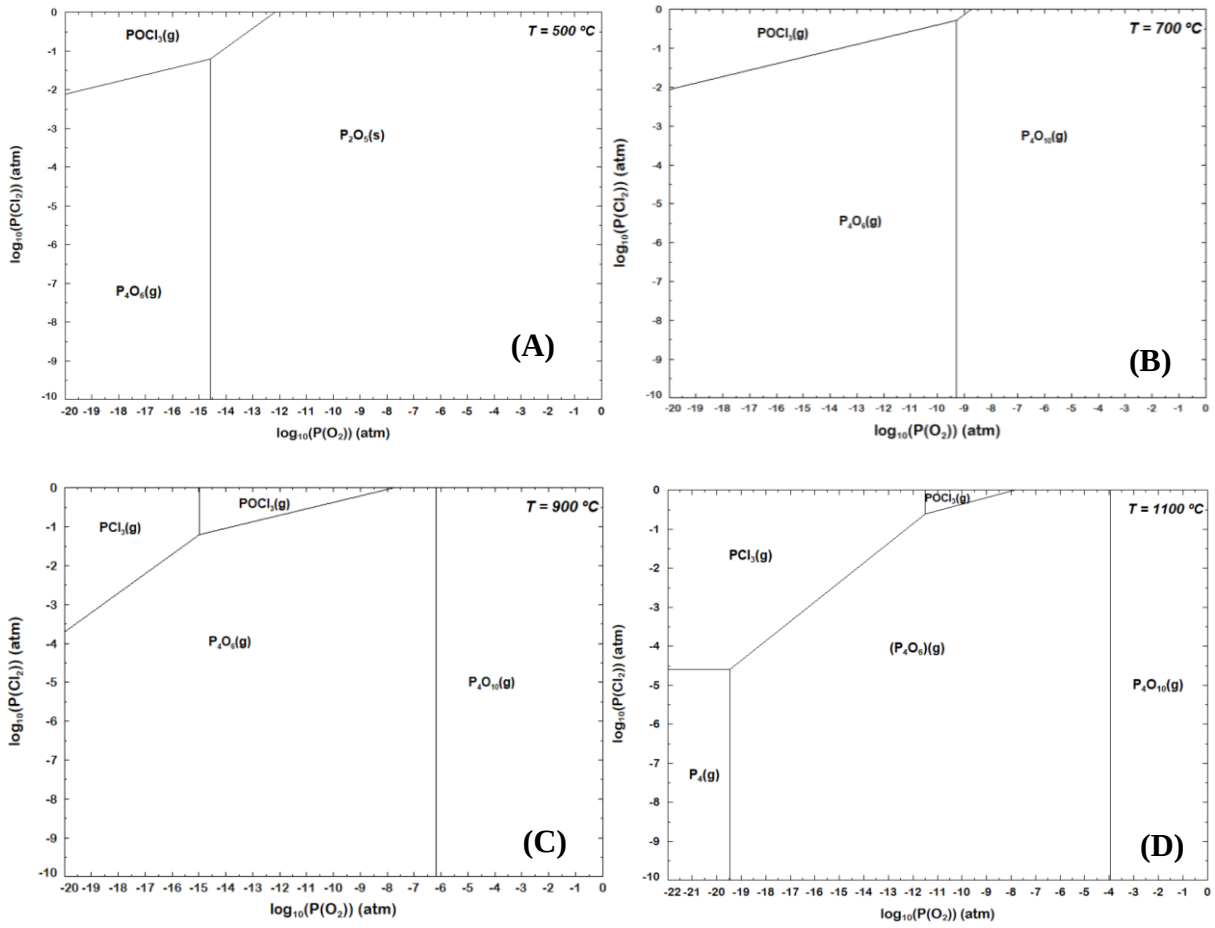

Figure 5.3. Evolution of the phase stability area of the P-O-Cl system as a function of oxygen partial pressure at (A) 500 ºC, (B) 700 ºC, (C) 900 ºC, and (D) 1100 ºC

Nevertheless, phosphorus trichloride (PCl_3) was the predominant product of the carbochlorination reaction at high temperatures, i.e., above 700 ºC, low oxygen partial pressure ($P_{O2} \leq 10^{-15}$ atm) and high chlorine partial pressure. For an oxygen partial pressure, e.g., higher than 10^{-9} atm above 700 ºC, phosphorus pentoxide (P_4O_{10}) is the only stable phase in the P-O-Cl.

The phase predominance diagrams were also studied as a function of temperature, and chlorine and oxygen partial pressures for the main gangue minerals, i.e., calcite and dolomite, and thus for the systems Ca-O-Cl and Mg-O-Cl. The diagrams in Figure 5.4 were established using the database on the phase diagram module on FactSage. According to the evolution of chlorine partial pressure in terms of temperature, the predominant phases in both systems at a high partial pressure of Cl_2, are calcium chloride $CaCl_2$ and magnesium chloride $MgCl_2$. However, a high oxygen partial pressure is more likely to induce the formation of calcium and magnesium oxides (CaO and MgO).

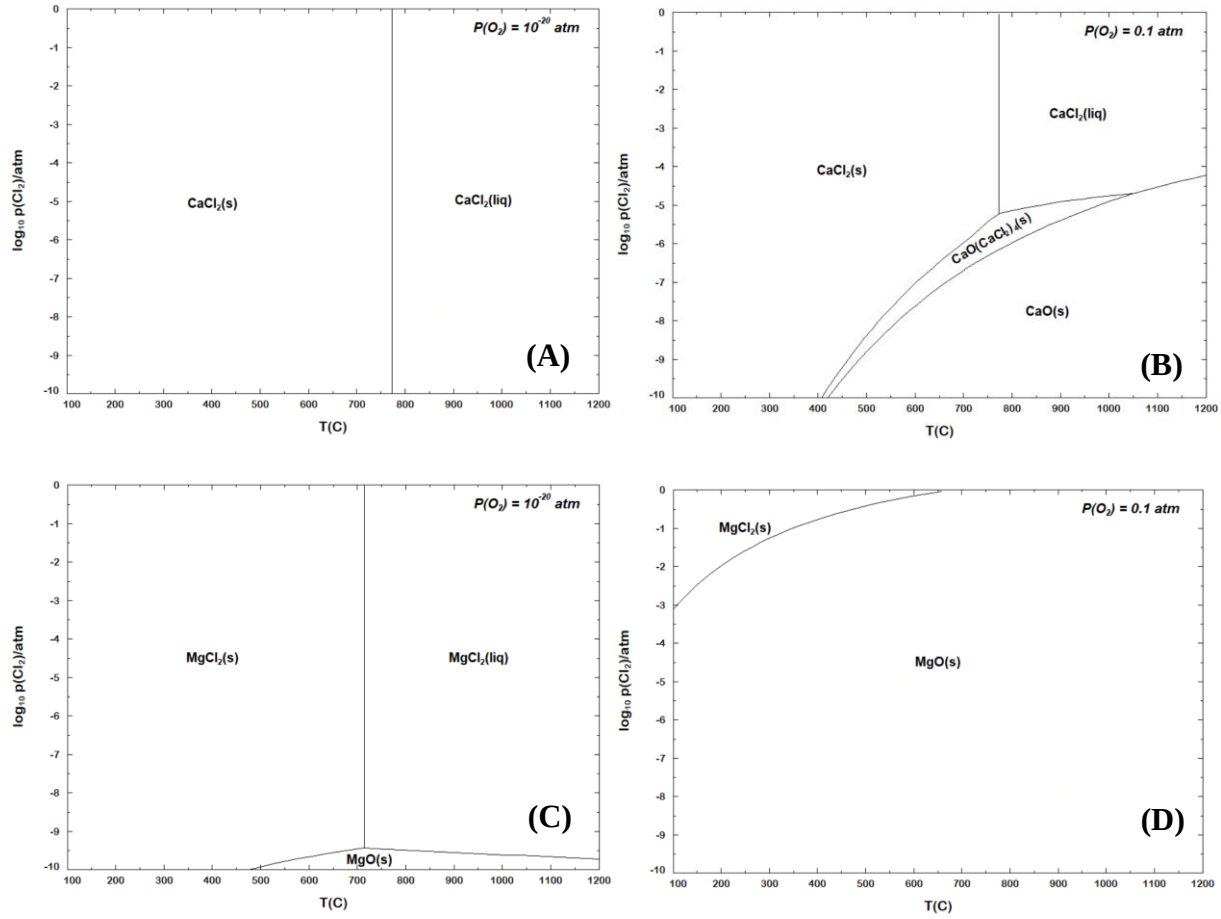

Figure 5.4 Evolution of the phase stability area as a function of temperature of (A) Ca-O-Cl system at P_{O2} = 10 $^{-20}$ atm, (B) Ca-O-Cl system at P_{O2} = 0.1 atm, (C) Mg-O-Cl system at P_{O2} = 10^{-20} atm, and (D) Mg-O-Cl system at P_{O2} = 0.1 atm

Furthermore, the phase diagram area shows the transition, herein melting of calcium and magnesium chloride at 772 ºC and 714 ºC, respectively. These temperatures were considered for the experimental work to avoid the formation of liquid calcium or magnesium chloride that would affect the carbochlorination process. According to the literature, the carbochlorination rate of phosphate ore may be affected by the physical properties of the synthesized products, like the melting point or volatilization. [86, 87] This is explained by the fact that this melted salt may cover the phosphate ore particles acting thus as a barrier for the diffusion of chlorine gas to the reaction zone. Similar phenomena have been reported previously for the carbochlorination of magnesium oxide. [87] For these reasons, it is recommended to work at temperatures lower than the melting

point of $MgCl_2$, below 714 ºC, to achieve an effective carbochlorination reaction and a higher phosphate conversion rate.

As given in Figure 5.2, the standard free energy change ΔG° of the carbochlorination reaction of fluorapatite is inversely proportional to the temperature. So, the higher the temperature, the lower is ΔG° and the more favorable is the reaction. For this reason, the following thermodynamic studies were performed at the highest possible temperature, considering the mentioned limit of 714 ºC. Hence, we set up a temperature of 700 ºC for the rest of the simulation. In addition, a nitrogen environment was assumed to reduce or minimize the oxygen partial pressure.

Following the predominant products diagram, the ternary phase diagram for the ore – Cl_2 – C mixture was studied to predict the different phases and intermediates formed according to the ratios of the three components at 700 ºC and 1 atm. Figure 5.5 illustrates the ternary diagrams for the carbochlorination reactions of the different minerals of the phosphate ore, i.e., fluorapatite, dolomite, calcite, and silicate, with Cl_2 and carbon. Herein, in the case of fluorapatite's carbochlorination reaction, several solid intermediates are formed, but more importantly, phosphorus is found in the gas phase from which the $POCl_3$. This product is mainly found in the zones highlighted in orange in fluorapatite's ternary diagram (Figure 5.5), where the apatite is completely converted, and all the phosphorus is found in the gas phase. This means that $POCl_3$ is formed for a high mole fraction of Cl_2 (over 0.5) and for carbon mole fraction ranging from 0.1 to 0.45. As fluorapatite decomposes and phosphorus evaporates in the form of chloride complexes, solid calcium chloride forms. When a low chlorine mole fraction (less than 0.5) or low carbon content (less than 0.3) are used, fluorapatite only dissociates into other solid form and most of the phosphorus remains in the solid phase ($Ca_3Mg_3(PO_4)_4$, $Ca_2Mg_2P_2O_{21}$, MgP_2O_6, $Ca_3P_2O_8$). Therefore, with this diagram, specific reagent concentration ranges should be considered in order to maximize the formation of phosphorous chloride compounds. The best range of condition concluded are as follow: maximum mole fraction of fluorapatite (0.1), minimum chlorine mole fraction (0.5), and carbon ranging from 0.1 to 0.45. The total decomposition of fluorapatite under these optimum conditions leads to the formation of calcium chloride as the main solid product. Regarding the other gaseous products formed, carbon dioxide CO_2 and monoxide CO were the major ones.

Figure 5.5-B shows that dolomite decomposes at this temperature to form mainly calcium chloride $CaCl_2$, Magnesium chloride $MgCl_2$ and magnesium oxide MgO as solid products, and carbon dioxide CO_2 and monoxide CO as gaseous products. The MgO formation is only observed for low carbon (<0.3) and chlorine (<0.5) content. According to figure 5.5-C, Calcite decomposed completely into $CaCl_2$ for high chlorine content (<0.5), independently of the carbon content. The released gases from this reaction are mainly CO and CO_2. Regarding the SiO_2, figure 5.5-D indicates the total decomposition of SiO_2 under high chlorine (>0.5) and Carbon (>0.2) content. In this case, the major gaseous products formed are $SiCl_4$, CO and CO_2.

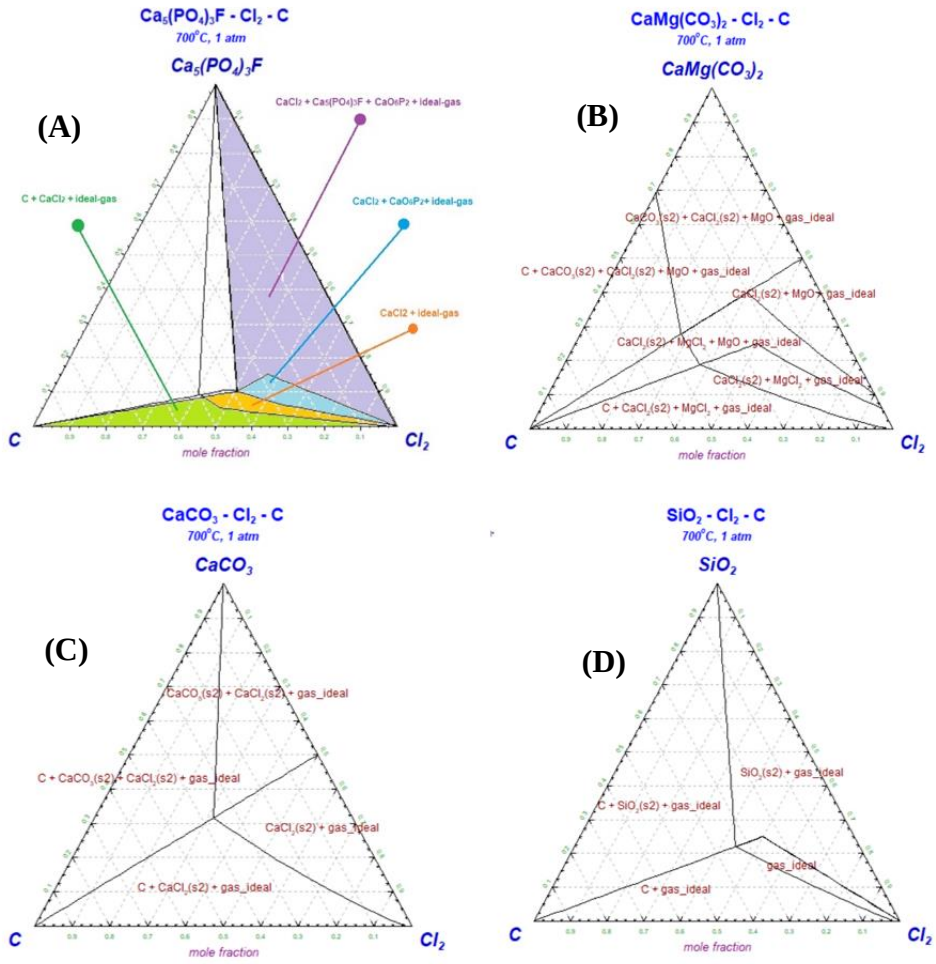

Figure 5.5 Ternary diagrams of the carbochlorination reactions with (A) Fluorapatite, (B) Dolomite, (C) Calcite, and (D) Quartz

With the potential products of the molar fractions of interest to achieve a full fluorapatite conversion and after balancing the reactions, the carbochlorination reactions of each mineral of the

phosphate ore including their respective standard free energy change ΔG° are listed below, where fluorapatite's reaction includes the formation of the main phosphorous gases, $POCl_3$, and POF_3. Herein, all the described reactions have a negative Gibbs energy and are thus spontaneous, indicating that all minerals from the phosphate ore are at the specified conditions.

$3\ Ca_5(PO_4)_3F + 27\ Cl_2 + 14\ C \rightarrow 15\ CaCl_2 + POF_3 + 8\ POCl_3 + 13\ CO_2 + CO$ C1

$\Delta G° = -92.6$ KJ/mol Cl_2

$0.75\ CaMg(CO_3)_2 + 1.5\ Cl_2 + C \rightarrow 0.75\ CaCl_2 + 0.75\ MgCl_2 + 2\ CO_2 + 0.5\ CO$ C2

$\Delta G° = -62.5$ KJ/mol Cl_2

$0.32\ CaCO_3 + 0.32\ Cl_2 + 1.28\ C \rightarrow 0.32\ CaCl_2 + 0.32\ CO_2 + 0.32\ CO$ C3

$\Delta G° = -160$ KJ/mol Cl_2

$0.55\ SiO_2 + 1.1\ Cl_2 + 1.1\ C \rightarrow 0.55\ SiCl_4 + 1.1\ CO$ C4

$\Delta G° = -68.7$ KJ/mol Cl_2

Subsequently, additional simulations were conducted using the equilib module on FactSage to ascertain the optimal composition of the ore, chlorine, and carbon mixture, leading to the highest yield of $POCl_3$. Figure 5.6 vividly depicts the variations in the mass of phosphorus-chlorinated compounds formed in relation to the amount of added reducing agent (carbon).

For the simulation, a 1 kg quantity of phosphate ore was considered, adhering to the ore composition of low-grade phosphate as depicted in Figure 4.1: 650 g of fluorapatite, 160 g of dolomite, 70 g of calcite, and 120 g of silicate. Concerning chlorine, the stoichiometric amount required was calculated, and an additional 10% excess was included to ensure complete reaction. The stoichiometric total number of moles of Cl_2 needed was determined from balanced equations, equating to 18 moles (1280 g). Hence, the mass of introduced chlorine in the simulation was approximately 1420 g. Figure 5.6 illustrates that the maximum production of $POCl_3$ occurred when the mass of carbon was 108.5 g, corresponding to roughly 10% w/w of the total solid reactant.

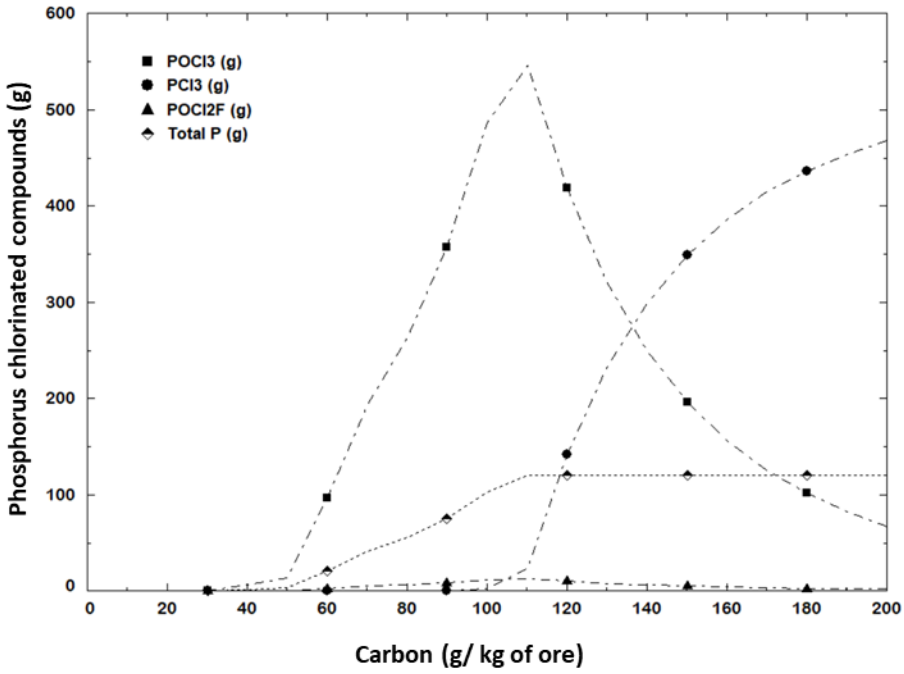

Figure 5.6 Mass of phosphorus-chlorinated compounds produced vs the mass of reacted carbon.

An excess of carbon results in the production of phosphorus trichloride, while the total amount of converted phosphorus (in the gas phase) remains unchanged. This implies that the excess carbon facilitates the reduction of phosphorus oxychloride into phosphorus trichloride. Additionally, a chlorinated phosphorus by-product, namely phosphoryl dichloride fluoride ($POCl_2F$), was detected in trace amounts.

Furthermore, Figure 5.7 displays the mass of elemental phosphorus formed in the gas phase, which reaches a peak of 120 g with 108.5 g of carbon. This mass signifies a complete conversion of phosphorus.

Moreover, the analysis also encompassed the evaluation of solid compounds (both intermediates and end products) concerning the mass of carbon, as depicted in Figure 5.7. The plot illustrates that the only solids remaining at the end of the reaction are $MgCl_2$ and $CaCl_2$. Their values remain constant beyond the optimum value of carbon (108.5 g), even when an excess of the reducing agent is introduced.

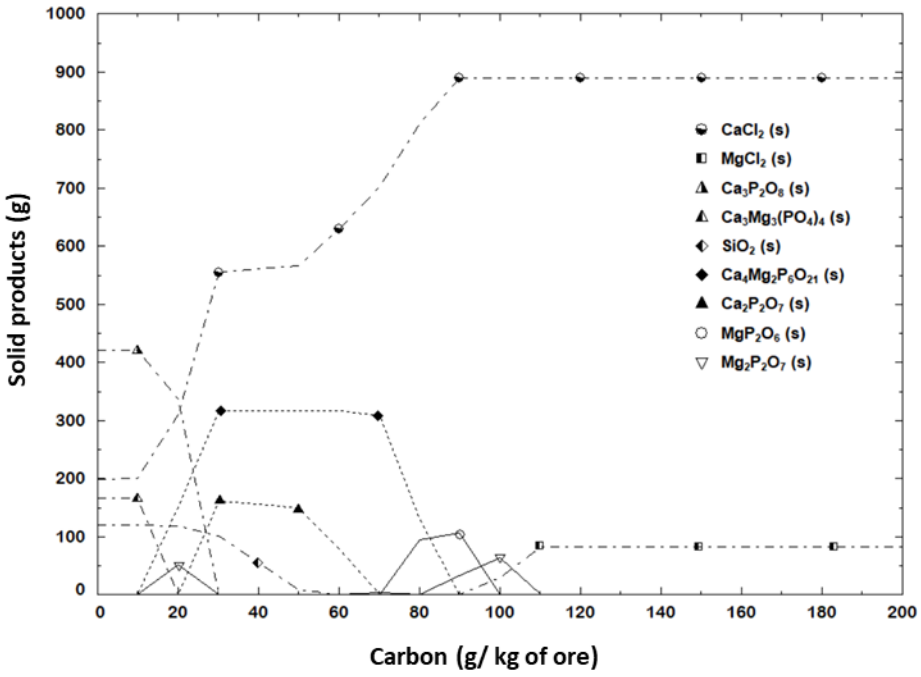

Figure 5.7 Mass of solid intermediates and products vs the mass of reacted carbon.

The graph clearly indicates that the phosphate ore undergoes several intermediate reactions before releasing the total phosphorus content. At 50 g of added carbon, complete conversion of quartz into $SiCl_4$ is observed. Moreover, the graph elucidates that in the absence of carbon at this temperature (700 °C), the phosphate ore mineral no longer exists in the form of fluorapatite, but instead transforms into $Ca_3P_2O_8$ and $Ca_3Mg_3(PO_4)_4$, which can be attributed to the calcination reaction.

CHAPTER 6 EXPERIMENTAL RESULTS

The experimental conditions (temperature, pressure, mole fractions) considered in the coming test were selected according to the thermodynamic analysis discussed in the previous chapter. The ranges of operational conditions are summarized in Table 6.1.

Table 6.1 General operational conditions for the carbochlorination experiments

Atmosphere	Nitrogen
Temperature range	600 °C to 750 °C
Reaction time	30 min to 7 hours
Phosphate Ore type	High and low-grade
Chlorine content	50% to 250 %Excess*
Carbon content	30% Excess*
**Excess is calculated according to the stoichiometric ratios*	

6.1 Carbochlorination reaction

The first carbochlorination tests were performed with high and low grade at 700 ºC in a 1.4 mm ID round-bottomed quartz reactor that was available in the laboratory and whose inlet gas flow was not directly in contact with the solid sample, see Figure 6.1. The tests were performed for 1 h on a 2.2 g of solid sample containing 90% of phosphate ore and 10% of activated carbon to study the effect of chlorine concentration (3 to 23%), reaction time and, in the case of the high-grade phosphate ore, the effect of particle size. The samples were then analyzed by ICP-OES to determine the amount of phosphorus and other major and minor elements.

Although the primary focus of this study was the conversion of apatite to phosphorous chloride compounds, thus the phosphorous conversion considered as the phosphor removed from the phosphate ore was considered.

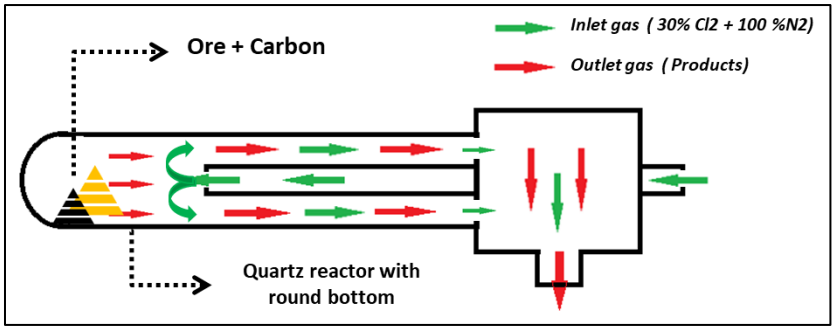

Figure 6.1. Schematic of the old reactor design with inlet and outlet gas trajectory

When applied on very fine low-grade phosphate ore, a low phosphate conversion of 4.8% was achieved after 1h of residence time under a 23% Cl_2 gas concentration and a 7 L/h flowrate. It should be noted that this flow rate was selected after studying the effect of the flow rate (7 to 25 L/h) at the same conditions, however, the flow rate did not affect the phosphate conversion. Although the effect of the chlorine concentration on apatite's conversion (Figure 6.2) was not significant, a lower apatite conversion was achieved at 3% Cl_2 concentration.

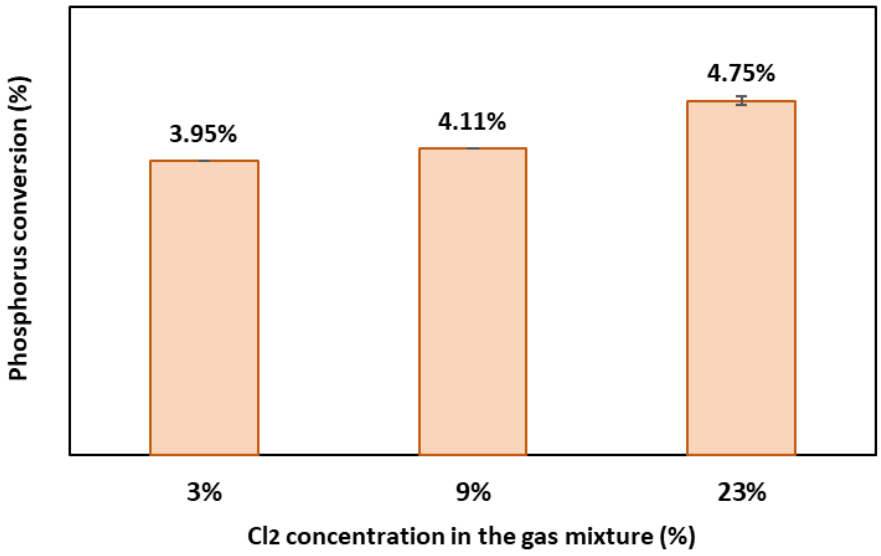

Figure 6.2 Conversion % of phosphorus for the first preliminary tests with low-grade phosphate ore

As the low-grade phosphate ore contains higher undesired gangue, e.g., calcite, dolomite or quartz, a high-grade phosphate ore containing ~95.5% of carbonate fluorapatite (Figure 4.2) was tested in order to evaluate apatite's conversion with the carbochlorination process. Herein, tests were performed with a 30% chlorine concentration at a 4.5 L/h flowrate to ensure a longer gas residence

time. The effect of temperature (700 ºC and 750 ºC), time (1 – 5 h), and particle size, i.e., combined as received (<5 mm) and 45 to 150 µm, were tested. Based on thermodynamics, the first tests at 750 ºC were applied on the high-grade phosphate ore as received. At said temperature, the activated carbon supposedly reacts, as per the Boudouard reaction, with the CO_2 generated by the decomposition of carbonatite minerals producing carbon monoxide. This gas, along with the activated carbon has a reducing role. Although based on thermodynamics using CO as a reducing agent was not as advantageous as using carbon, it may favor the carbochlorination reaction by having a gas-solid reaction and increasing the mass transfer of the reducing agent. Nevertheless, apatite's conversion after 2 h of residence time was still low, approximately 6.7%, and the effect of the time was low (Figure 6.3). The low effect of time, in this case, could be attributed to the mass transfer of chlorine since the particle size varied from approximately 20 µm up to 500 µm. Therefore, the low surface area and low ore porosity hindered chlorine diffusion and contact between the apatite and the reactive gas.

In addition, at 750 ºC, the formation of calcium and magnesium chlorides makes the ore sinter. In fact, both chlorides are produced during the reaction and have respective melting points at 714 ºC and 775 ºC. In the case of calcium chloride and given the intricate nature of the phosphate matrix, its combination with certain impurities of the ore weakens the lattice structure of the solid salt and reduces its stability thus lowering the melting point compared to the pure phase. A similar phenomenon has been reported previously for the carbochlorination of MgO, and dicalcium phosphate [86, 88]. There is therefore the possibility that $CaCl_2$ fuses at 750 ºC. As a result, it was difficult to retrieve the final product from the reactor. Therefore, to avoid sintering and to reduce the effect of mass transfer on the desired reaction, the following tests were performed on a lower particle size high-grade phosphate ore, i.e., 45 to 150 µm, at 700 ºC.

The carbochlorination of the fine high-grade phosphate ore with a 45 – 150 µm particle size, was performed for 1 and 5 h residence time. By reducing the particle size of the ore, a higher apatite's conversion was achieved, i.e., 10.6%, and as a matter of fact, the effect of chlorine's diffusion caused by the previous tests on particle sizes was neglected. Indeed, after 5 h of reaction, apatite's conversion remained at 10.6% (Figure 6.3).

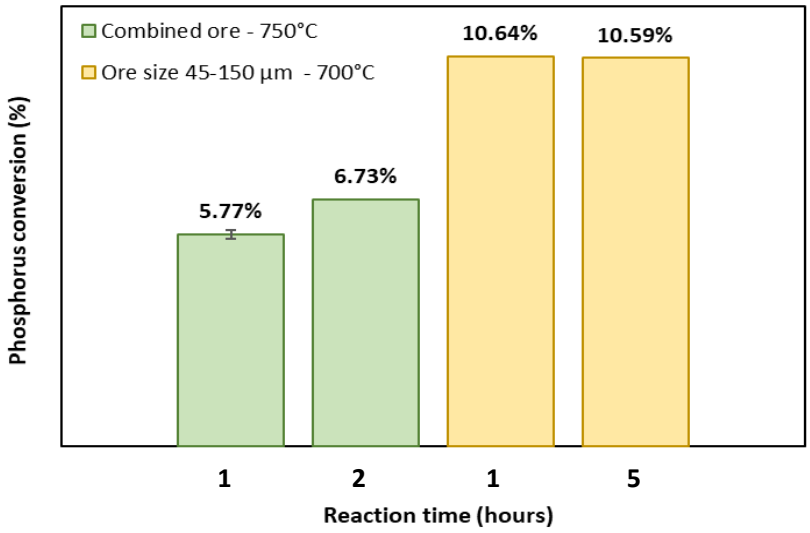

Figure 6.3 Conversion % of phosphorus for the first preliminary tests with high-grade phosphate ore

Although a higher conversion was achieved when reducing the particle size, this conversion was too low, and it was assumed to be caused by the low gas-solid contact due to a wrong reactor design. Indeed, in the previous design, Figure 6.1, the inlet chlorine gas was getting mixture with the outlet gas and part of it was being directly entrained to the outlet thus diluting the chlorine concentration and limiting the chlorine-apatite contact. This situation proved the importance of an appropriate reactor design and setup even at the laboratory scale.

To overcome this problem, a new reactor was designed in order to have a continuous feed of chlorine inside the reactor. The new setup, presented in Figure 6.4, consists of a 1.4 mm ID U-tube shape with a separated inlet and outlet. A quartz frit with 40 µm pores was added to the reactor to prevent solid particle entrainment. The reactor was made in-house by a glassblower.

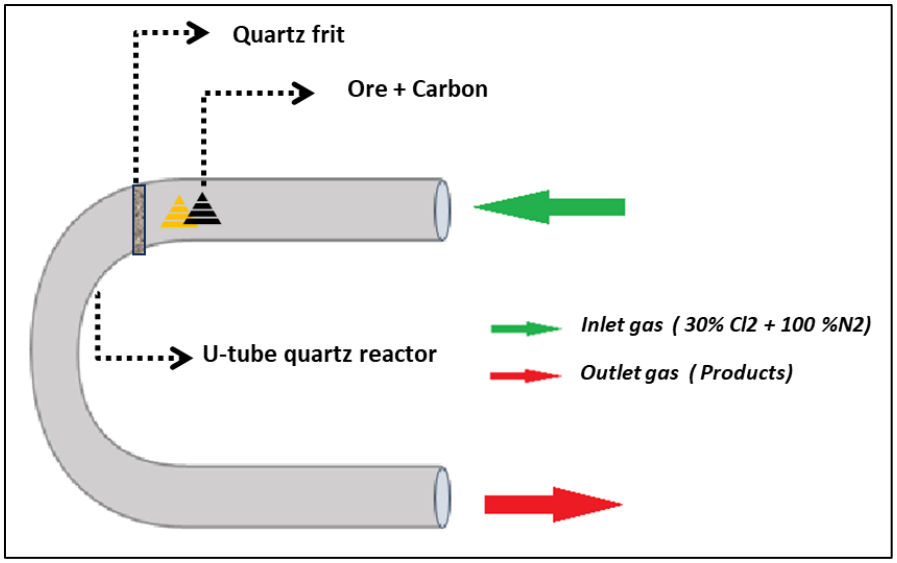

Figure 6.4 Schematic of the new reactor design with inlet and outlet gas trajectory

6.2 Carbochlorination of the high-grade phosphate ore

As per the new setup, the effect of time (0.5 to 7 h) and temperature (600 ºC to 700 ºC) on the carbochlorination process of high-grade phosphate ore was studied. Figure 6.5 presents the effect of both parameters on apatite's conversion, where the temperature has a noticeable on apatite's reaction rate. As a matter of fact, the conversion rate increases rapidly with the temperature since at 600 ºC only 17% of apatite was converted after 7 h, while 48% and 70% of apatite were converted into phosphorous chloride compounds at 650 ºC and 700 ºC respectively after 7 h. The achieved conversion, although it is a slow reaction, proves the viability of the process to thermally valorize apatite while confirming thermodynamic results (Chapter 5). Herein, it was experimentally proven that phosphorus in its natural carbonate-fluorapatite form reacts with the chlorine gas to form phosphorus chlorinated compound: phosphorus oxychloride $POCl_3$ and phosphorus trichloride PCl_3. According to the modelled phase diagram in Chapter 4, the reaction seemed to be more selective towards phosphorus oxychloride ($POCl_3$) at 700 °C with a high partial pressure of chlorine gas. Experimentally, carbochlorination's selectivity towards $POCl_3$ and PCl_3 still needs to be studied. In addition to the proof of concept of apatite's carbochlorination reaction, the results confirmed the reactor's selection discussed in the previous section as a much higher conversion was achieved at same conditions.

The effect of temperature sheds some light on the reaction rate of apatite's carbochlorination reaction, but the kinetics of this reaction was not studied as the reaction's selectivity was unknown.

In addition, despite its low presence in the ore, the presence of gangue minerals, i.e., mainly calcite, dolomite, and quartz, may certainly affect the reaction kinetics. In fact, in order to obtain more accurate kinetics, the carbonate fluorapatite should be purified, or the effect of gangue minerals on kinetics should be accounted for by studying that kinetics. On top of that, the ratio of added activated carbon and mainly the partial chlorine partial pressure must also be part of the kinetic study.

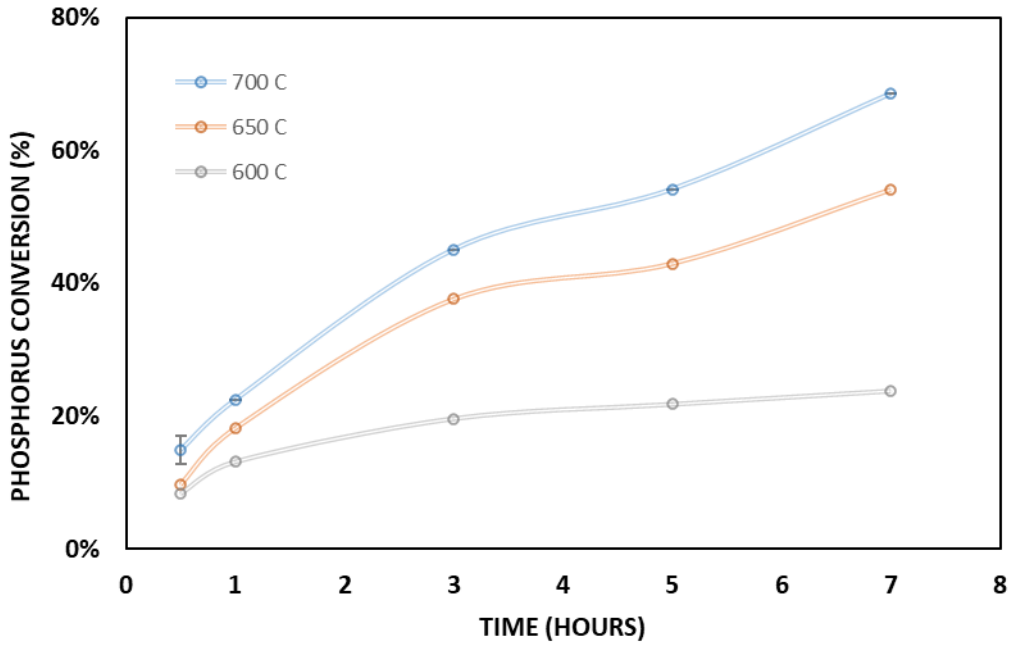

Figure 6.5 Effect of time and temperature on the phosphorus conversion %

A mass balance was conducted for all samples to assess the process gains and losses and to validate the phosphorus conversion results obtained using ICP-OES. The underlying assumption was that the principal solid products at the end of the reaction comprised the remaining fluorapatite ($Ca_5(PO_4)_3F$) and carbon, alongside the newly formed calcium chloride ($CaCl_2$). Based on this assumption, the masses of the major elements (Calcium and phosphorus) determined through ICP analysis were utilized to calculate the masses of $Ca_5(PO_4)_3F$ and $CaCl_2$. The quantification of the remaining carbon in the collected solid product was carried out using the LECO technique. Subsequently, the calculated masses of the remaining solids were compared to their recorded masses after the reaction. Specific example of the calculations performed for the high-grade phosphate ore treated at 700 °C for 7 hours is summarized in Table 6.2 below. Notably, the maximum error encountered during the mass balance procedure was approximately 7%. It is

important to acknowledge that this error might be attributed to the adherence of some solid products to the walls of the quartz reactor, thereby impeding the complete collection of all solid products.

Table 6.2 Example of mass balance calculation for low-grade ore treated at 700 °C for 7 h

Conditions	**m Ca (g)**	**m P (g)**	**m $CaCl_2$ (g)**	**m F-apt (g)**	**m tot (g)**	**m C (g)**	**Error (%)**
700C- 7 hours	*1.161*	*0.127*	*2.458*	*0.687*	*3.140*	*0.014*	*0.03%*

Ca: Calcium, P: Phosphorus, F-Apt: Fluorapatite, C: Carbon, m: mass, m tot: total mass of solid collected

Following the carbochlorination reaction, the mineralogy of the obtained products was qualitatively and semi-quantitatively analyzed by X-Ray Diffraction (XRD) with the perspective to obtain a preliminary reaction mechanism. This mechanism should certainly be validated once the condensed phosphorus chloride compounds are analyzed. Figure 6.6 presents the diffractograms of the remaining products at each temperature after 7h of reaction.

First of all, to validate the interest in analyzing the samples with XRD, the diffractogram of the high-grade apatite (feed) was compared to the QEMSCAN mineralogy presented in Figure 4.2. The presence of carbonate-fluorapatite ($Ca_{9.55}(PO_4)_{4.96}F_{1.96}(CO_3)_{1.283}$) as the main phase, and calcite ($CaCO_3$), dolomite ($CaMg(CO_3)_2$), and quartz (SiO_2) as minor phases combined to the quantitative analysis by Rietveld confirmed that the XRD analysis was in good agreement with the mineralogy.

As a matter of fact, Table 6.3 shows that the estimated composition obtained by XRD was close to the QEMSCAN, although it should be noted that Rietveld methods often present a ±20% error. The minor differences between XRD and QEMSCAN may be caused by said error and by the limited surface that is analyzed by XRD.

Table 6.3 High-grade ore composition obtained by XRD and QEMSCAN

Mineral	**Phase % (XRD)**	**Phase % (QEMSCAN)**
Carbonate-fluorapatite	*94.5*	*95.5*
Dolomite	*1*	*0.1*
Calcite	*2.6*	*1.9*
Silicate	*1.9*	*2.5*

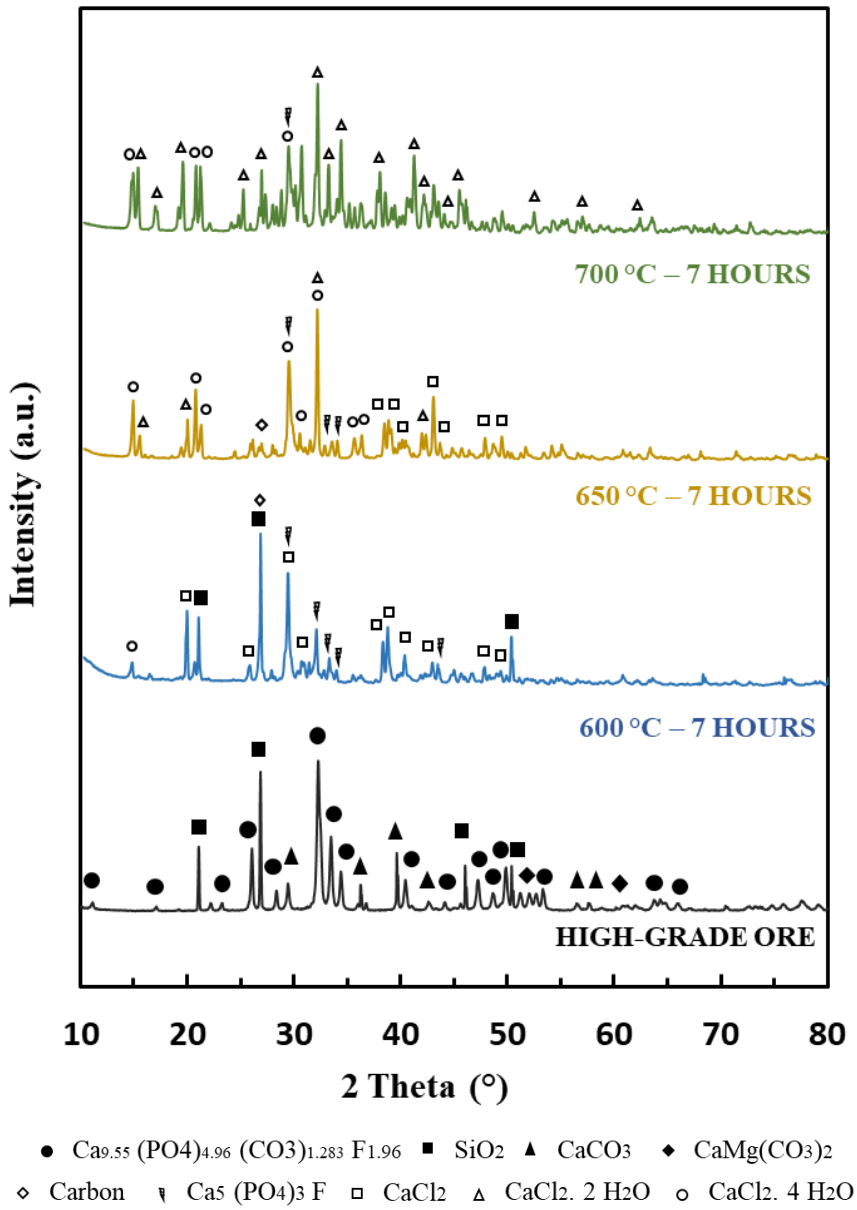

Figure 6.6 XRD of high-grade ore before and after treatment at different temperatures (600, 650, and 700 °C) after 7h of reaction

The XRD spectra presented in Figure 6.6 exhibit the distinct crystalline phases observed during different stages of the carbochlorination process applied to high-grade phosphate ore (600°C, 650°C, and 700°C) over a 7-hour reaction time.

At 600°C, the major phases identified are calcium chloride ($CaCl_2$), fluorapatite ($Ca_5(PO_4)_3F$), and silica (SiO_2). Notably, the peaks associated with carbonate-fluorapatite diminish, with the

simultaneous emergence of fluorapatite ($Ca_5(PO_4)_3F$), indicating the decarbonization of carbonate-fluorapatite and liberation of carbon dioxide (CO_2) gas.

The absence of dolomite and calcite peaks at 600°C confirms their complete consumption, likely forming $CaCl_2$ and $MgCl_2$. The presence of $CaCl_2$ in the carbochlorination residue supports this proposition, while the low dolomite content in the raw ore hinders the detection of $MgCl_2$. Furthermore, the generation of $CaCl_2$ predominantly stems from the decomposition of carbonate-fluorapatite and fluorapatite, accompanied by the production of gaseous phosphorus-chlorinated compounds containing CO and CO_2.

At 650°C, the disappearance of SiO_2 peaks confirms its consumption, yielding $SiCl_4$ gas according to previous FactSage simulations. The relatively reduced intensity of fluorapatite peaks suggests its higher consumption at this temperature. Moreover, the prevalent phase in the carbochlorination residue is identified as hydrated $CaCl_2$ ($CaCl_2.4H_2O$), resulting from the hygroscopic nature of $CaCl_2$ and its transformation into hydrate forms during XRD sample preparation. Finally, at 700°C, fluorapatite ($Ca_5(PO_4)_3F$) exhibits a single prominent peak, indicating heightened reactivity at this temperature. The main phases detected are hydrate species of $CaCl_2$ in the form of $CaCl_2.2H_2O$ and $CaCl_2.4H_2O$, reaffirming the influence of temperature on the reaction dynamics and product formation.

The influence of time on the carbochlorination process of high-grade phosphate ore was also explored within the time interval of 1 hour to 7 hours at 700 °C as illustrated in Figure 6.7.

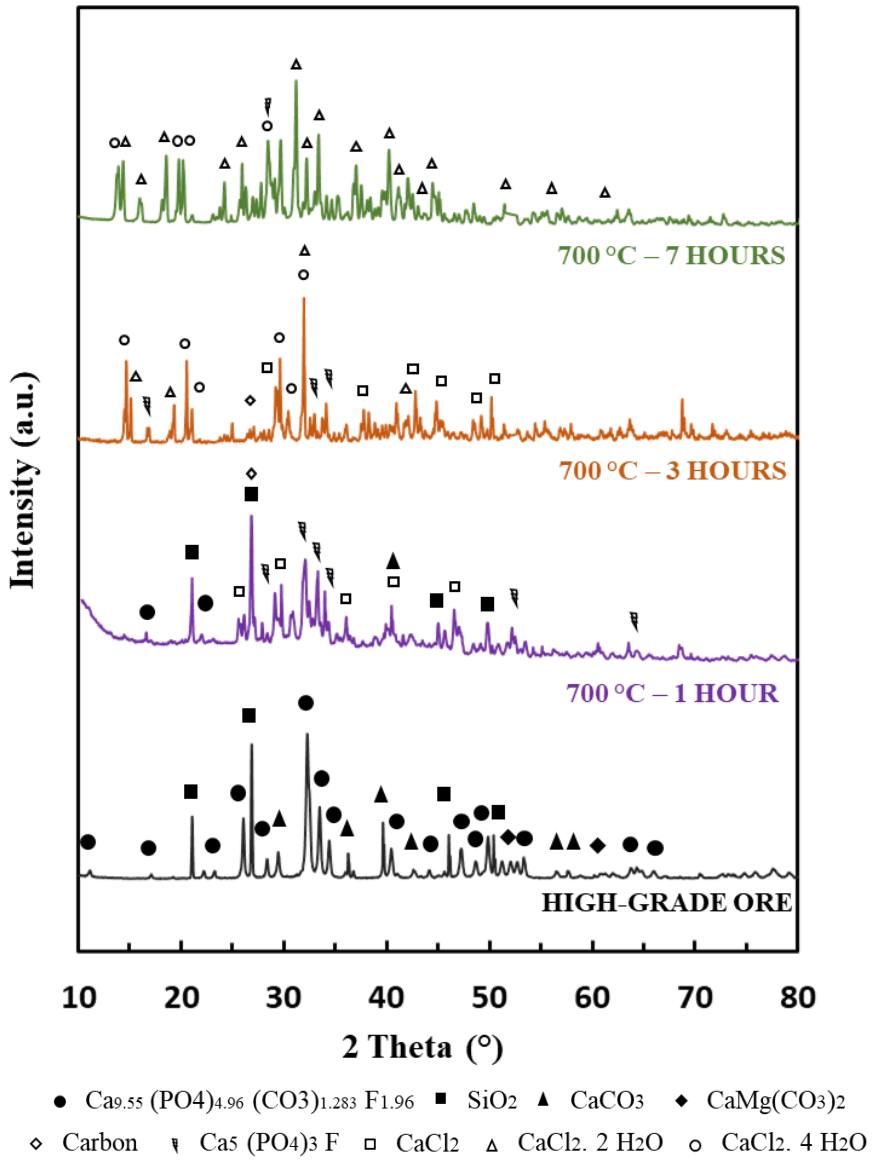

Figure 6.7 XRD of high-grade ore before and after treatment at 700 °C for 1, 3, and 7 hours

The XRD spectra in Figure 6.7 depicted the diverse crystalline phases present at various stages of the carbochlorination process, for 1, 3 and 7 hours, as well as the untreated raw phosphate sample. After one hour of carbochlorination, a similar trend to previous observations was observed, wherein carbonate fluorapatite underwent decarbonization, transforming into fluorapatite, and potentially generating calcium chloride through carbochlorination.

The relatively low intensity of the calcium chloride peak emphasized the limited conversion of fluorapatite or carbonate-fluorapatite at this early stage. Furthermore, a complete breakdown of dolomite occurred within one hour. From a thermodynamic standpoint, the dolomite primarily

dissociates into $CaCl_2$ and $MgCl_2$. Although clear $CaCl_2$ peaks were evident, the detection of $MgCl_2$ was not observed due to its expected low concentration resulting from the low dolomite content in the raw ore material. Similarly, calcite and silicate exhibited only partial dissociation, as evidenced by the persistence of their respective peaks, indicating that one hour of reaction time was insufficient for a complete reaction with SiO_2.

At the 3-hour mark, substantial dissociation of SiO_2 and $CaCO_3$ was observed. As predicted by the thermodynamic analysis, they primarily decomposed into $SiCl_4$, $CaCl_2$, and CO_2. The prominent phases observed at this time were $CaCl_2$ and its hydrate species ($CaCl_2.2H_2O$ and $CaCl_2.4H_2O$). The intensity reduction in fluorapatite peaks suggested further dissociation into solid $CaCl_2$ and gaseous $POCl_3$, CO_2, and CO.

After 7 hours, the major phases detected at this condition were the hydrate species of $CaCl_2$, specifically $CaCl_2.2H_2O$ and $CaCl_2.4H_2O$, with only a small peak of fluorapatite remaining. This indicates further progression of the reaction, leading to the prevalence of the aforementioned hydrates for CaCl2. Overall, the XRD analyses provided valuable insights into the evolving phases and reaction kinetics throughout the carbochlorination process over different time intervals at 700°C.

General spectra of the SEM-EDS analysis regarding the raw phosphate ore sample and the carbochlorination residues at 700 °C at different reaction times (1h, 3h and 7h) are grouped in Figure 6.8.

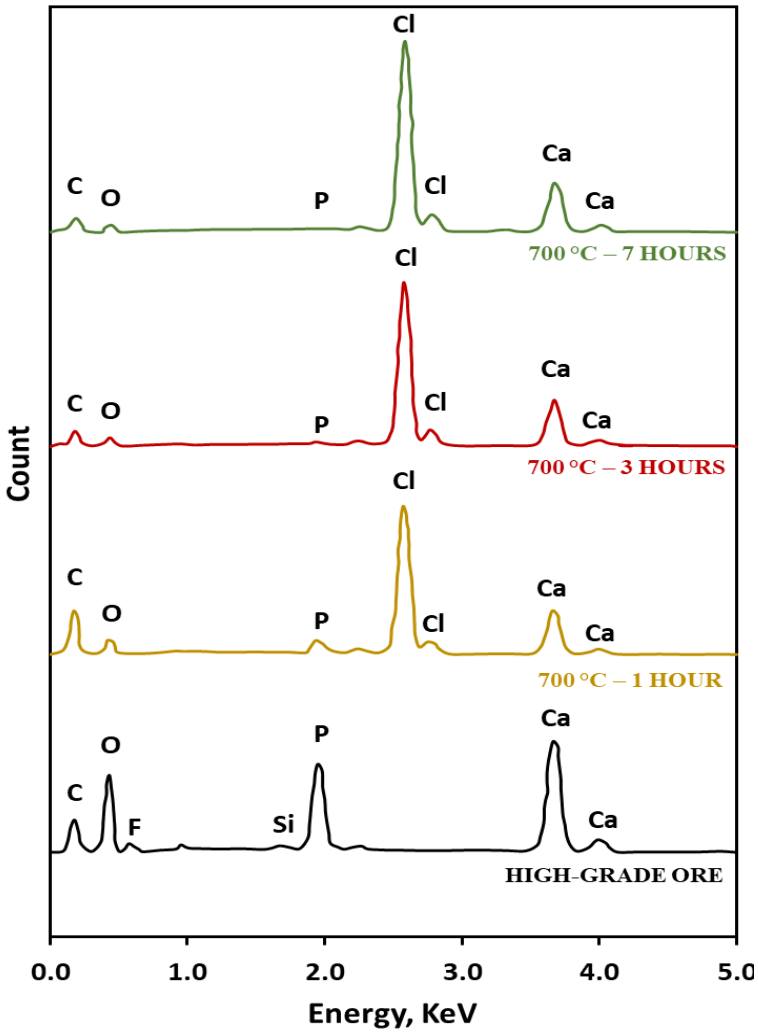

Figure 6.8 SEM-EDS of high-grade ore before and after treatment at 700 °C at different reaction times (1, 3, and 7h)

Consistent with expectations, the initial sample of the raw high-grade phosphate ore primarily comprises elements such as Ca, P, O, F, and C. In the carbochlorination residue at 700 °C for all reaction times, a prominent chlorine peak is evident, attributed to the formation of calcium chloride salt. Notably, a significant reduction in phosphorus peak intensity is observed within the tested time interval at 700 °C, indicating the removal of phosphorus in the form of gaseous phosphorus chloride, owing to its high volatility.

Additionally, the carbon peak intensity decreases with increasing reaction time, aligning with the results obtained from carbon analysis conducted with LECO. Moreover, a noteworthy decline in oxygen peak intensity is observed during the 700 °C treatment, further supporting the hypothesis

of oxygen removal through the decarbonization of carbonate-fluorapatite, resulting in the formation of carbon oxide. The SEM-EDS analysis corroborates the conclusions drawn from the interpretation of XRD diffractograms, reinforcing the consistency and reliability of the findings.

SEM images, shown in Figure 6.9, were captured for both the low-grade and high-grade phosphate samples both before and after treatment at 700 °C for 7 hours. The surface images of the samples were acquired at various magnifications, covering a scale ranging from 30 to 500 µm.

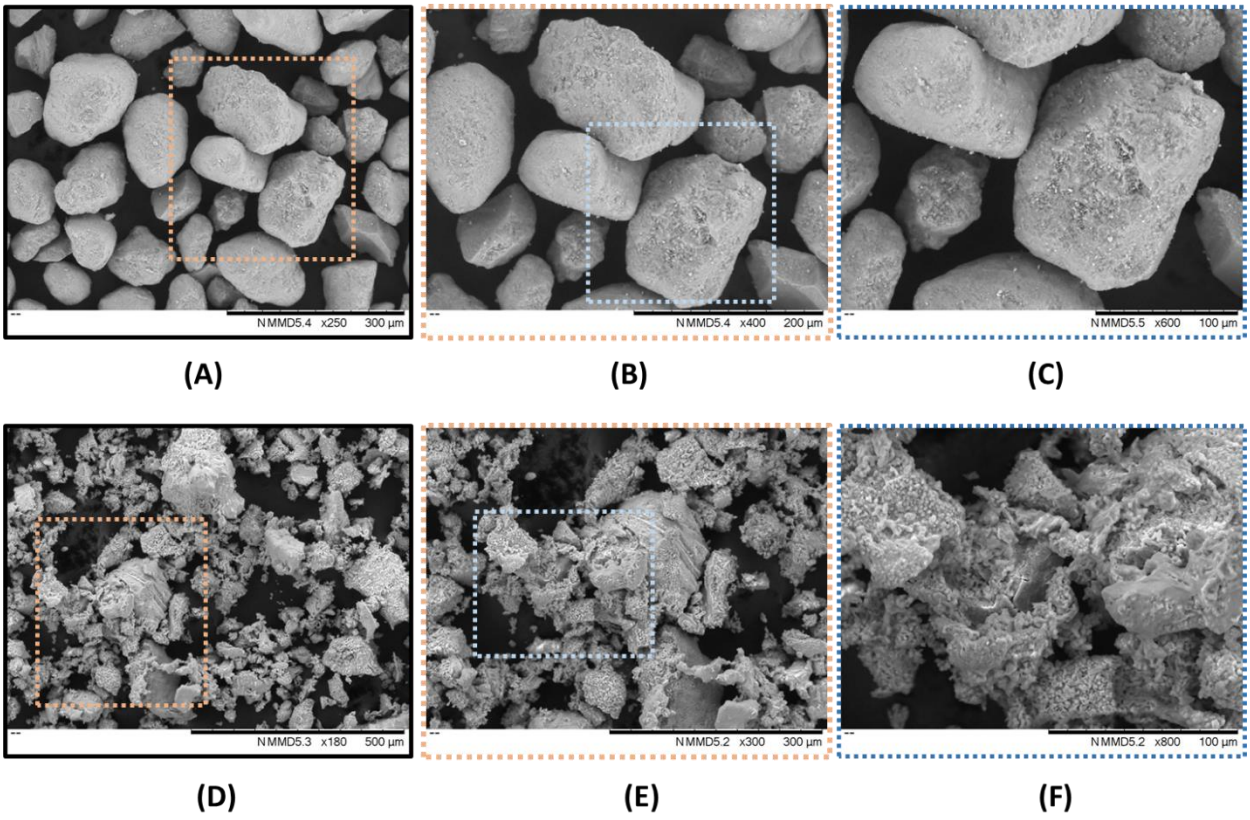

Figure 6.9 SEM images of high-grade ore before treatment (A, B, C) and after carbochlorination treatment (D, E, F) at 700 °C for 7 hours

Figure 6.9 presents the material morphologies of the high-grade phosphate ore both before treatment (A, B, C) and after carbochlorination treatment (D, E, F) at 700 °C for 7 hours. The initial raw high-grade phosphate ore (Figure 6.9-A) exhibits a relatively smooth surface with particles displaying irregular morphologies. These particles appear homogeneous, comprising over 95% carbonate-fluorapatite, and can be easily distinguished from one another. The observed particle size falls within the range obtained from the particle size distribution (45-150 µm), indicating that these particles correspond to carbonate-fluorapatite. Figures 6.9-B and 6.9-C are locally enlarged

views of Figure 6.9-A, offering a better understanding of the ore's morphology. In contrast, Figure 6.9-D reveals a notable increase in the average particle size due to agglomeration caused by the formation of a $CaCl_2$ layer. This layer, as seen in the enlarged view (Figure 6.9-F), covers most of the ore particles, hindering the access of chlorine gas to the ore. This hypothesis was highlighted and further validated through image analysis.

6.3 Carbochlorination of the low-grade phosphate ore

The low-grade phosphate ore was subjected to the same treatment conditions as the high-grade ore, undergoing treatment at 700 °C for 7 hours, to assess the phosphorus conversion percentage. The objective was to investigate the influence of gangue presence on the chlorination of phosphate ore. The phosphorus conversion percentage of the low-grade phosphate ore reached 76% under these specified conditions, and the conversion of other heavy metals will be elaborated on in section 5.4.

To comprehend the reasons behind the relatively slow conversion, SEM imaging and XRD analysis were employed to monitor the evolution of the mineralogical composition of both the treated and untreated ore. Figure 6.10 showcases the results of the XRD analysis applied to the low-grade phosphate ore and the treated sample (700 °C and 7 hours). To ascertain the reliability of analyzing the samples with XRD, a comparison was made between the diffractogram of the low-grade apatite (feed) and the QEMSCAN mineralogy presented in Figure 4.1. Table 6.4 summarize the results collected by both techniques.

Table 6.4 Low-grade ore composition obtained by XRD and QEMSCAN

Mineral	**Phase % (XRD)**	**Phase % (QEMSCAN)**
Carbonate-fluorapatite	64.2	65.2
Dolomite	15.5	16.2
Calcite	9.8	6.8
Silicate	10.2	11.6

The main phases detected by XRD, which included carbonate-fluorapatite ($Ca_{9.55}(PO_4)_{4.96}F_{1.96}(CO_3)_{1.283}$), calcite ($CaCO_3$), dolomite ($CaMg(CO_3)_2$), and quartz ($SiO_2$), were found to be consistent with the results of the quantitative analysis by Rietveld and confirmed through QEMSCAN. The XRD analysis demonstrated good agreement with the mineralogical

composition, as evidenced by the close match between the obtained composition and the QEMSCAN results, as illustrated in the Table 6.4.

Figure 6.10 displays the XRD spectra, revealing the distinct crystalline phases observed during the carbochlorination process applied to low-grade phosphate ore at 700 °C for a 7-hour reaction time.

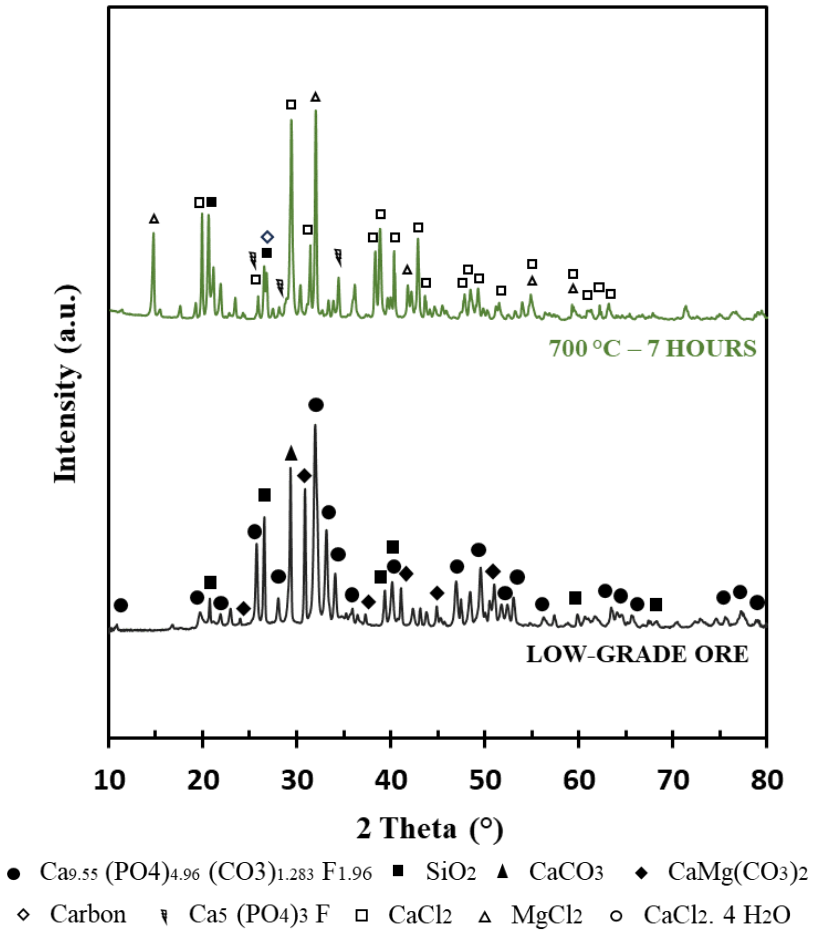

Figure 6.10 XRD diagram of low-grade phosphate ore and the treated sample (700 °C and 7 hours)

The major identified phases include calcium chloride ($CaCl_2$) and its hydrate ($CaCl_2.4H_2O$), fluorapatite ($Ca_5(PO_4)_3F$), and silica (SiO_2). Interestingly, the peaks associated with fluorapatite exhibit very low intensities, indicating its near-complete consumption during the chlorination reaction. The absence of dolomite and calcite peaks further confirms their total consumption, likely resulting in the formation of $CaCl_2$ and $MgCl_2$. The presence of $CaCl_2$ and $MgCl_2$ in the carbochlorination residue strongly supports this proposition.

Additionally, the generation of $CaCl_2$ is primarily attributed to the decomposition of fluorapatite, concurrently leading to the production of gaseous phosphorus-chlorinated compounds containing CO and CO_2. As for SiO_2, it appears to undergo only partial conversion at this temperature, indicating that the reaction with SiO_2 is not yet complete at the given conditions.

SEM image displayed in Figure 6.11 displays the material morphologies of the low-grade phosphate ore before treatment (A, B, C) and after carbochlorination treatment (D, E, F) at 700 °C for 7 hours. The untreated low-grade phosphate ore (Figure 6.11-A) exhibits non-homogeneous particles with irregular morphologies, reflecting the complex matrix containing carbonate-fluorapatite, calcite, dolomite, and silicate in substantial proportions. The particle size observed falls within the range of the obtained particle size distribution (< 45µm), but unlike the high-grade ore, it is challenging to distinguish individual particles due to their independent distribution.

Figures 6.11-B and 6.11-C provide local enlarged views of Figure 6.11-A, offering further insight into the ore's morphology. A prominent large particle, corresponding to carbonate-fluorapatite, holds the other gangue materials forming the ore.

Figure 6.11-D reveals a clear increase in average particle size, attributed to pronounced agglomeration resulting from the formation of a $CaCl_2$ layer and potentially the melting of chloride salts. Notably, agglomeration is more pronounced in the low-grade phosphate ore compared to the high-grade one. Enlarged views (Figures 6.11-E and 6.11-F) confirm the formation and expansion of cracks, likely caused by the decarbonization of carbonate-fluorapatite, leading to the release of carbonic gases that induced these cracks.

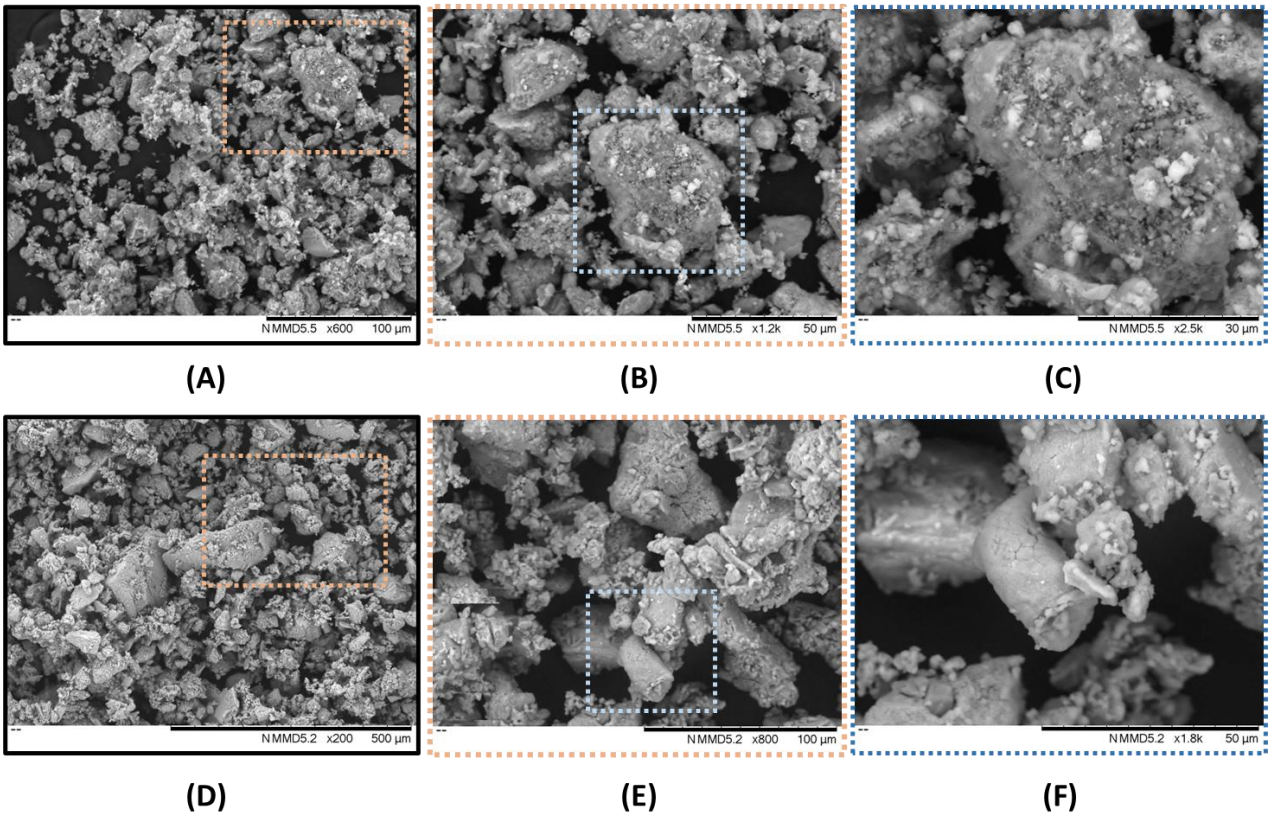

Figure 6.11 SEM images of low-grade ore before treatment (A, B, C) and after carbochlorination treatment (D, E, F) at 700 °C for 7 hours

It is important to note that particle size distribution analysis for the treated ores was not feasible due to the presence of calcium chloride, which rapidly dissolves in the available solvents used for particle size analysis.

By combining phase transformation and mineralogical composition provided by XRD and SEM-EDS, along with the thermodynamic analysis with Factsage, the following reaction scheme is proposed during the carbochlorination process of low-grade ore:

$$Ca_{9.55}(PO_4)_{4.96}F_{1.96}(CO_3)_{1.28} \rightarrow 0.826\ Ca_{10}(PO_4)_6F_2 + 0.153\ CO_2 + 0.153\ CaF_2 + 1.13\ CaCO_3 + 0.076\ O_2 \quad \text{C5}$$

$$3Ca_5(PO_4)_3F + 13.5\ C + 27\ Cl_2 \rightarrow 15\ CaCl_2 + 8\ POCl_3 + POF_3 + 13.5\ CO_2 \quad \text{C6}$$

$$2\,CaCO_3 + C + 2\,Cl2 \rightarrow 2\,CaCl_2 + 3\,CO_2 \quad \text{C7}$$

$$CaMg(CO_3)_2 + C + 2\,Cl_2 \rightarrow CaCl_2 + MgCl_2 + 3\,CO_2 \quad \text{C8}$$

$$SiO_2 + C + 2Cl_2 \rightarrow SiCl_4 + CO_2 \quad \text{C9}$$

6.4 Heavy metals outcome

The investigation of heavy metals in both low and high-grade ores revealed significant recovery through the chlorination process, except for aluminum, which showed a consistent recovery extent. For cadmium (Cd) and vanadium (V), nearly complete recovery was achieved after 7 hours at 700 °C for both ore grades. However, nickel (Ni) was absent in the high-grade ore, thus it was not detected in the analysis. Conversely, the recovery of nickel (Ni) from the low-grade ore reached 80%. Regarding Zinc (Zn), Chromium (Cr), and Iron (Fe), the recovery percentages ranged from 80% to 90% in the case of low-grade ore, whereas for the high-grade ore, the recovery rates were slightly lower, falling between 60% and 80%. Figure 6.12 illustrates these findings comprehensively.

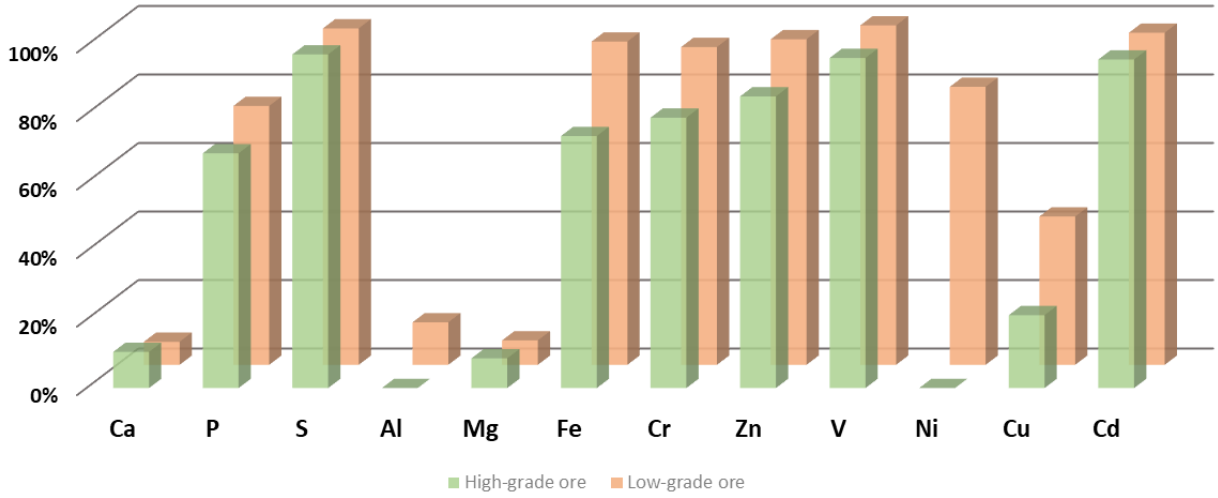

Figure 6.12 Heavy metals recovery for high- and low-grade ore at 700 °C after 7h

CHAPTER 7 ASPEN SIMULATION AND ECONOMIC ANALYSIS

To investigate the mass and energy balance of an industrial-scale phosphate ore valorization plant and assess its economic viability, the development of a process flow diagram (PFD) is essential. Previous studies focused on techno-economic evaluations of ore and/or ore waste valorization plants, prompting us to create a process flow diagram and conduct subsequent techno-economic analyses for a plant with a feed capacity of 1,000,000 tons per year of waste phosphate ore. [89] The utilization of industrial process simulators facilitates the validation of mass and energy balance within the systems and enables us to conduct sensitivity analyses and optimize the process effectively.

The accomplishment of a techno-economic assessment of the plant, as delineated in this chapter, necessitates the initial adoption of an appropriate industrial process simulator. In the context of validating the mass and energy balance of the process, the Aspen Plus software emerges as an efficacious instrument, given its track record in successfully aiding in the techno-economic evaluation and process development of analogous studies in the past.

7.1 Aspen Simulation

The primary advantages of implementing Aspen Plus software for the validation of the mass and energy balance of the plant involves:

i) Its user-friendly interface paired with potent mathematical functionality.
ii) A comprehensive library containing several thermodynamic packages for gas, liquid, and solid phases.
iii) The ability to interface with other mathematical software, such as MATLAB, for the detailed simulation and modeling of process equipment.
iv) The competency to manage both steady-state and dynamic systems.

Thus, this industrial process simulator is deemed fit for the validation of the mass and energy balance of the process, serving as a precursor to the accomplishment of equipment design and subsequent economic evaluations. Equations and correlations used for equipment design and techno-economic analysis are mainly taken from the literature. [89-92]

7.1.1 General process description

Displayed in Figure 7.1 is the general Block Flow Diagram (BFD) of the carbochlorination process of Low-grade phosphate ore.

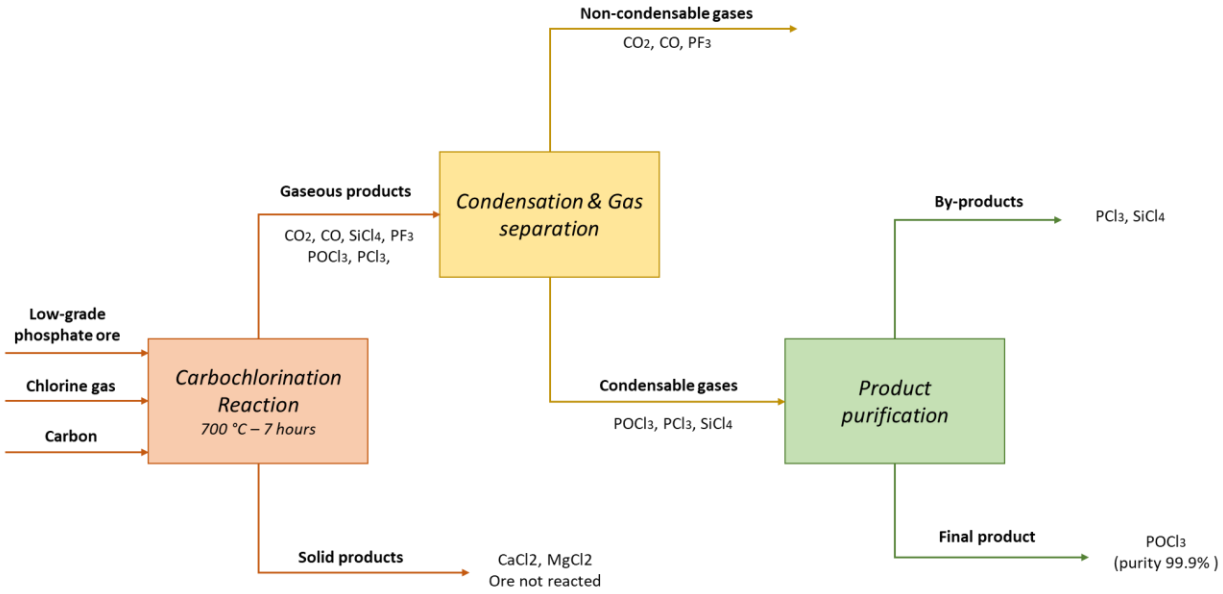

Figure 7.1 Bock flow diagram of the carbochlorination process of phosphate wastes

In this study, the carbochlorination process of low-grade phosphate ore is comprehensively examined, including three key unit operations, as depicted in Figure 7.1: the carbochlorination of phosphate waste utilizing a rotary kiln reactor, the subsequent separation of condensable and non-condensable product gases, and the purification of the condensate to obtain the final pure product ($POCl_3$).

The initial stage of the process involves blending low-grade phosphate ore with charcoal, and subsequently introducing chlorine gas (Cl_2) into the reactor to facilitate solid-solid and gas-solid reactions. The carbochlorination reaction is conducted at a temperature of 700°C, resulting in the formation of two distinct phases: solid and gaseous mixtures. The solid phase mainly consists of calcium and magnesium chlorides ($CaCl_2$ and $MgCl_2$), along with some unreacted ore. Due to the continuous production nature of the process, immediate handling of the hot solids leaving the reactor is crucial, accomplished using high-capacity rotary coolers.

Concurrently, the gaseous products from the carbochlorination process include both condensable ($POCl_3$, PCl_3, $SiCl_4$) and non-condensable (CO_2, CO, PF_3) gases. To separate these components,

successive cooling steps are applied downstream of the rotary kiln reactor till reaching a low temperature (-10 °C). Subsequently, the liquid and gas mixture undergo further processing in a vertical separator to segregate the liquid from the gaseous products. The gaseous product exiting the separator at -10°C finds utility as a cooling medium in another part of the production process, enhancing the overall efficiency and sustainability of the carbochlorination operation. Finally, the separated liquid is heated to 30°C using a heat exchanger (economizer) before being directed to a distillation column. Within the distillation column, the highly pure $POCl_3$ is extracted from the liquid mixture at the bottom, achieving an impressive purity level of 99.99%. The remaining distillate, which predominantly contains $SiCl_4$ and PCl_3, holds potential for further treatment and valorization.

7.1.2 Process simulation and design

To analyze the gaseous components, the Peng-Robinson thermodynamic package within the Aspen Plus software was utilized. For examining the solid components, the UNIFAC and SOLID thermodynamic packages were similarly employed. For a thorough understanding of the plant operations, the reaction involving low-grade phosphate ore, charcoal, and Cl_2 is examined, based on both thermodynamic analysis and conversion data derived from the experimental investigations in this study.

The initial phase of this study involved performing preliminary simulations using the RGibbs reactor, which were subsequently compared to the thermodynamic results obtained. The outcomes demonstrated a high degree of agreement with the thermodynamic analysis conducted using FactSage, thereby validating the previously identified optimum conditions concerning temperature, pressure, and composition for leading to a higher phosphorus conversion. The preliminary tests using RGibss reactor were not added to this section.

Building upon this, a comprehensive Process Flow Diagram (PFD) for the plant was developed, with a particular focus on utilizing the RStoic reactor within the Aspen Plus software framework. The RStoic reactor, employed in Aspen Plus, is characterized as a stoichiometry-based reactor with specified extents of reaction. This selection was motivated by the absence of kinetic data for the reaction at this stage of the research. However, the stoichiometry and conversion of the reaction have been accurately determined through experimental. The PFD constructed based on the RStoch reactors is illustrated in Figure 7.2.

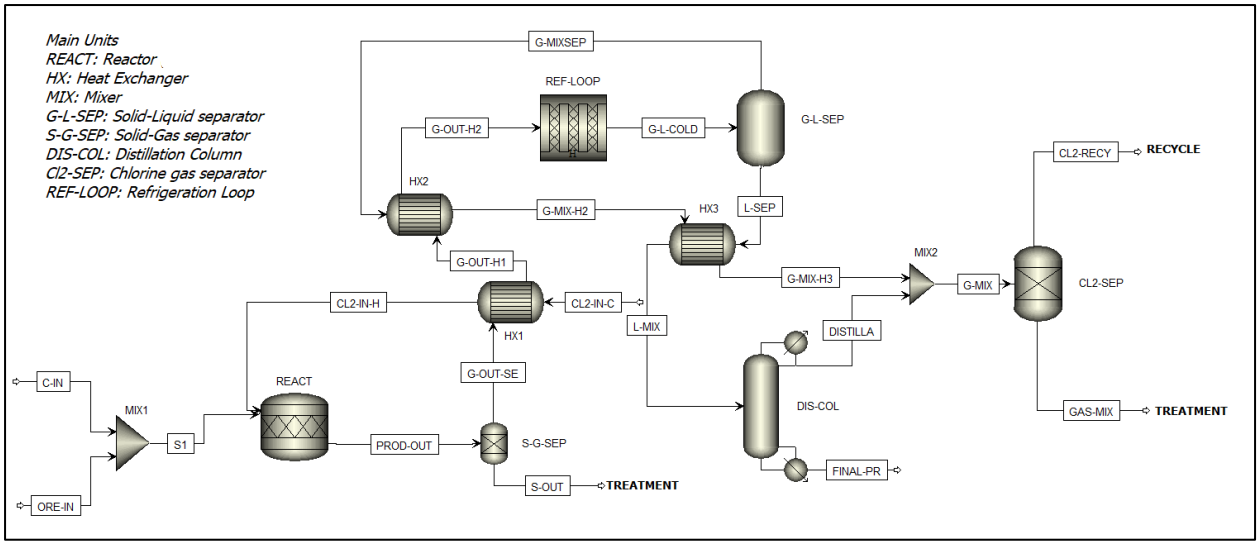

Figure 7.2 Process flow diagram of the low-grade phosphate ore carbochlorination process

The selection of reactor temperature and pressure at 700 °C and 1 bar, respectively, was determined based on thermodynamic and experimental investigations conducted in preceding chapters. These parameters were identified as the most favorable conditions to achieve optimal process efficiency and phosphorus yield.

In the RStoic reactor model, the overall chemical reaction considered involves the interaction of low-grade phosphate ore, comprising Fluor-apatite, dolomite, calcite, and silicate, with Chlorine gas and carbon, acting as the initial reagents. The reaction is described by the following equation:

$$3\ Ca_5(PO_4)_3F + 2\ CaMg(CO_3) + 1.6\ CaCO_3 + 4.6\ SiO_2 + 41.8\ Cl_2 + 21.4\ C \rightarrow$$

$$18.6\ CaCl_2 + 2\ MgCl_2 + 8\ POCl_3 + PF_3 + 4.6\ SiCl_4 + 27\ CO_2$$

In the simulation, a conversion of 0.76 for fluorapatite was utilized. This value was based on experimental data obtained from earlier investigations.

Table 7.1 presents a comprehensive summary of the main equipment employed in the carbochlorination process, along with their respective specifications. Units were designed based on both literature and aspen plus data. Table 7.1 also emphasizes the size parameter S, which will be taken into account during the calculation of equipment costs.

Table 7.1 Specifications of the unit operations in the carbochlorinations process

Unit	Specifications	Ref
Reactor	Rotary kiln reactor	[92]
	Isothermal	
	Solid-solid and solid-gas reactions	
	Required power: 23 MW	
	Operation temperature: 700 °C	
	Designed pressure: 1 bar	
	*Total volume: 558 m^3	
	Number of units: 8	
Heat Exchanger HX1	Plate and frame heat exchanger	[91]
	Net heat exchanged: 13.5 MW	
	*Heat exchanger area: 79 m^2	
	Number of units: 1	
Heat Exchanger HX2	Plate and frame heat exchanger	[91]
	Net heat exchanged: 7.9 MW	
	*Heat exchanger area: 235 m^2	
	Number of units: 1	
Heat Exchanger HX3	Plate and frame heat exchanger	[91]
	Net heat exchanged: 1.1 MW	
	*Heat exchanger area: 3.7 m^2	
	Number of units: 1	
Distillation column	Trayed distillation tower.	[90]
	Number of stages: 25	
	Column height: 15 m	
	Column diameter: 1.4 m	
	*Total weight (Shell & plates): 17.2 tons	
	Number of units: 1	

Gas/Liquid separator	Vertical separator Vessel height: 4.9 m Vessel diameter: 2.2 m *Vessel weight: 4 tons Number of units: 1	[90]
Condenser (Refrigeration loop)	Shell and tube heat exchanger Net heat exchanged: 18.5 MW *Heat exchanger area: 2560 m^2 Number of units: 1	[91]
Chiller (Refrigeration loop)	Shell and tube heat exchanger Net heat exchanged: 13.8 MW *Heat exchanger area: 360 m^2 Number of units: 1	[91]
Compressor (Refrigeration loop)	*Required power: 6.6 MW Efficiency: 80% Number of units: 1	[90]

*** The star represent the size parameter S used to calculate the equipment cost in eq 4**

Table 7.2 and Table 7.3 provide an overview of the all the product streams generated from the rotary kiln reactor operating at 700 °C, which include both gaseous and solid components. The solid product stream exiting the reactor at this temperature predominantly consists of $CaCl_2$, $MgCl_2$, and some unreacted phosphate. To optimize energy utilization, these solids can be directed to high-capacity rotary coolers, thus exploiting the heat content of the stream, and offering potential avenues for further valorization of these salts. Considering the main objective of this study, the corresponding units of the treatment of the mentioned solids is not brought in this discussion.

Table 7.2 Mass balance and properties of each stream given in the PFD (part 1)

Stream	Temperature	$CA_{10}(PO_4)_6F_2$	$CaMg(CO_3)_2$	$CaCO_3$	SiO_2	Cl_2	C
Unit	***C***	***kg/hr***	***kg/hr***	***kg/hr***	***kg/hr***	***kg/hr***	***kg/hr***
C-IN	*25*	*0*	*0*	*0*	*0*	*0*	*14080*
CL2-IN-C	*30*	*0*	*0*	*0*	*0*	*167000*	*0*
CL2-IN-H	*600*	*0*	*0*	*0*	*0*	*167000*	*0*
CL2-RECY	*121*	*0*	*0*	*0*	*0*	*44093*	*0*
DISTILLA	*32*	*0*	*0*	*0*	*0*	*4814*	*0*
FINAL-PR	*42*	*0*	*0*	*0*	*0*	*0*	*0*
G-L-COLD	*-10*	*0*	*0*	*0*	*0*	*44093*	*0*
G-MIX	*121*	*0*	*0*	*0*	*0*	*44093*	*0*
G-MIX-H2	*276*	*0*	*0*	*0*	*0*	*39279*	*0*
G-MIX-H3	*226*	*0*	*0*	*0*	*0*	*39279*	*0*
G-MIXSEP	*-10*	*0*	*0*	*0*	*0*	*39279*	*0*
G-OUT-H1	*346*	*0*	*0*	*0*	*0*	*44093*	*0*
G-OUT-H2	*187*	*0*	*0*	*0*	*0*	*44093*	*0*
G-OUT-SE	*700*	*0*	*0*	*0*	*0*	*44093*	*0*
GAS-MIX	*121*	*0*	*0*	*0*	*0*	*0*	*0*
L-MIX	*30*	*0*	*0*	*0*	*0*	*4814*	*0*
L-SEP	*-10*	*0*	*0*	*0*	*0*	*4814*	*0*
ORE-IN	*25*	*82550*	*20320*	*8890*	*15240*	*0*	*0*
PROD-OUT	*700*	*19812*	*5026*	*2249*	*3779*	*44093*	*3421*
S1	*25*	*82550*	*20320*	*8890*	*15240*	*0*	*14080*
S-OUT	*700*	*19812*	*5026*	*2249*	*3779*	*0*	*3421*

The gaseous products exiting the reactor at 700 °C undergo a stepwise cooling process, initially passing through two heat exchangers (economizers), where its heat is utilized efficiently, before reaching a propane refrigeration unit.

Table 7.3 Mass balance and properties of each stream given in the PFD (part 2)

Stream	Temperature	$POCl_3$	$MgCl_2$	$CaCl_2$	PF_3	$SiCl_4$	CO_2
Unit	***C***	***kg/hr***	***kg/hr***	***kg/hr***	***kg/hr***	***kg/hr***	***kg/hr***
C-IN	*25*	*0*	*0*	*0*	*0*	*0*	*0*
CL2-IN-C	*30*	*0*	*0*	*0*	*0*	*0*	*0*
CL2-IN-H	*600*	*0*	*0*	*0*	*0*	*0*	*0*
CL2-RECY	*121*	*0*	*0*	*0*	*0*	*0*	*0*
DISTILLA	*32*	*418*	*0*	*0*	*0*	*27268*	*594*
FINAL-PR	*42*	*49716*	*0*	*0*	*0*	*2*	*0*
G-L-COLD	*-10*	*50868*	*0*	*0*	*3648*	*32409*	*49276*
G-MIX	*121*	*1152*	*0*	*0*	*3648*	*32407*	*49276*
G-MIX-H2	*276*	*734*	*0*	*0*	*3648*	*5139*	*48682*

G-MIX-H3	*226*	*734*	*0*	*0*	*3648*	*5139*	*48682*
G-MIXSEP	*-10*	*734*	*0*	*0*	*3648*	*5139*	*48682*
G-OUT-H1	*346*	*50868*	*0*	*0*	*3648*	*32409*	*49276*
G-OUT-H2	*187*	*50868*	*0*	*0*	*3648*	*32409*	*49276*
G-OUT-SE	*700*	*50868*	*0*	*0*	*3648*	*32409*	*49276*
GAS-MIX	*121*	*1152*	*0*	*0*	*3648*	*32407*	*49276*
L-MIX	*30*	*50133*	*0*	*0*	*0*	*27270*	*594*
L-SEP	*-10*	*50133*	*0*	*0*	*0*	*27270*	*594*
ORE-IN	*25*	*0*	*0*	*0*	*0*	*0*	*0*
PROD-OUT	*700*	*50868*	*7897*	*85603*	*3648*	*32409*	*49276*
S1	*25*	*0*	*0*	*0*	*0*	*0*	*0*
S-OUT	*700*	*0*	*7897*	*85603*	*0*	*0*	*0*

A comprehensive Process Flow Diagram (PFD) for the refrigeration unit is presented in Figure 7.3. The decision to employ a propane refrigeration loop was based on a sensitivity analysis conducted to determine the optimal cooling temperature allowing a better recuperation of ($POCl_3$) in the liquid phase with an acceptable purity. Figure 7.4 illustrates the variation in $POCl_3$ liquid purity and recuperation % with respect to the cooling temperature.

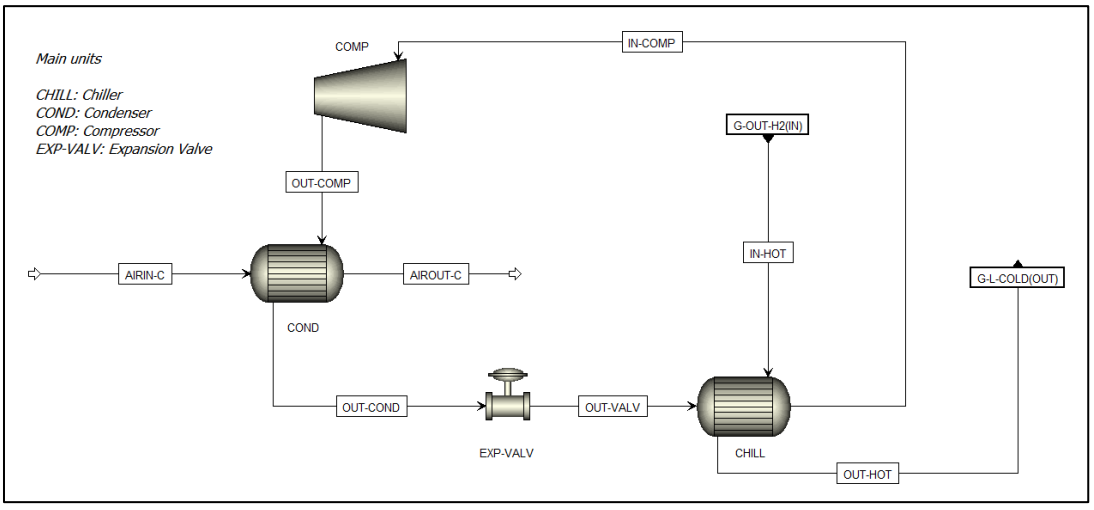

Figure 7.3. Process flow diagram of the propane refrigeration unit

The sensitivity analysis revealed that temperatures below -40 °C would permit total condensation of $POCl_3$. However, such low temperatures demand a significant amount of power and may not be viable in terms of the operational cost of the refrigeration unit. Additionally, under these conditions, a portion of Cl_2 and CO_2 was also observed to condense, which could potentially complicate the subsequent purification process of the liquid.

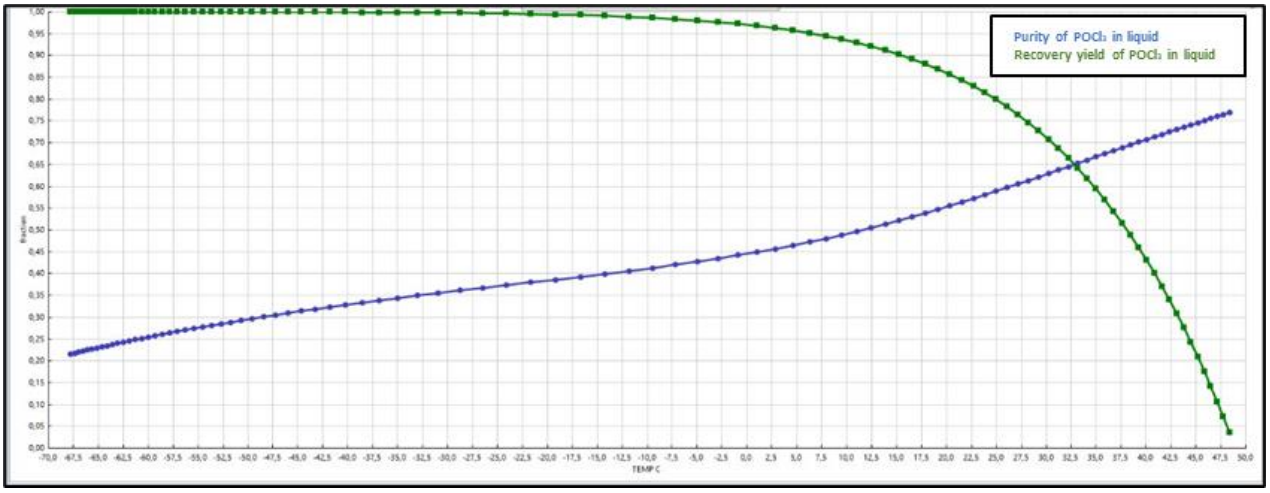

Figure 7.4. Variation of the recovery yield and purity of $POCl_3$ in liquid in terms of temperature

Moreover, very low temperature favors the condensation of other non-condensable gases (PCl_3, $SiCl_4$) which affects the purity of the $POCl_3$ liquid. For these reasons, an operational temperature of -10 °C was selected, allowing for the condensation of 98.5% of the total $POCl_3$ present in the gaseous phase with acceptable purity. This temperature strikes a balance between effective condensation and practical operational considerations.

To separate the vapor-liquid mixture leaving the refrigeration unit, a vertical separator was chosen due to the significantly high gas-liquid ratio. After the gas-liquid separation, the condensed liquid, mainly containing $POCl_3$, PCl_3, and $SiCl_4$, was preheated to 30°C before being directed to the distillation column. This preheating step aims to minimize the energy requirements in both the condenser and reboiler. The distillation column, as depicted in Figure 7.2, was specifically designed to achieve optimal purification of $POCl_3$, reaching a purity level of 99.99%. The resulting $POCl_3$ liquid product should then be collected and stored. It is highly recommended to store this product under Nitrogen atmosphere in securely sealed containers within a cool, well-ventilated environment.

7.2 Techno-economic analysis

In the context of the techno-economic evaluation in this study, only the Stoic reactor will be evaluated, which, besides the RGibbs reactor, is more realistic as it incorporates the fractional conversion of phosphate ore and the stoichiometry of the reaction.

7.2.1 Detailed costs calculation procedure

The determination of total cost is carried out employing a commonly utilized method for TCOP calculation, as expressed in Equation (7.1): [89, 90]

$$\mathrm{TCOP} = \mathrm{VCOP} + \mathrm{FCOP} + \mathrm{ACC} \tag{7.1}$$

VCOP denotes variable costs of production, while FCOP and ACC stand for fixed costs of production and annual capital charges, respectively. VCOP comprises expenses related to electricity, propane, reagents (chlorine gas and charcoal), and utilities, including the fuel needed for the reactor. On the other hand, FCOP represents costs that remain independent of the plant production rate, including the following items: [89, 90]

- Operating labor: The workforce consists of 6 operators assigned to various critical aspects of the process. This allocation includes responsibilities such as overseeing the reactor's feed, monitoring product output, managing liquid products, overseeing the control room of both the reactor and the distillation column, and supervising the refrigeration unit. The selection of 6 operators was based on the specific requirements and complexity of each operational component. The work shift in this case was selected to be 4.8.
- Supervision: Assumed to be 30% of the operating labor cost.
- Direct salary overhead: Assumed to be 40% of the sum of operating labor cost and supervision cost.
- Maintenance costs: Considered 5% of the annual capital charge ACC.
- Insurance and property taxes: Assumed to be 5% of the annual capital charge ACC.
- The land rent: Assumed at 5% of the annual capital charge ACC.

The annual capital charge (ACC) is given by Equation (7.2): [89, 90]

$$\mathrm{ACC} = \mathrm{FCI} \times \mathrm{CRF} \tag{7.2}$$

where, CRF denotes the capital recovery factor, and FCI stands for fixed capital investment. The factor CRF, is calculated using Equation (7.3): [89, 90]

$$CRF = \frac{i(1+i)^n}{(1+i)^n-1} \tag{7.3}$$

Where n is the equipment lifetime time and i is the discount rate.

The Fixed Capital Investment (FCI) itself comprises four major components:

- ISBL Investment: This depicts the cost associated with the installation and procurement of all process equipment within the plant. The ISBL cost constitutes the total cost of the plant.
- Offsite Costs or OSBL Capital Costs: These costs pertain to the infrastructure of the site, including expenses incurred for adding new units or renovating the existing plant.
- Engineering Costs: This includes the expenditures related to engineering services, particularly detailed design work for the projects.
- Contingency Charges: Additional costs are factored in as contingency charges to accommodate potential variations in the estimated costs, considering that the final installed costs may not be fixed due to uncertainties in calculations.

The formula applied for all equipment cost calculations is given by Equation (7.4):

$$C_{PE} = f_m\,(a + bS^n) \tag{7.4}$$

where f_m is the material cost factor, a and b are the cost constants, S denotes the size parameter, and n is the constant exponent. Constants used in Eq. (4) are taken from the literature. [90] Along with the references aspen plus was also used to complete the design of the equipment.

Installed equipment cost (C_{IE}) is calculated by the cost index correlation given in Equation (7.5) based on the 2020 cost index:

$$C_{IE} = f_i \times C_{PE} \times \frac{Cost\ index\ in\ year\ A}{Cost\ index\ in\ year\ B} \tag{7.5}$$

where f_i stands for the installation factor. The main items considered in the economic analysis for calculating TCOP are summarized in Table 7.4.

Table 7.4 Items calculated in the techno-economic analysis.

VCOP	**FCI**
• Chlorine gas	• ISBL investment
• Carbon	• Rotary kiln reactor
• Propane	• Distillation column
• Electricity	• Vertical G/L separator
• Fuel	• Compressor
FCOP	• Heat exchangers (Heating & cooling)
• Operating labor	• Engineering Costs
• Supervision	• Contingency Charges
• Direct salary overhead	
• Maintenance	
• Insurance and property taxes	
• Rent of land	

7.2.2 Results

To evaluate all the impacts that affect the TCOP, the following assumptions were also considered:

- Plant life: 20 years
- $POCl_3$ selling price: 1200 $/ ton $POCl_3$. [97]
- Discount rate: 30%

Table 7.5 provides the installation factors of equipment.

Table 7.5 Installation factors of the different equipment used[90]

Equipment	**Installation factor**
Reactor	3.5
Distillation column	4
Separator	4
Compressor	2.5

Chlorine gas, charcoal, propane, fuel electricity in US$ per year are considered in the utility cost shown in Table 7.6. The costs of raw materials and utilities, based on United, are given in Table 7.6. [93- 96]

Table 7.6 Summary of the costs of raw materials and utilities

Parameter	**Value**
Chlorine gas	160 $/ton
Charcoal	72 $/ton
Propane	5.5 $/kg
Fuel (CH_4)	0.03 $/kWh
Electricity	0.077 $/ kWh

The detailed cost results (ACC, FCI, FCOP, TCOP) are summarized in Table 7.7. The FCI is estimated to be 165,616,019 US$/year, with equipment costs contributing significantly at 78%. Notably, the rotary kiln reactors constitute the largest proportion, accounting for 67% of the total FCI. The calculated ACC amounts to 19,453,195 US$/year.

Table 7.7 Detailed costs to produce 50 ton/h of $POCl_3$ assuming 127 ton/h of treated phosphate waste, 8000 working hours/year and based on the equipment purchase cost (fi = 1.3)

FCI	
• Rotary kiln reactor ($)	*112,444,996*
• Distillation column ($)	*2,653,925*
• Vertical G/L separator ($)	*731,861*
• Compressor ($)	*7,604,741*
• Heat exchangers (Heating & cooling) ($)	*4,546,394*
• Engineering Costs ($)	*25,596,384*
• Contingency Charges ($)	*12,037,718*
• Discount rate (%)	*10*
• Plant life	*20*
• CRF	*0.117*
FCI	***165,616,019***
ACC	***19,453,195***

VCOP	
• Chlorine gas ($/year)	*213,760,000*
• Charcoal ($/year)	*8,135,111*
• Propane ($/year)	*1,309,000*
• Electricity ($/year)	*4,073,608*
• Fuel (CH4) ($/year)	*5,520,000*
FCOP	
• Operating labor ($/year)	*1,036,800*
• Supervision ($/year)	*311,040*
• Direct salary overhead ($/year)	*539,136*
• Maintenance ($/year)	*972,660*
• Insurance and property taxes ($/year)	*972,660*
• Rent of land ($/year)	*972,660*
FCOP	***237,602,674***
TCOP ($/year)	***257,055,870***
TCOP ($/kg $POCl_3$)	***0.64***

An analysis of the different parameters affecting the operating cost reveals that chlorine gas plays a crucial role, contributing 90% to the TCOP. Furthermore, chlorine gas emerges as the most significant component in determining the FCOP, making up 82% of the FCOP, as illustrated in Table 7.7. The TCOP is estimated to be 0.64 $/kg $POCl_3$.

Finally, considering the minimum selling price of $POCl_3$ (1.2 $/kg $POCl_3$), the techno-economic evaluation demonstrates that the carbochlorination process is economically viable and profitable.

CHAPTER 8 CONCLUSION

In this study, a carbochlorination process for the valorization of low-grade phosphate waste materials was investigated. The study including the thermodynamic analysis and laboratory experiments aimed to develop the proof of concept of this process. The carbochlorination consists in the reduction of the phosphate ore under the presence of chlorination and reductive reagents that may produce value-added gas phosphorous chloride components such as phosphoryl chloride. These gaseous phosphorous products can be used as reagents in the synthesis of valuable chemical products, e.g., phosphate esters and phosphine oxides, or to synthesize phosphoric acid, as part of the chain value of the OCP Group.

The preliminary thermodynamic analysis for carbochlorination systems within a specific temperature range was conducted using FactSage software. Our findings indicate that the carbochlorination reaction employing chlorine gas and carbon is more thermodynamically favorable than chlorination. Subsequently, equilibrium and phase diagram calculations were conducted to determine the ideal composition and process conditions that lead to the optimal conversion of phosphate ore to phosphorus trichloride ($POCl_3$). This thermodynamic investigation lays out the fundamental elements for the selective extraction of phosphorus-chlorinated compounds from phosphate ore during carbochlorination.

The carbo-chlorination experimental setup, along with a chlorine gas generator, was constructed and tested successfully. Under the carefully selected optimal conditions, the low and high-grade phosphate ore was subjected to rigorous testing, at different temperatures and reaction time, to ascertain the feasibility of the carbochlorination process using industrial low-grade phosphate waste. To gain comprehensive insights into the underlying phenomena and reaction mechanisms during the carbochlorination of low-grade phosphate waste, a multifaceted approach was employed. This approach involved integrating thermodynamic predictions with advanced analytical techniques, including ICP, SEM-EDS and XRD.

The findings obtained from the experimental investigations revealed notable differences in phosphorus recovery between high and low-grade phosphates, reaching 70% and 76%, respectively, at a temperature of 700 °C during a 7-hour duration. The observed relatively sluggish reaction rate was attributed to the solid-solid interactions prevailing between carbon and ore, primarily governed by the diffusion of carbon within the ore matrix. Additionally, the gradual

formation of $CaCl_2$ on the solid particles resulted in a reduced contact surface area between the chlorine gas and the ore, thus impeding its diffusion and slowing down the overall progress of the reaction.

The carbochlorination technique represents a promising approach for valorizing low-grade phosphate waste and extracting phosphorus from its source material. This proposed process emerges as a compelling alternative to conventional wet and thermal methods utilized for the beneficiation of low-grade phosphorus ore. The carbochlorination technique offers several advantages, making it an attractive option for sustainable phosphorus resource management.

Furthermore, it is noteworthy that the carbochlorination process yields a significant quantity of $SiCl_4$ as a byproduct. This $SiCl_4$ has the potential for valorization in various applications, particularly in the production of semiconductors and silica gel. Additionally, the carbochlorination reactions generate a substantial amount of CO_2 as a secondary product. Given the increasing global focus on carbon capture and utilization, exploring viable methods for capturing and utilizing this CO_2 emission is of paramount importance to minimize environmental impacts and enhance the process's sustainability. Moreover, the solid product collected at the reactor outlet, a result of the carbochlorination process, exhibits potential value for other applications leading to further economic and environmental benefits.

The techno-economic analysis revealed that the production cost of $POCl_3$ (0.64 \$/kg $POCl_3$) is lower than its selling price of 1.2 \$/kg $POCl_3$, considering the minimum selling market price. Consequently, the viability and profitability of the carbochlorination process for the treatment of low-grade phosphate ore waste have been substantiated through economic analysis.

In conclusion, the carbochlorination technique holds significant promise as an alternative and selective approach for valorizing low-grade phosphate waste and extracting phosphorus from its source material. This process presents an appealing alternative to traditional beneficiation methods and opens up opportunities for utilizing byproducts such as $SiCl_4$, $CaCl_2$ and $MgCl_2$ and addressing CO_2 emissions.

REFERENCES

[1] R. W. Scholz, A. E. Ulrich, M. Eilittä, and A. J. S. o. t. T. E. Roy, "Sustainable use of phosphorus: a finite resource," vol. 461, pp. 799-803, 2013.

[2] S. Kouzbour, B. Gourich, F. Gros, C. Vial, F. Allam, and Y. J. H. Stiriba, "Comparative analysis of industrial processes for cadmium removal from phosphoric acid: A review," vol. 188, pp. 222-247, 2019.

[3] M. A. De Boer, L. Wolzak, J. C. J. P. r. Slootweg, and recycling, "Phosphorus: reserves, production, and applications," pp. 75-100, 2019.

[4] A.-Z. M. J. I. j. o. m. p. Abouzeid, "Physical and thermal treatment of phosphate ores—An overview," vol. 85, no. 4, pp. 59-84, 2008.

[5] Y. Fu, Q. Wei, G. Zhang, and S. J. A. E. M. Sun, "Advanced phosphorus-based materials for lithium/sodium-ion batteries: recent developments and future perspectives," vol. 8, no. 13, p. 1703058, 2018.

[6] E. Commiss, "Best available techniques for the manufacture of large volume inorganic chemicals-Ammonia, Acids and Fertilisers," ed: European Page of Commission-Integrated Pollution Prevention and Control, 2007.

[7] M. Schorr and B. J. C. R. Valdez, "The phosphoric acid industry: equipment, materials, and corrosion," vol. 34, no. 1-2, pp. 85-102, 2016.

[8] L. Dong, X. Tong, X. Li, J. Zhou, S. Wang, and B. J. J. o. C. P. Liu, "Some developments and new insights of environmental problems and deep mining strategy for cleaner production in mines," vol. 210, pp. 1562-1578, 2019.

[9] R. Hakkou, M. Benzaazoua, and B. J. P. E. Bussière, "Valorization of phosphate waste rocks and sludge from the Moroccan phosphate mines: challenges and perspectives," vol. 138, pp. 110-118, 2016.

[10] Y. Taha and M. J. M. Benzaazoua, "Editorial for Special Issue “Towards a sustainable management of mine wastes: Reprocessing, reuse, revalorization, and repository”," vol. 10, ed: MDPI, 2019, p. 21.

[11] R. Dabbebi, P. Perumal, and S. Moukannaa, "Management and valorization of phosphate beneficiation slime: a critical review," *International Journal of Environmental Science and Technology*, pp. 1-14, 2023.

[12] N. Kanari, E. Allain, R. Joussemet, J. Mochón, I. Ruiz-Bustinza, and I. Gaballah, "An overview study of chlorination reactions applied to the primary extraction and recycling of metals and to the synthesis of new reagents," *Thermochimica acta*, vol. 495, no. 1-2, pp. 42-50, 2009.

[13] M. Djona, "Nouveau procédé pour la récupération de Co, Ni, Mo et V à partir des catalyseurs usés," Vandoeuvre-les-Nancy, INPL, 1994.

[14] X. Yu, X. Lang, and Z. Wang, "Extraction of rare earths from Baotou concentrating mill’s tailing by MgO roasting and carbochlorination reaction," *J Chin Rare Earth Soc*, vol. 27, no. 2, p. 309, 2009.

[15] P. M. Vitousek and W. A. Reiners, "Ecosystem succession and nutrient retention: a hypothesis," *BioScience,* vol. 25, no. 6, pp. 376-381, 1975.

[16] V. Smil, "Phosphorus in the environment: natural flows and human interferences," *Annual review of energy and the environment,* vol. 25, no. 1, pp. 53-88, 2000.

[17] S. A. Barber, *Soil nutrient bioavailability: a mechanistic approach*. John Wiley & Sons, 1995.

[18] T. Mitran, R. S. Meena, R. Lal, J. Layek, S. Kumar, and R. Datta, "Role of soil phosphorus on legume production," *Legumes for soil health and sustainable management,* pp. 487-510, 2018.

[19] D. Cordell, J.-O. Drangert, and S. White, "The story of phosphorus: global food security and food for thought," *Global environmental change,* vol. 19, no. 2, pp. 292-305, 2009.

[20] S. B. Sharma, R. Z. Sayyed, M. H. Trivedi, and T. A. Gobi, "Phosphate solubilizing microbes: sustainable approach for managing phosphorus deficiency in agricultural soils," *SpringerPlus,* vol. 2, pp. 1-14, 2013.

[21] H. Malhotra, S. Sharma, and R. Pandey, "Phosphorus nutrition: plant growth in response to deficiency and excess," *Plant nutrients and abiotic stress tolerance,* pp. 171-190, 2018.

[22] B. S. Don Ankerman, Richard Large, Ph.D. , "The Agronomy Handbook, Midwest Laboratories.," Page 25, p. 138, 2019.

[23] M. S. Khan, A. Zaidi, and P. A. Wani, "Role of phosphate solubilizing microorganisms in sustainable agriculture-a review," *Sustainable agriculture,* pp. 551-570, 2009.

[24] W. Li, H. Gao, Y. Luo, and J. Gao, "Status, trends and suggestions of phosphorus ore resources at home and abroad," *China Min. Mag,* vol. 24, pp. 6-10, 2015.

[25] R. Cui, Y. Zhang, J. Guo, Z. Guo, and Y. Xiao, "Development strategy of phosphate rock in China under global allocation of resources," *Strategic Study of Chinese Academy of Engineering,* vol. 21, no. 1, pp. 128-132, 2019.

[26] T. G. Langton, "Phosphate rock," in *Natural Resources in US-Canadian Relations*: Routledge, 2019, pp. 123-142.

[27] S.-c. LIU, S.-l. WANG, and R.-g. CUI, "Information Center of Ministry of Land and Resources," *Geological Bulletin of China,* vol. 28, no. 2-3, pp. 160-165, 2009.

[28] S. J. Van Kauwenbergh, *World phosphate rock reserves and resources*. Ifdc Muscle Shoals, 2010.

[29] C. E. Beigie, *Natural Resources In Us-canadian Relations, Volume 2: Patterns And Trends In Resource Supplies And Policies*. Routledge, 2019.

[30] C. B. Chernoff and G. Orris, "Data set of world phosphate mines, deposits, and occurrences: Part A. geologic data; Part B. location and mineral economic data," *US Geol. Surv. Open-File Rep,* p. C6, 2002.

[31] X. Meng, Q. Huang, J. Xu, H. Gao, and J. Yan, "A review of phosphorus recovery from different thermal treatment products of sewage sludge," *Waste Disposal & Sustainable Energy,* vol. 1, pp. 99-115, 2019.

[32] S. Larmagnat, "GLG-1000: Planète Terre," 2015.

[33] A.-Z. M. Abouzeid, "Physical and thermal treatment of phosphate ores—An overview," *International journal of mineral processing,* vol. 85, no. 4, pp. 59-84, 2008.

[34] S. Jasinski, "Geological Survey, Mineral Commodity Summaries: Phosphate Rock," ed.

[35] R. J. Singh and J. Bushee, "The rock cycle," *Journal of Geological Education,* vol. 25, no. 5, pp. 146-147, 1977.

[36] M. Derhy, Y. Taha, R. Hakkou, and M. Benzaazoua, "Review of the main factors affecting the flotation of phosphate ores," *Minerals,* vol. 10, no. 12, p. 1109, 2020.

[37] A. CHAABOUNI, C. CHTARA, A. NZIHOU, and H. EL FEKI, "Study the Nature and the Effects of the Impurities of Phosphate Rock in the Plants of Production of Phosphoric Acid," *Journal: Journal of Advances in Chemistry,* vol. 7, no. 2, 2014.

[38] T. Al-Fariss, H. Ozbelge, and H. El-Shall, "On the phosphate rock beneficiation for the production of phosphoric acid in Saudi Arabia," *Journal of King Saud University-Engineering Sciences,* vol. 4, no. 1, pp. 13-31, 1992.

[39] S. K. Kawatra and J. Carlson, *Beneficiation of phosphate ore*. Society for Mining, Metallurgy, and Exploration, 2013.

[40] A. Özer, M. Gülaboglu, S. Bayrakçeken, and W. J. A. P. T. Weisweiler, "Changes in physical structure and chemical composition of phosphate rock during calcination in fluidized and fixed beds," vol. 17, no. 5, pp. 481-494, 2006.

[41] M. Gharabaghi, M. Irannajad, and M. J. H. Noaparast, "A review of the beneficiation of calcareous phosphate ores using organic acid leaching," vol. 103, no. 1-4, pp. 96-107, 2010.

[42] G. Reta *et al.,* "Environmental impact of phosphate mining and beneficiation: review," vol. 2, no. 4, pp. 424-431, 2018.

[43] M. A. Mange and H. Maurer, *Heavy minerals in colour*. Springer Science & Business Media, 2012.

[44] S. S. MUKHOPADHYAY, "Beneficiation of phosphate rock for the segregation of phosphorus containing heavy metal free minerals," Patent WO2015159140A1, 2015.

[45] Z. I. Zafar, M. Anwar, and D. J. M. E. Pritchard, "Selective leaching of calcareous phosphate rock in formic acid: Optimisation of operating conditions," vol. 19, no. 14, pp. 1459-1461, 2006.

[46] P. J. A. Ptácek, S. Their Synthetic Analogues-Synthesis, Properties, and A. I. h. d. org/10./62214, "Phosphate rocks," 2016.

[47] M. J. A. j. o. c. Barakat, "New trends in removing heavy metals from industrial wastewater," vol. 4, no. 4, pp. 361-377, 2011.

[48] J.-f. Peng, Y.-h. Song, P. Yuan, X.-y. Cui, and G.-l. J. J. o. h. m. Qiu, "The remediation of heavy metals contaminated sediment," vol. 161, no. 2-3, pp. 633-640, 2009.

[49] E. A. Deliyanni, G. Z. Kyzas, and K. A. J. J. o. M. L. Matis, "Various flotation techniques for metal ions removal," vol. 225, pp. 260-264, 2017.

[50] A. V. Slack, *Fertilizer Science and Technology Series* (no. 1). Marcel Dekker, 1968.

[51] T. F. Al-Fariss, H. Özbelge, and H. J. J. o. K. S. U.-E. S. El-Shall, "Process technology for phosphoric acid production in Saudi Arabia," vol. 4, no. 2, pp. 239-254, 1992.

[52] P. Becker, *Phosphates and phosphoric acid*. Marcel Dekker, Inc., 1983.

[53] R. Gilmour, *Phosphoric acid: purification, uses, technology, and economics*. CRC Press, 2013.

[54] R. Guilmour, "Phosphoric Acid," ed: CRC Press, Florida, 2014.

[55] R. Boussen, "Valorisation de l'acide phosphorique par précipitation du cadmium et pertraction de l'uranium," 2007.

[56] W. MECIBAH, "Élimination des métaux lourds de l'acide phosphorique par un procédé membranaire," 2013.

[57] J. Bessiere, M. Bruant, E. Jdid, and P. J. I. j. o. m. p. Blazy, "Flottation ionique du cadmium et de l'arsenic par un dithiophosphate dans les solutions concentrées en acide phosphorique," vol. 16, no. 1-2, pp. 63-74, 1986.

[58] K. Bahsaine, M. E. M. Mekhzoum, H. Benzeid, R. J. J. o. I. Bouhfid, and E. Chemistry, "Recent progress in heavy metals extraction from phosphoric acid: a short review," 2022.

[59] M. Echchad and A. S. M. J. S.-P. A. o. S. GHAITH, "Green Marketing In Morocco," no. 28, pp. 7-16, 2022.

[60] W. Stowasser and M. y. a. r. I. Bureau of Mines %J Bureau of Mines, "The mineral industry of Morocco," vol. 3, pp. 623-632, 1973.

[61] M. J. E. C. Ahmed and R. P. C. Approaches, "Characterization of the Youssoufia-Morocco-MineFluoride-Contaminated Water and Their Detrimental Effects on Human Health," p. 3, 2019.

[62] A. Becker *et al.*, "Toward global food security: Transforming OCP through analytics," vol. 52, no. 1, pp. 90-107, 2022.

[63] M. J. M. Y. Taib, "The mineral industry of Libya," vol. 3, p. 20, 2010.

[64] M.-C. Meyer-Joly, "Valorisation du Concentré Mixte d'Echassières," Ph. D. Thesis, Institut National Polytechnique de Lorraine, France, 1988.

[65] N. Kanari, E. Allain, R. Joussemet, J. Mochón, I. Ruiz-Bustinza, and I. J. T. a. Gaballah, "An overview study of chlorination reactions applied to the primary extraction and recycling of metals and to the synthesis of new reagents," vol. 495, no. 1-2, pp. 42-50, 2009.

[66] N. Kanari, I. Gaballah, E. Allain, N. J. M. Menad, and M. T. B, "Chlorination of chalcopyrite concentrates," vol. 30, pp. 567-576, 1999.

[67] N. Kanari, I. Gaballah, and E. J. T. A. Allain, "A low temperature chlorination–volatilization process for the treatment of chalcopyrite concentrates," vol. 373, no. 1, pp. 75-93, 2001.

[68] N. Kanari, "Extraction des métaux de valeur des concentrés de chalcopyrite et de chromite par chloruration," INPL-Institut National Polytechnique de Lorraine, 1995.

[69] N. Kanari, I. Gaballah, E. J. M. Allain, and M. T. B, "A study of chromite carbochlorination kinetics," vol. 30, pp. 577-587, 1999.

[70] N. Kanari, I. Gaballah, and E. J. T. a. Allain, "Kinetics of oxychlorination of chromite: Part I. Effect of temperature," vol. 371, no. 1-2, pp. 143-154, 2001.

[71] N. Kanari, I. Gaballah, E. J. M. Allain, and M. T. B, "Kinetics of oxychlorination of magnesium oxide," vol. 30, pp. 1009-1015, 1999.

[72] B. Nowak, L. Perutka, P. Aschenbrenner, P. Kraus, H. Rechberger, and F. Winter, "Limitations for heavy metal release during thermo-chemical treatment of sewage sludge ash," *Waste Management*, vol. 31, no. 6, pp. 1285-1291, 2011.

[73] N. Kanari, N. Menad, F. Diot, E. Allain, and J. Yvon, "Phosphate valorization by dry chlorination route," *Journal of Mining and Metallurgy, Section B: Metallurgy*, vol. 52, no. 1, pp. 17-24, 2016.

[74] G. Fraissler, M. Jöller, H. Mattenberger, T. Brunner, and I. Obernberger, "Thermodynamic equilibrium calculations concerning the removal of heavy metals from sewage sludge ash by chlorination," *Chemical Engineering and Processing: Process Intensification*, vol. 48, no. 1, pp. 152-164, 2009.

[75] C. J. Menéndez, E. J. Nolasco, E. L. Tavani, and E. Pereira, "Kinetic aspects of the chlorination of wolframite and of scheelite with chlorine and sulphur dioxide," *Materials chemistry and physics*, vol. 40, no. 4, pp. 273-280, 1995.

[76] I. Gaballah and M. Djona, "Recovery of Co, Ni, Mo, and V from unroasted spent hydrorefining catalysts by selective chlorination," *Metallurgical and Materials Transactions B*, vol. 26, pp. 41-50, 1995.

[77] N. Kanari, B. Reddy, and I. Gaballah, "Kinetics of carbochlorination of chromium (III) oxide," *Metallurgical and Materials Transactions B*, vol. 29, pp. 729-738, 1998.

[78] A. Anderson, *Investigation of the carbochlorination process for the conversion of rare earth oxides into chlorides and measurement of their solubility in inert molten salts*. Colorado School of Mines, 2015.

[79] D. Mishra, J. Mochón Muñoz, L. F. Verdeja González, F. Diot, and E. J. R. d. m. Allain, 46, "Some kinetics aspects of chlorine-solids reactions," 2011.

[80] D. Brown, "HALIDES OF THE LANTHANIDES AND ACTINIDES," 1968.

[81] K. Jacob, A. Dixit, and A. J. B. o. M. S. Rajput, "Stability field diagrams for Ln–O–Cl systems," vol. 39, pp. 603-611, 2016.

[82] F. J. Pomiro, J. P. Gaviría, G. G. Fouga, A. E. Bohé, G. J. M. De Micco, Metallurgy, and Exploration, "A Panoramic Overview of Chlorination and Carbochlorination of Light Rare Earth Oxides, Including Thermodynamic, Reaction Mechanism, and Kinetic Aspects," pp. 1-18, 2021.

[83] D. W. Gaede *et al.*, "Chlorination roasting of rare earth element oxides," pp. 11-18, 2016.

[84] J. A. Gamboa, A. E. Bohé, and D. M. Pasquevich, "Carbochlorination of TiO2," *Thermochimica acta*, vol. 334, no. 1-2, pp. 131-139, 1999.

[85] D. M. Pasquevich, J. A. Gamboa, and A. Caneiro, "On the role of carbon in the carbochlorination of refractory oxides," *Thermochimica acta*, vol. 209, pp. 209-222, 1992.

[86] N. Kanari, "Phosphate valorization by dry chlorination route," *Journal of Mining and Metallurgy, Section B: Metallurgy*, vol. 52, no. 1, pp. 17-24, 2016.

[87] N. Kanari, I. Gaballah, and E. Allain, "Kinetics of oxychlorination of chromite: Part I. Effect of temperature," *Thermochimica acta*, vol. 371, no. 1-2, pp. 143-154, 2001.

[88] N. Kanari and I. Gaballah, "Chlorination and carbochlorination of magnesium oxide," *Metallurgical and Materials Transactions B*, vol. 30, pp. 383-391, 1999.

[89] M. Khodabandehloo, A. Larimi, and F. Khorasheh, "Comparative process modeling and techno-economic evaluation of renewable hydrogen production by glycerol reforming in aqueous and gaseous phases," *Energy Conversion and Management*, vol. 225, p. 113483, 2020.

[90] G. Towler and R. Sinnott, *Chemical engineering design: principles, practice and economics of plant and process design*. Butterworth-Heinemann, 2021.

[91] S. Hall, *Rules of thumb for chemical engineers*. Butterworth-Heinemann, 2017.

[92] A. A. Boateng, *Rotary kilns: transport phenomena and transport processes*. Butterworth-Heinemann, 2015.

[93] https://www.indexbox.io/blog/chlorine-price-per-ton-april-2022/

[94] https://www.carel.com/blog/-/blogs/six-reasons-to-use-propane-as-refrigerant

[95] https://www.eia.gov/energyexplained/coal/prices-and-outlook.php

[96] https://www.eia.gov/dnav/ng/hist/n3035us3m.htm

[97] https://www.intratec.us/chemical-markets/phosphorus-oxychloride-price